

Master Thesis, Department of Geosciences

# Sedimentology, Petrology and Diagenesis of Mesozoic Sandstones in the Mandawa Basin, Coastal Tanzania.

Ellen Gundersveen



**UNIVERSITY OF OSLO**

**FACULTY OF MATHEMATICS AND NATURAL SCIENCES**



# **Sedimentology, Petrology and Diagenesis of Mesozoic Sandstones in the Mandawa Basin, Coastal Tanzania.**

**Ellen Gundersveen**



Master Thesis in Geosciences

Discipline: Geology

Department of Geosciences

Faculty of Mathematics and Natural Sciences

University of Oslo

**June 2<sup>nd</sup>, 2014**

© **Ellen Gundersveen, 2014**

Tutors(s): Prof. Henning Dypvik (UiO).

This work is published digitally through DUO – Digitale Utgivelser ved UiO

<http://www.duo.uio.no>

It is also catalogued in BIBSYS (<http://www.bibsys.no/english>)

All rights reserved. No part of this publication may be reproduced or transmitted, in any form or by any means, without permission.



## **Acknowledgments**

First of all I would like to thank my supervisor Henning Dypvik at the Department of Geosciences at UiO. Thank you for always being supportive, helping and motivating me. You have been a big inspiration for me during my time at UiO.

Great thanks to all the people involved in the MBP project. Thanks to Katrine Fossum who have helped me and supported me throughout the year, an always being available for questions and discussions. Special thanks to fellow MSc students Kristine Nerbråten and Orhan Mahmic, for good collaboration in the field work in Tanzania in September and throughout the year.

I would also like to thank my fellow students in room 210 for helpful discussion, noumerous coffebreaks and fun times throughout the year.

Further I would like to thank Statoil for financial support to the project. Thanks to Erik Holtar and Mogens Ramm who have provided their time and effort to help the project running.

Thanks to Erik Zakariassen who created maps and proof read my thesis. You have been a great help.

Several people have helped me throughout the year at UiO. Thanks to Berit Løkenberg for assisting me during SEM analysis; Muriel Erambert for assisting me during EMP analysis, Marteen Aert for running my XRD.

I would like to thank my family, especially my mom and dad, who always have supported me throughout my academic years, and put out with me being stressed about my master thesis. You all made this year a lot easier for me. Thank you Lars for you love and patience. You have seen minimal of me the last months, but always being supportive and putting a smile back on my face.

## **Abstract**

Sedimentary successions of Mesozoic age have been studied in the Mandawa Basin, with the emphasis on describing facies and facies associations to provide information about the depositional environments. The diagenetic history of the sandstones is outlined by the use of petrographical studies. Further, the Mandawa Basin is the most promising hydrocarbon prospective onshore in Tanzania, and the petrographic and diagenetic observations in this study will provide information about the reservoir properties of the sandstones. With the recently discovery of the offshore gas field by Statoil in Block 2, the onshore-offshore relation of the sandstones is of great interest. Two samples of the offshore areas will be compared to the onshore sandstones studied in this thesis.

The study of field outcrops consisting of sandstones of the Upper Kipatimu Mb., Upper Mitole Mb., and Makonde Fm. display deposition environment within different alluvial regimes. Upper Kipatimu Mb. was deposited in a braided river system, and authigenic kaolinite is the dominant diagenetic cement, reducing the porosity and permeability. Upper Mitole Mb. deposited in and tidal channel, whereas Makonde Fm. deposited in an terminal distributary channel. Both Upper Mitole Mb. and Makonde Mb. experienced mechanical infiltration of clay in an early stage, and developed severe authigenic clay coatings of a smectite-chlorite mixed clay.

The studied cores from well site 21 and 24 displays a marine depositional setting within the outer shelf and upper slope environment. These sandstones consists of highly cemented turbiditic sandstones, where sparitic calcite cement is the major cement. In addition dolomite and ankerite is present. Porosities are generally low in the cemented units, but few units without any cement and high porosities is observed within the cores.

The study reveals that the reservoir quality of the Mesozoic sandstones within Mandawa Basin are significantly affected by early diagenetic processes related to the sedimentary facies in alluvial and marginal marine environments. The precipitation of early diagenetic cements has strongly influenced the present-day porosity. Knowledge of the influence of sedimentology on diagenetic patterns is an important element for improved understanding and predictions of reservoir quality in the Mandawa Basin sandstone.

The onshore-offshore comparison shows similarities in composition, which could indicate that the sediments offshore could have derived from the Mandawa Basin.

# Contents

<b>1. INTRODUCTION .....</b>	<b>1</b>
1.1 STUDY AREA .....	3
1.2 PREVIOUS STUDIES .....	3
<b>2. REGIONAL SETTING: DEVELOPMENT OF MANDAWA BASIN.....</b>	<b>5</b>
2.1 PERMIAN TO MID JURASSIC.....	8
2.2 MID JURASSIC TO LATE CRETACEOUS.....	10
2.3 LATE CRETACEOUS TO LATE PALEOGENE.....	12
2.4 LATE PALEOGENE TO PRESENT .....	13
2.5 OFFSHORE TANZANIA .....	13
<b>3. METHODS.....</b>	<b>14</b>
3.1 CORE LOGGING AND FIELD WORK.....	14
3.1.1 <i>Sampling</i> .....	14
3.1.2 <i>Offshore</i> .....	15
3.2 FACIES DESCRIPTION AND FACIES ASSOCIATIONS .....	17
3.3 DIGITALIZING OF SEDIMENTARY LOGS .....	18
3.4 PETROGRAPHICAL AND MINERALOGICAL ANALYSIS .....	19
3.4.1 <i>Thin section</i> .....	19
3.4.2 <i>Point counting</i> .....	20
3.4.3 <i>XRD - X-ray diffraction analysis</i> .....	22
3.4.4 <i>SEM – Scanning electron microscope</i> .....	24
3.4.5 <i>EMP – Electron microprobe analysis</i> .....	24
3.4.6 <i>IGV (Intergranular volume)</i> .....	25
<b>4. RESULTS.....</b>	<b>26</b>
4.1 FACIES.....	26
4.1.1 <i>Field outcrops (Late Jurassic – Mid Cretaceous)</i> .....	26
4.1.2 <i>Facies description – core from well site 24 and 21</i> .....	35

4.2	FACIES ASSOCIATIONS AND SEDIMENTOLOGICAL DESCRIPTION.....	42
4.2.1	<i>Facies associations – outcrops</i> .....	43
4.2.2	<i>Facies associations – cores</i> .....	47
4.3	PETROGRAPHIC DESCRIPTION .....	51
4.3.1	<i>Upper Kipatimu Mb. (Kimmeridgian - Tithonian)</i> .....	51
4.3.2	<i>Upper Mitole Mb. (Kimmeridgian – Berriasian)</i> .....	55
4.3.3	<i>Makonde Fm. (Aptian – Albian)</i> .....	58
4.3.4	<i>Well site 24 (Albian – Turonian)</i> .....	61
4.3.5	<i>Well site 21 (Cenomanian – Coniacian)</i> .....	64
4.3.6	<i>Offshore samples</i> .....	66
4.4	EMP – ELECTRON MICRO PROBE.....	69
4.4.1	<i>Kaolinite</i> .....	69
4.4.2	<i>Dolomite zonation</i> .....	71
4.4.3	<i>Feldspar overgrowth</i> .....	72
4.4.4	<i>Smectite-chlorite coating</i> .....	73
4.5	POROSITY AND IGV (INTERGRANULAR VOLUME) .....	73
<b>5.</b>	<b>DISCUSSION.....</b>	<b>79</b>
5.1	FACIES ASSOCIATIONS AND DEPOSITIONAL ENVIRONMENT .....	79
5.1.1	<i>FA2 - Upper Kipatimu Mb.</i> .....	79
5.1.2	<i>FA3 - Upper Mitole Mb.</i> .....	80
5.1.3	<i>FA4 - Makonde Fm.</i> .....	81
5.1.4	<i>Well site 24 (Albian – Turonian)</i> .....	82
5.1.5	<i>Well site 21 (Cenomanian – Coniacian)</i> .....	83
5.2	PETROGRAPHY AND DIAGENETIC HISTORY .....	85
5.2.1	<i>Field outcrops</i> .....	86
5.2.2	<i>Well sites 24 and 21</i> .....	92
5.2.3	<i>Offshore samples</i> .....	95
5.3	RESERVOIR SANDSTONES .....	95

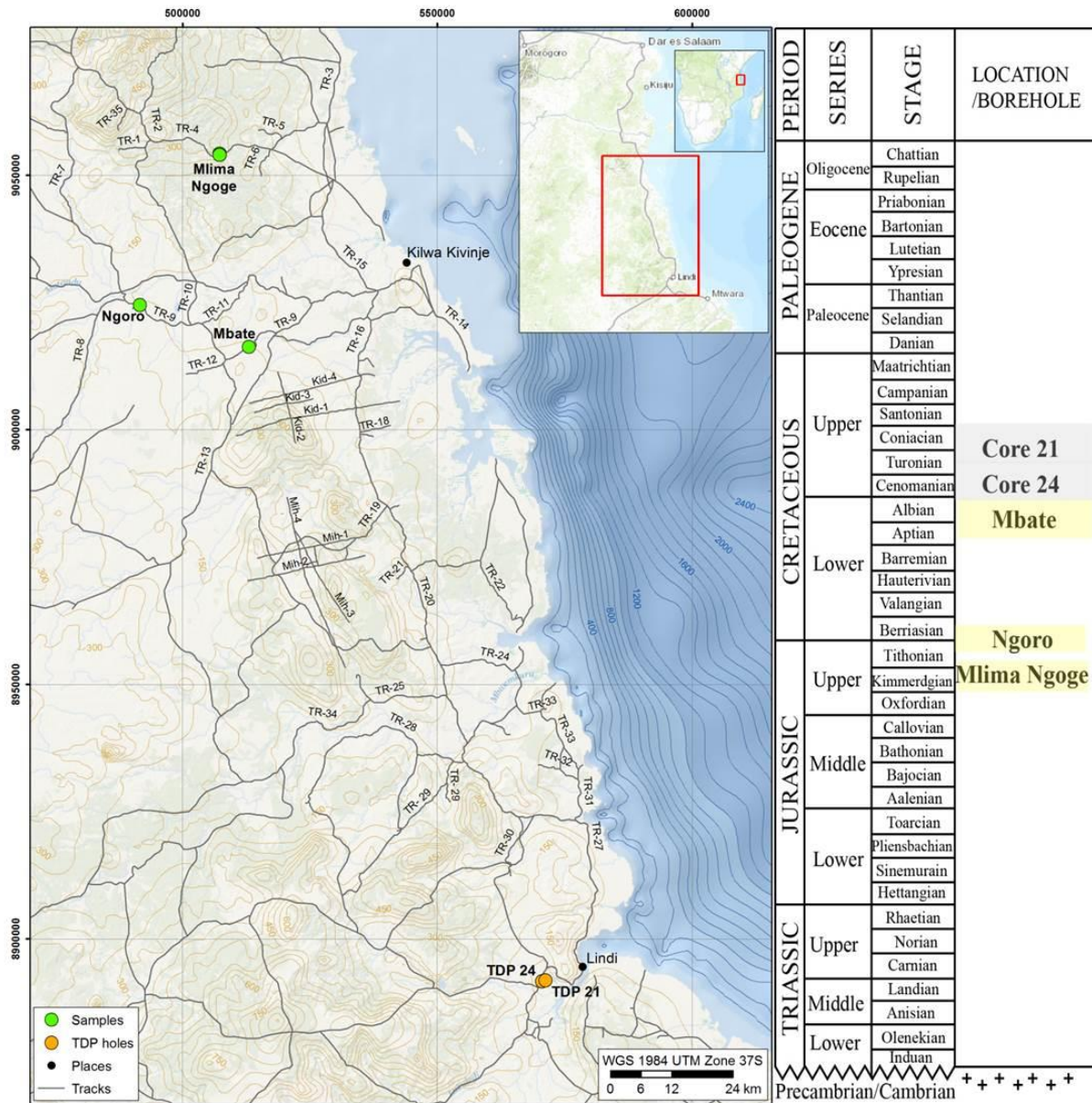
5.3.1	<i>Field outcrops</i> .....	95
5.3.2	<i>Well site 21 and 24</i> .....	96
5.4	OFFSHORE-ONSHORE RELATION .....	97
5.5	CONCLUSION .....	98
<b>REFERENCES</b> .....		<b>101</b>
<b>APPENDIX</b> .....		<b>I</b>

# 1. Introduction

This master thesis uses field observations and petrographical studies to give a sedimentological and petrographic description of Late Jurassic and Mid Cretaceous sandstones within the Mandawa Basin in coastal Tanzania. The main goal of this study is to assess the depositional environment and diagenetic history of the studied sandstones. Further, the study provides information about the reservoir properties of selected sandstone formations within the basin.

This thesis is a part of a four year (2013–2017) international research project, named Mandawa Basin Project (MBP). The Mandawa Basin Project is organized by University of Dar Es Salaam (UDSM), Department of Geosciences at University of Oslo (UiO) and Tanzania Petroleum Development Corporation (TPDC) in cooperation with Norwegian Petroleum Directorate (NPD) and Statoil. Scientists from UDSM, UiO and TPDC along with master students and PhD students from both universities are involved in this project. The aim of the project is to disclose sedimentary and structural history of the Mandawa Basin in order to better understand the stratigraphical developments, sediment formation and transportation as well as sediment provenance. The final goal of the project is to compare onshore studies with available material from offshore sites (Statoil), to tie land and offshore geology together.

During two weeks of fieldwork (18 – 24 September, 2013), three outcrops and two cored boreholes were logged, studied and sampled (Figure 1.1). The corings were performed by TDP (Tanzania Drilling Project). Key sandstone samples from outcrops and cores were selected and studied in detail to provide sedimentological, petrographical and reservoir related information in the Mandawa Basin. The post-depositional diagenetic history of the sandstone will be outlined to relate the petrography to the sedimentological evolution. In addition, two offshore samples provided by Statoil, were briefly compared to the onshore samples from the Mandawa Basin. The comparison of the offshore and onshore samples provides information about the onshore-offshore relation.

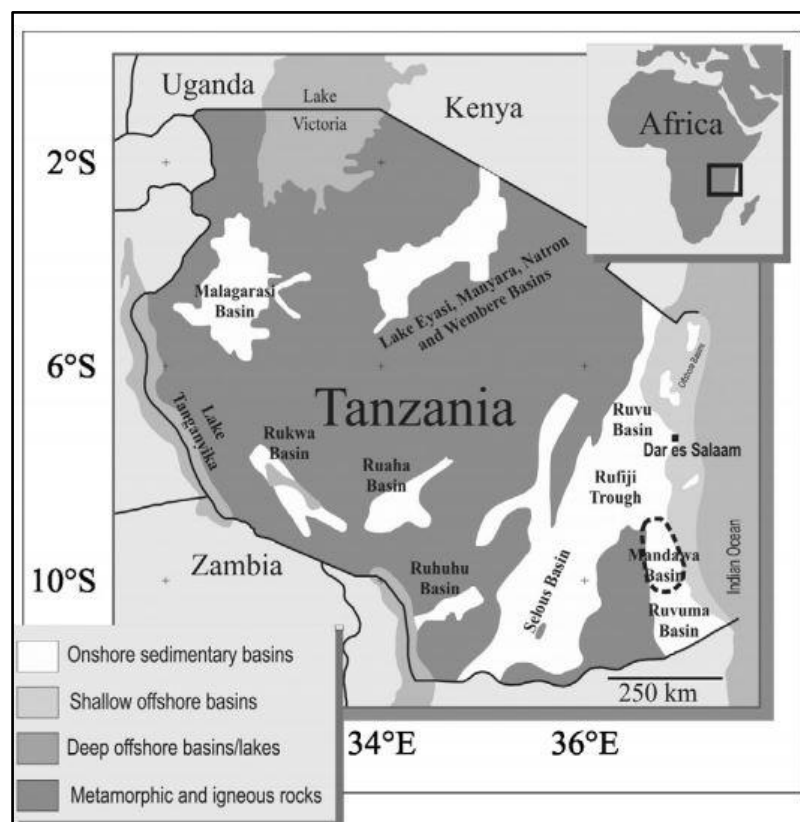


**Figure 1.1:** Map of the study area in coastal Tanzania. The main localities studied are indicated with green dots for the field formations; Kipatimu Fm. at Mlima Ngoge, Mitole Fm. at Ngoro and Makonde Fm. at Mbate, modified by Zakariassen (2014) from Esri (2014). The studied cores from well site 24 and 21 are marked with orange dots. The simplified stratigraphical column displays the field formations marked with yellow boxes and the studied well sites marked with grey boxes, modified from Hudson (2011).



## 1.1 Study area

Mandawa basin is a sub-basin within the coastal belt of Tanzania, along with the Ruvu and Ruvuma basins. Mandawa basin is structurally situated between the Ruvuma basin to the south, separated by the Ruvuma Saddle, the metamorphic basement to the west, the offshore basins to the east, and bound to the Rufiji Trough to the north (Hudson and Nicholas, 2014) (Figure 1.2). Mandawa basin is probably the most prospective onshore basin for hydrocarbons in Tanzania. With discoveries of large gas and oil reserves offshore in southern Tanzania/Mozambique and the conjugate margin in Madagascar, the Mandawa basin has become the focus of a new phase of exploration (Hudson, 2011, Nicholas, 2013).



*Figure 1.2: Location of Mandawa basin in the dotted line. Situated between Ruvuma and Ruvu basins, and bound to metamorphic basement to the west and Rufiji Trough in the north (Hudson and Nicholas, 2014).*

## 1.2 Previous studies

Mandawa Basin was initially explored by British Petroleum (BP) in 1950s and 1960s. They conducted geological and geophysical work, and the drilling of 7 boreholes took place. The

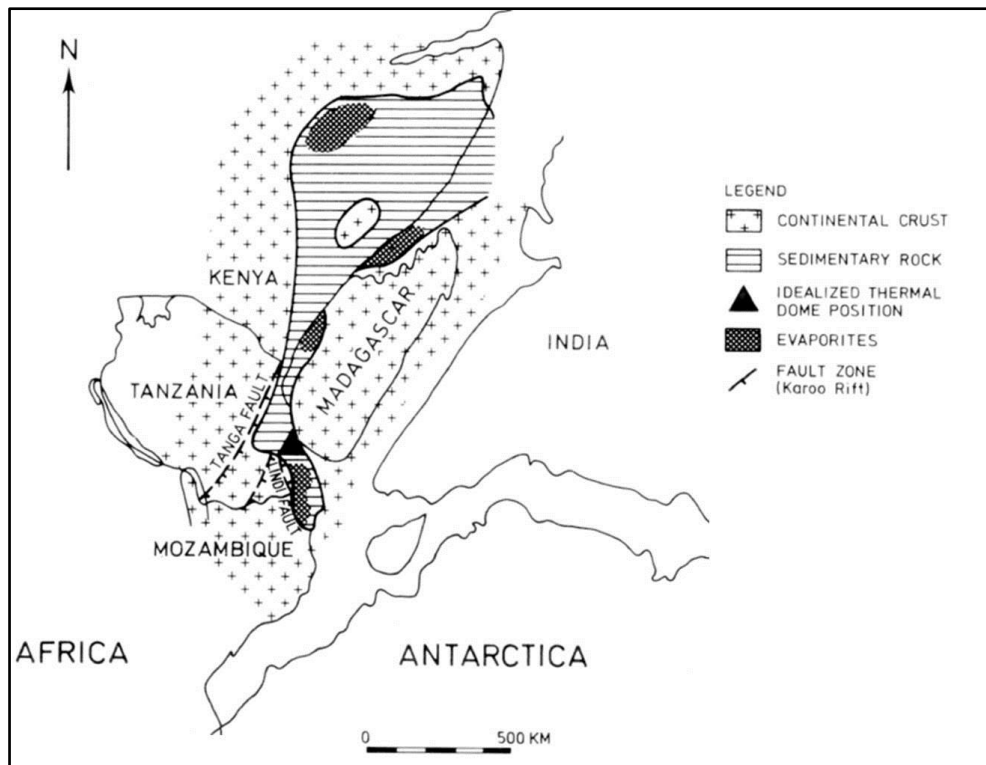
first geological mapping by BP was done in the northern part of the basin. No commercial hydrocarbons were discovered during this survey (Kent et al., 1971). Between 1970 and 2011 Mandawa was explored by several companies: Agip, Shell Petroleum Development Tanzania, Dublin International and TPDC/Dominion Petroleum Limited. These companies acquired seismic data and drilled a total of 8 deep wells in the Mandawa Basin, without encountering any hydrocarbons in commercial quantities. The wells did, however, encounter shales with source rock quality. Most of the studies intended for mineral and petroleum exploration are not published and classified information is kept within the oil companies (Hudson, 2011, Hudson and Nicholas, 2014).

The regional stratigraphy and distribution of the Mesozoic to Tertiary sediments in the coastal basins of Tanzania is described in detail in Kent et al. (1971). Furthermore the TDP conducted drilling of 41 boreholes with the interest of paleoclimate research (Pearson et al., 2004, Nicholas et al., 2006, Nicholas et al., 2007). In addition Kagya et al. (1996) performed geochemical analysis on silty shales, with hydrocarbon generation potential. Hudson (2011) conducted a detailed surface mapping of the Mandawa Basin and synthesized the geological evolution of the basin using available geological and geophysical surface and subsurface data. Some of the latest work in the Mandawa basin includes studies of paleoenvironment and stratigraphy of the Pindi Group (Triassic to Early Jurassic) within the Mandawa basin done by Hudson and Nicholas (2014).

The basin is of significance for hydrocarbon prospectivity, where both source rocks and potential source rocks are proven. Considering only 8 deep wells are drilled in an area of approximately 7 000 km<sup>2</sup>, Mandawa Basin is underexplored (Hudson, 2011).

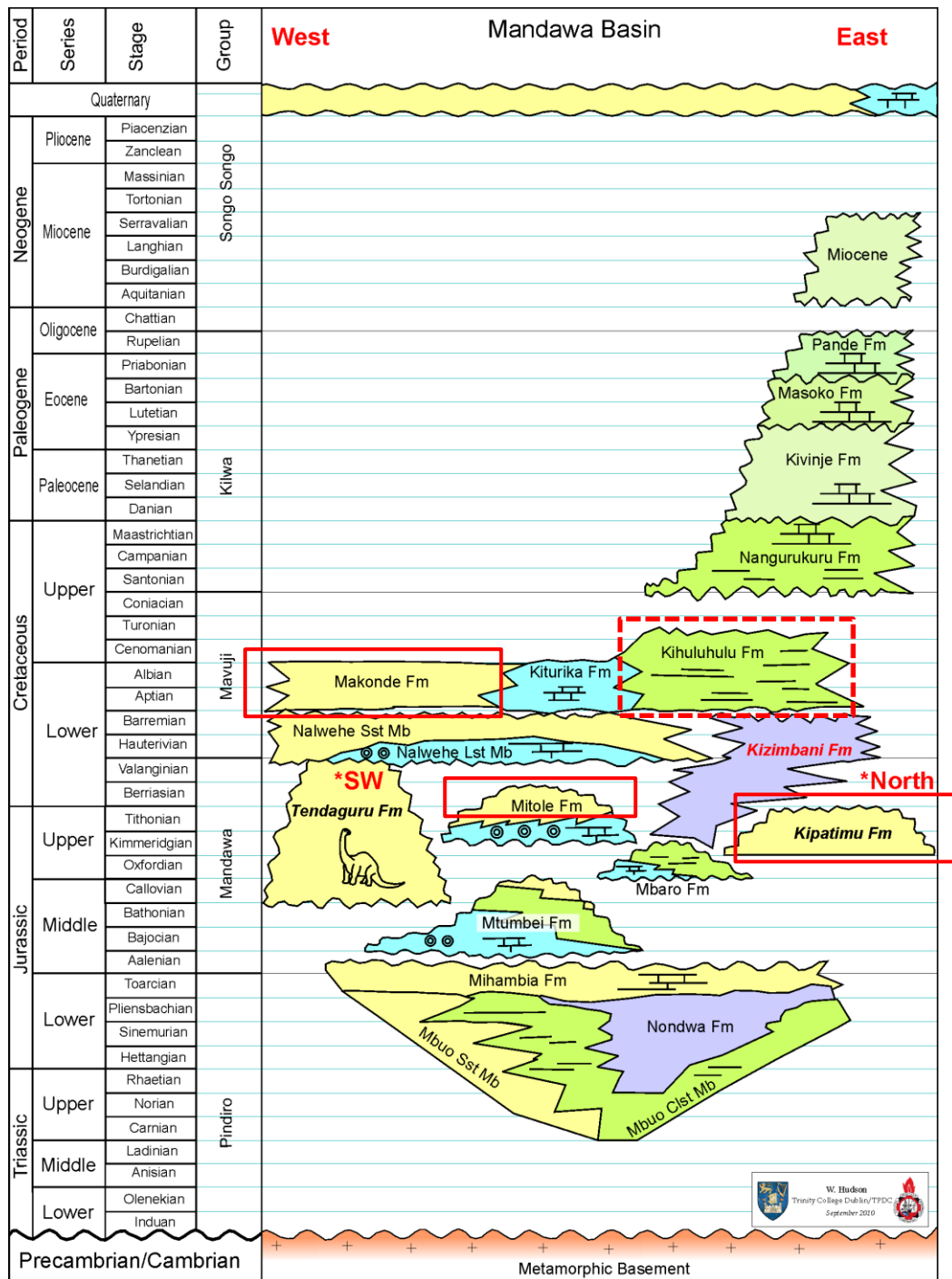
## 2. Regional setting: Development of Mandawa Basin

Mandawa Basin evolved from the Triassic as a result of rifting and break-up of Gondwana. The main factors considered to determine the geological history of the basin are the initial position of Madagascar within the Gondwana continental plate (Figure 2.1), and the relative drifting of the Madagascar and African continental blocks (Salman and Abdula, 1995).



*Figure 2.1: Plate reconstruction, showing the paleo-position of Madagascar with respect to Africa. This is before the break up of Gondwana, in Early Jurassic times (Mpanda 1997).*

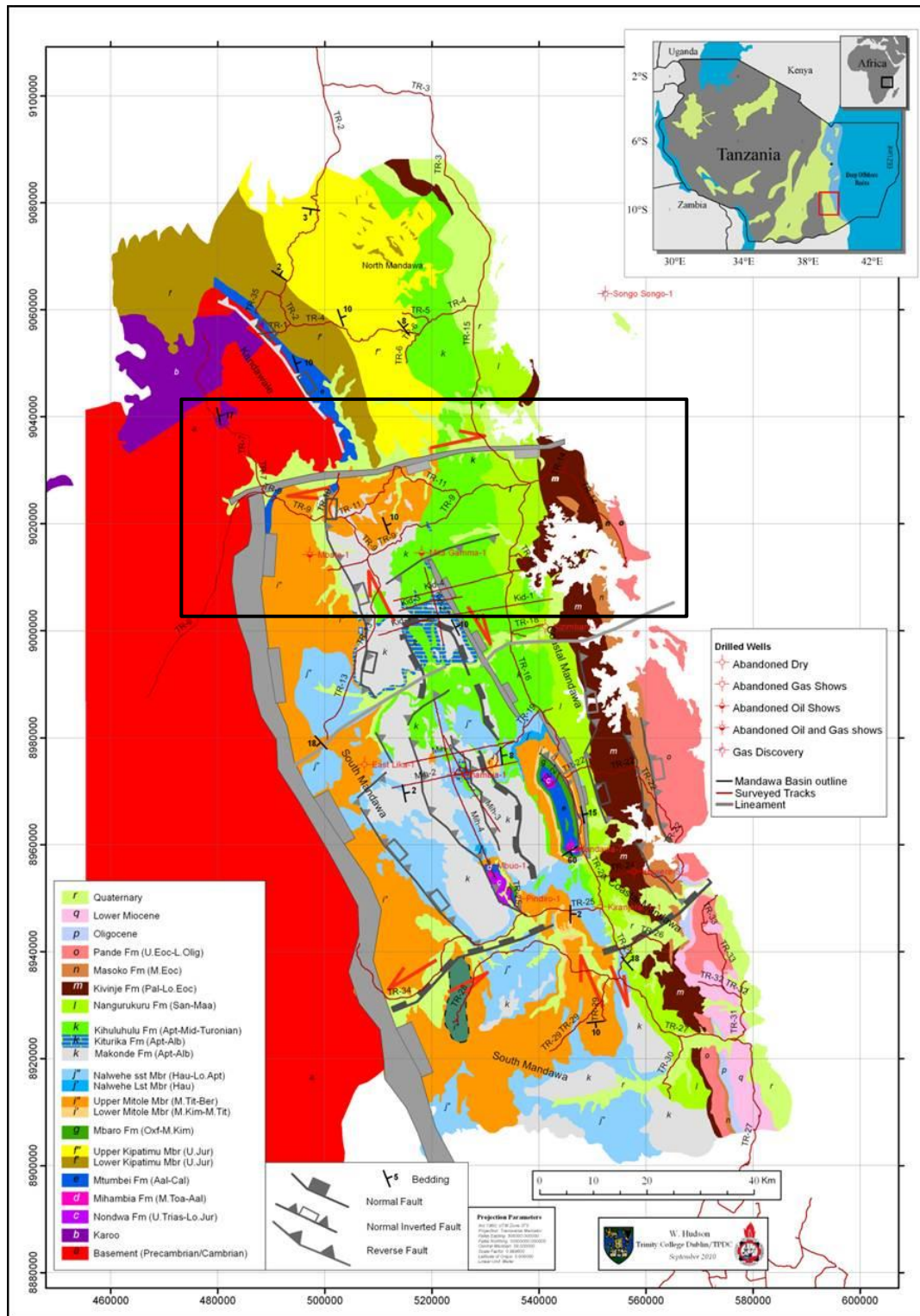
The sedimentary successions of the Mandawa Basin was by divided in to five groups Hudson (2011): Pindiro Mandawa, Mavuji, Kilwa and Songo Songo (Figure 2.2). These groups consist of associated formations with significant unifying lithological features. The studied field outcrops and cores in this study are represented by the Mandawa Gp. (Upper Kipatimu Mb. and Upper Mitole Mb.) and the Mavuji Gp. (Makonde Fm.) (1.1 and 2.2). The studied cores are equivalent in time with the Kihuluhulu Fm. (Albian – Coniacian) within the Mavuji Gp. (Figure 1.1. and 2.2).



**Figure 2.2** Revised litho- and chronostratigraphic framework of the Mandawa Basin.

*Studied formations are marked with red boxes. Modified after Hudson (2011).*

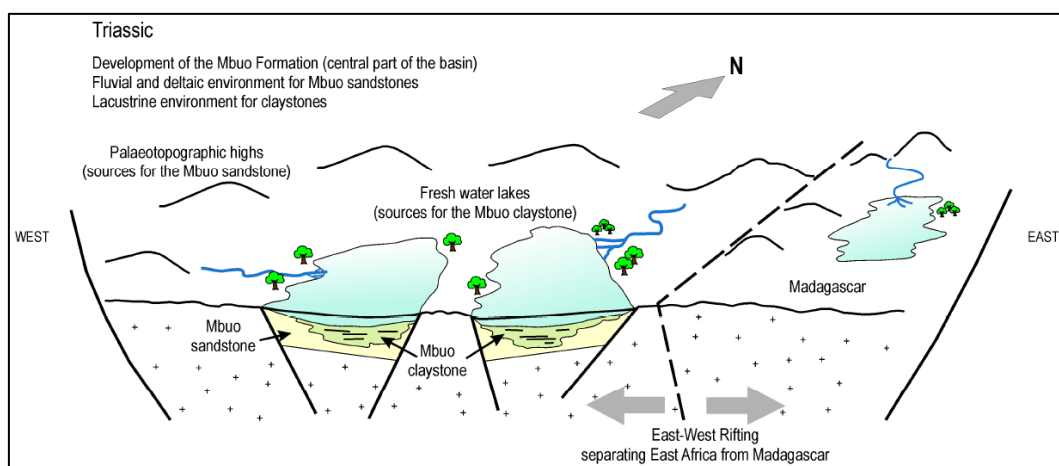
In addition, Hudson (2011) created a revised geological map of the Mandawa Basin (Figure 2.3). This map is used as the basis for the location of the sandstone formations studied in this thesis within the Mandawa Basin. The following chapter focuses on the tectostratigraphic development along with the basin infill history.



**Figure 2.3:** Revised Geological map of Mandawa Basin. The sedimentary successions within the basin have a gentle offshore dip. The study area is marked with a black box (Hudson, 2011).

## 2.1 Permian to Mid Jurassic

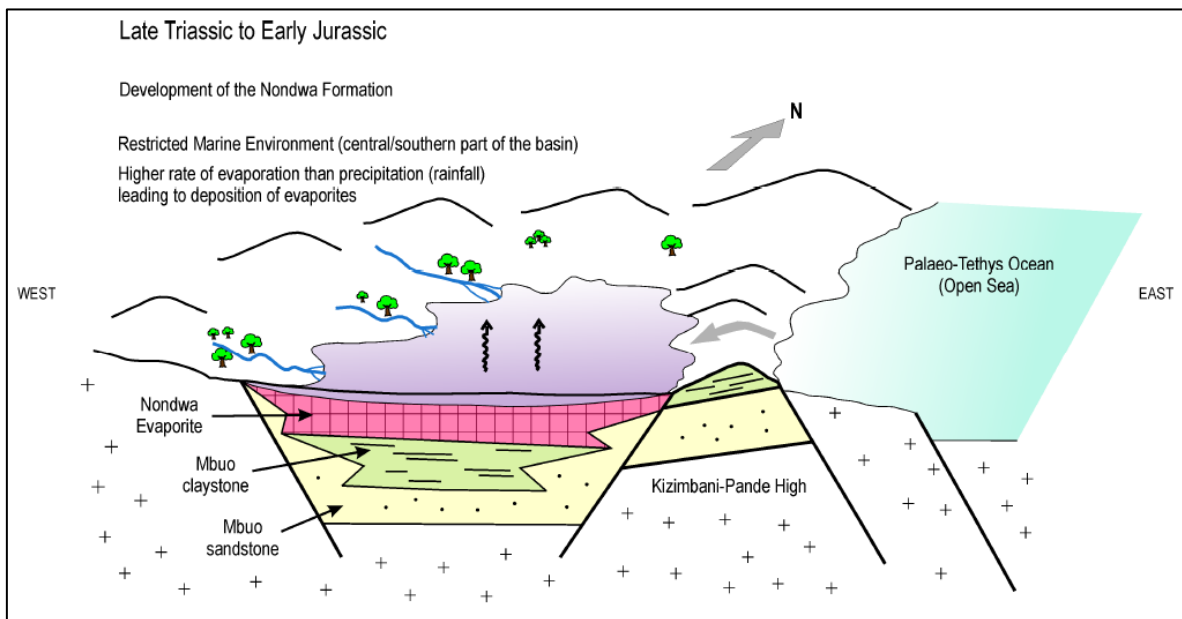
Mandawa Basin started to develop within the single Gondwana continental mass as Gondwana was breaking up. During the rifting phase of Gondwana, in Permian (300 – 205 Ma), extended rift structures were formed due to regional uplift. The uplifting, caused by thermal expansion, led to peripheral parts of the supercontinent starting to break up (Salman and Abdula, 1995). Block faulting occurred and created broad platform depressions (Mpanda, 1997). During Late Triassic, when the Indian Ocean started to open, seawater flooded the downfaulted belts. At the same time the southern and central part of Mandawa Basin subsided at a much higher rate than the adjacent areas, resulting in accumulation of thick sequences of terrestrial carbonate, fluvial and alluvial deposits in the depressions. These initial deposits lying unconformably on top of the Precambrian basement are known as the Karoo Group (Nicholas et al., 2007, Hudson and Nicholas, 2014, Hudson, 2011) (Figure 2.2). In the literature Karoo is used as a term for the depositional events ranging from Late Triassic to Late Cretaceous (Wopfner, 2002). Within the Mandawa Basin these deposits are named the Pindiro Group, consisting of Mbuo Fm., Nondwa Fm. and Mihambia Fm. (Figure 2.2 and 2.3). Mbuo Fm., as the first sediments deposited on top of the Precambrian metamorphic basement, consists of basal clastic conglomerates succeeded by claystones at the top of the formation. Mbuo Fm. was deposited within lacustrine, alluvial and fluvial environments (Hudson and Nicholas, 2014) (Figure 2.4).



**Figure 2.4:** Paleogeography of the deposition of the earliest sediment infill in the Mandawa Basin. These sediments were deposited in fresh water lakes. The sediments consist of conglomerates (yellow) at the base, and claystones (green) at the top. Madagascar was still connected to the continent, but the East-West rifting lineaments

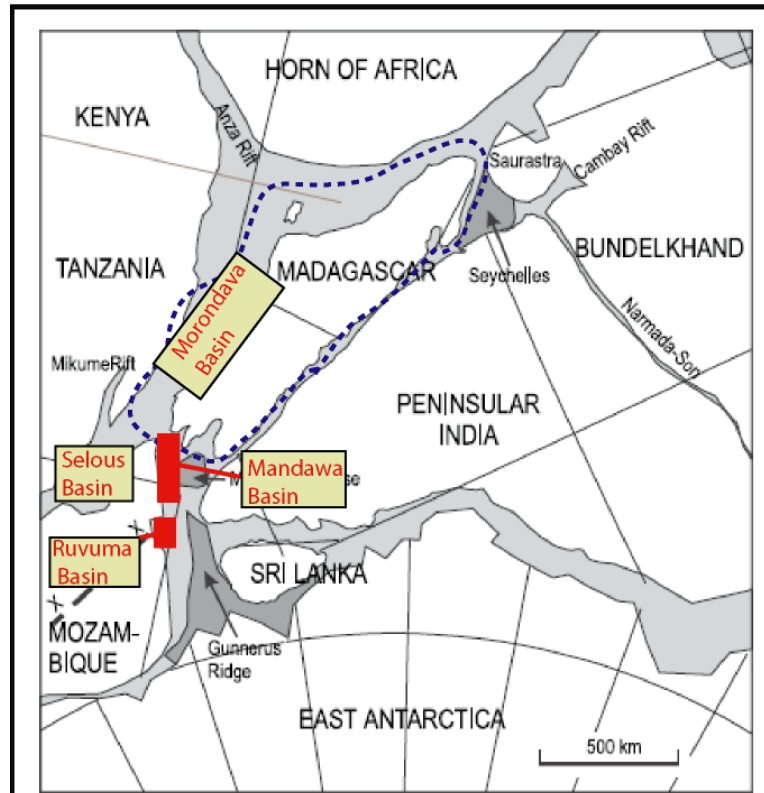
*that later separated Madagascar from East Africa is marked. From Hudson & Nicholas (2014).*

In Late Jurassic times Nondwa Fm. was deposited as salt evaporate sequences in the central basin, formed in lakes from the Triassic which had now turned into hypersaline lakes. The Kizimbani- Pande High to the east and Ruvuma Saddle to the South may have provided barriers, creating a restricted marine environment (Hudson & Nicholas 2014) (Figure 2.5). On top of Nondwa Fm., the Mihambia Fm. was deposited as clastic siltstones, sandstones, and carbonates within a shallow and marginal environment. The period from 205 to 157 Ma marks the end of the Gondwana continent, and the onset of the continent breaking up into separate blocks. Between Africa and Madagascar a deep depression formed, creating a marine seaway between the two blocks (Figure 2.6). During this time the Mandawa Basin experienced the Paleo-Thetys transgression (Salman and Abdula, 1995) (Figure 2.5).



**Figure 2.5:** *Paleogeography for the deposition of Nondwa Fm. (purple), consisting of evaporates deposited in a hypersaline lake, and the Mbuo Fm.(yellow and green). The Kizimbani-Pande high provided a barrier for the restricted marine environment. Later the Palaeo-Tethys from the east led to a marine transgression (Hudson and Nicholas, 2014).*



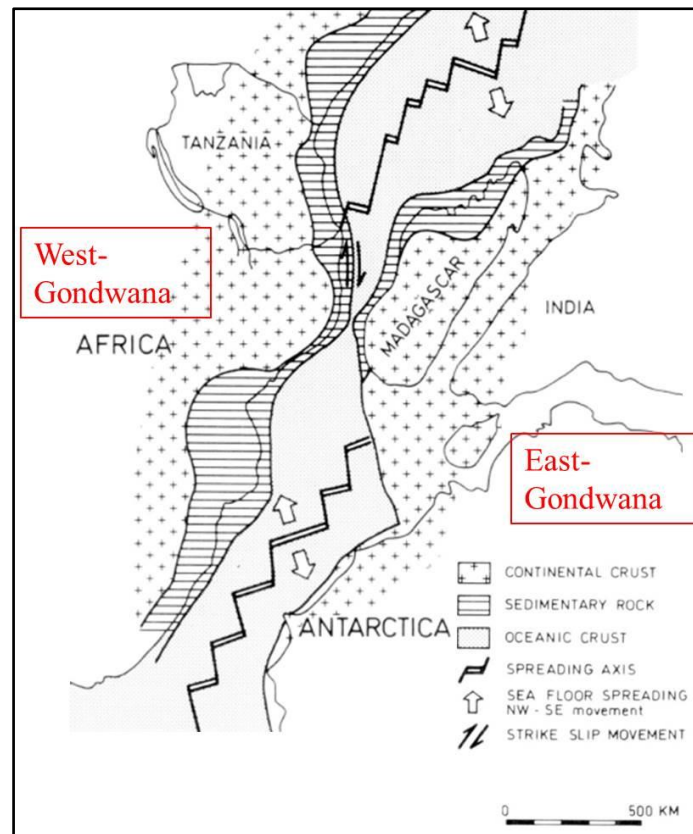


**Figure 2.6:** Position of Madagascar at 200 Ma, and the Mandawa basin. A marine seaway started developing between Africa and Madagascar. Modified by Nicholas (2013) after Reeves (2002).

## 2.2 Mid Jurassic to Late Cretaceous

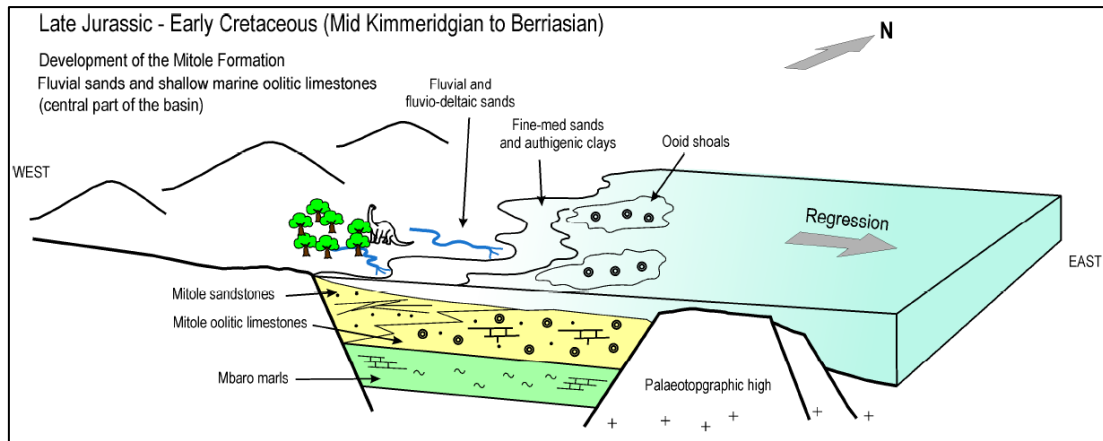
The period between 157 and 118 Ma is considered as the post-Gondwana stage, where active seafloor spreading dominated the study area. Gondwana successfully separated into two major blocks; (1) West Gondwana (Africa-South and America) and (2) East Gondwana (Madagascar, India, Sri Lanka, Seychelles, Australia and Antarctica) following zones of weakness created in Permian times (300-205 Ma) (Figure 2.7). Madagascar was separated from East Africa and moved east due to east-west dextral strike-slip movement. The opening of the East African basins, including Mandawa Basin, started at this point. Further, Madagascar moved to the south, parallel to the Davie Ridge Fracture Zone (Salman and Abdula, 1995, Hudson, 2011).





**Figure 2.7:** Early Cretaceous plate reconstruction showing the drift of Madagascar and the separation of Gondwana into West and East Gondwana. Modified from Mpanda (1997).

Seafloor spreading accompanied by a marine transgression covered the entire region and created fully marine conditions during Mid Jurassic times (Mpanda, 1997). Within the Mandawa Basin the sea was rising at a higher rate than the basin subsidence, and interbedded shallow-marine and shoreface deposits of the Mtumbei Fm. (Mandawa Gp.) (Figure 2.2) was deposited. In Late Jurassic the paleo-coastline stepped eastward and the basin was subsiding at an even higher rate. Marine shales and limestones were deposited in the central part of the basin, and at the same time the basin received clastic deposits from the paleohighs (Salman and Abdula, 1995, Hudson, 2011). These deposits consist of fluvio-deltaic sandstones and oolitic limestone beds of Kipatimu, Mbaro and Mitole formations (Mandawa Gp.) (Figure 2.8). In addition, sandstones of the Nalwehe Fm. (Mavuji Gp.) were deposited on top of the Mavuji Gp. in Lower Cretaceous (Figure 2.2). These friable quartz sandstones deposited during Lower Cretaceous age are potential reservoir rocks (Hudson, 2011).

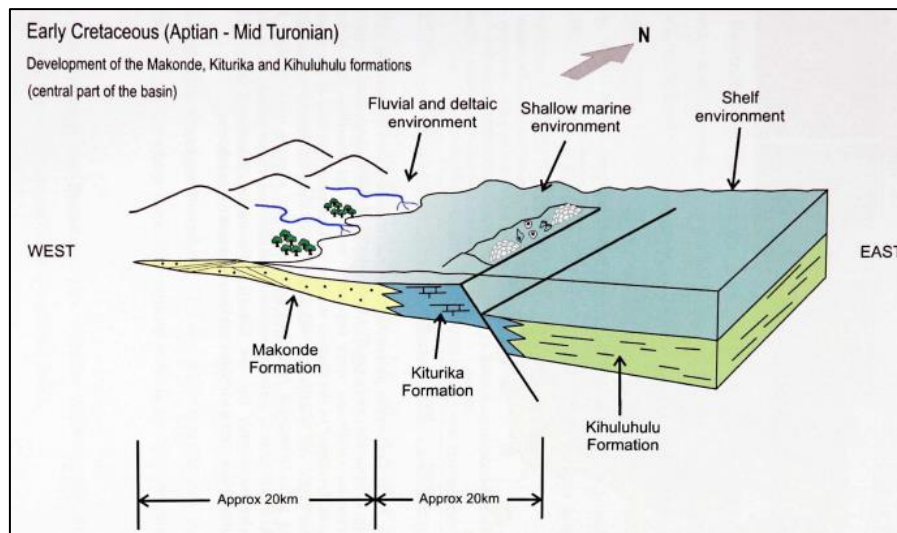


**Figure 2.8:** Paleogeography of the depositional environment from Late-Jurassic to Early Cretaceous where the central part of the basin is dominated by shallow marine oolitic limestone deposits, of Mbaro Fm. and Upper Mitole Mb. Within the western part fluvial and fluvio-deltaic sands were of Upper Mitole Mb. deposited (Hudson 2011).

From Mid Cretaceous to Late Cretaceous the basin was subsiding at a constant rate, and the rest of the Mavuji Gp. was deposited (Figure 2.2). Mavuji Group comprises Makonde, Kiturika, Kizimbani and Kihuluhulu formations (Figure 2.2). Makonde Fm. was deposited in the western part of the basin as fluvial sandstones contemporary with the carbonates of Kiturika Fm. and the marine clays of Kihuluhulu Fm. in the central and coastal part of the basin (Figure 2.9). A mid to outer shelf marine environment dominated, and this was a major sediment infill period in Mandawa Basin. Kizimbani Fm. was tectonically emplaced between Mbaro Fm. and Kihuluhulu Fm., and consists of evaporites (Figure 2.2) (Hudson, 2011).

### 2.3 Late Cretaceous to Late Paleogene

Drifting ended in Late Cretaceous (Santonian, 85 Ma.) and Mandawa experienced constant basin subsidence. The East African coast experienced very little extensional tectonics from Late Cretaceous to Oligocene, and the period was rather quiet. Deposition of thick massive clays with turbiditic sands happened in a mid- to outer shelf upper slope environment (Nicholas et al., 2007). These broadly homogenous deposits of marine clays are presently found within the Kilwa Gp. (Figure 2.2) (Nicholas et al. 2006). Kilwa Group consists of Nangurukuru, Kivinje, Masoko, and Pande formations (Figure 2.2).



**Figure 2.9:** Paleogeography of the contemporary deposition of the fluvial Makonde Fm. (yellow), carbonates of the Kiturika Fm. (blue) and marine clays of Kihuluhulu Fm. (green) (Hudson, 2011).

## 2.4 Late Paleogene to Present

Active fault movement created local accommodation space, along with minor sedimentation taking place within valleys and flood plains. A final marine regression occurred and the Songo Songo Gp. was deposited as the last basin infill succession. This group represent shallow lagoon, tidal flat marls and sand deposits (Hudson, 2011).

## 2.5 Offshore Tanzania

The offshore geology is strongly affected by extensional rifting related to the formation of the Indian Ocean. The separation of the African continental block from the Madagascar/Antarctica/India block was controlled by a strike slip movement (Figure 2.7). The offshore structural trends run parallel to the present day coastline (Mpanda, 1997). The continental shelf outside Tanzania is very narrow (3-10 km), and at the shelf edge the water depth declines rapidly with slope gradients locally being more than  $4.5^\circ$  (Bourget et al., 2008). The sediments located in the offshore areas were shed off the African craton from late Jurassic. The Jurassic-Tertiary sedimentary succession exceeds more than 4 km in thickness in the offshore areas of Tanzania (McDonough et al., 2013).

## **3. Methods**

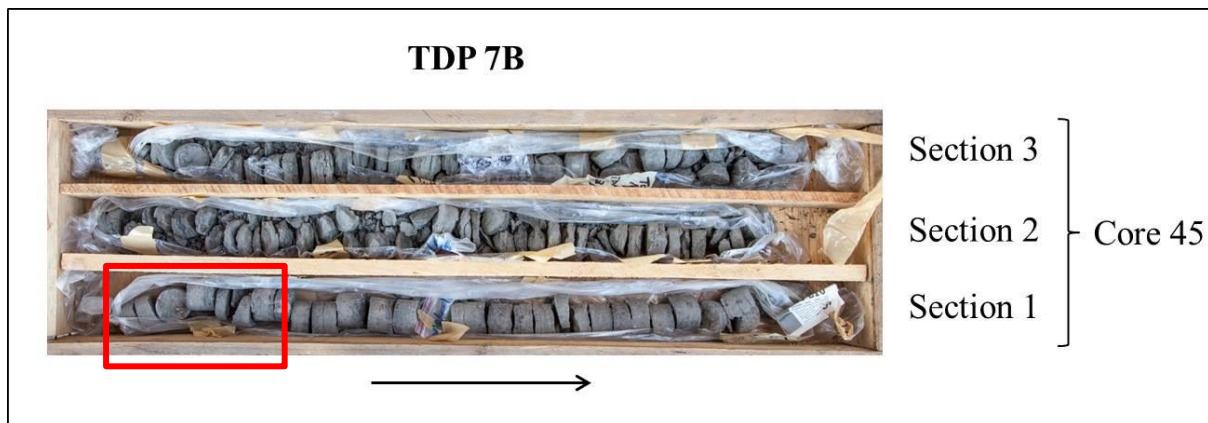
### **3.1 Core logging and field work**

Core logging and sampling was carried out at the TDP core storage facility in Dar Es Salaam for seven days (18. – 24. September 2013). Due to time restrictions seven wells were selected to get the best stratigraphic resolution from Late Cretaceous to Oligocene. Two of the logged wells, well 21 and well 24, are studied in this thesis (Figure 1.1). Field work was carried out in four days (26. – 29. September 2013) with Kilwa Masoko village as base station. Key localities were logged and sampled in the northern part of the basin, where the Kipatimu, Mitole and Makonde formations were studied (Figure 1.1, 2.2 and 2.3). In addition, Statoil provided two sandstone samples of Cenomanian age from offshore Tanzania.

Core logging and field work was a collaboration between the author, Kristine Nerbråten (MSc UiO, 2014), Orhan Mahmic (MSc UiO, 2014), Katrine Fossum (PhD, UiO), Justina Saroni (PhD UDS) and two master students from TPDC. Field work and core logging were done with assistance from Professor Henning Dypvik (UiO) and Dr. Charles Kaya (UoDS).

#### **3.1.1 Sampling**

Cores from well sites 24 and 21 were stored in boxes, with three meter long core pieces, divided in three sections of one meter (Figure 3.1). Sample identification numbers refer to borehole site/core number/section number/depth. Depth is measured in centimeters from the bottom of the sections. An example of a sample from core 45 is shown in Figure 3.1, where the sample name would be 7B/45/1 0- 20 cm. Samples collected from the cores were about 2 cm in thickness. The cores were logged and measured from the deepest part and upwards. Sedimentary logs of cores from well sites 24 and 21 thus displays the deepest part as zero meters, and the shallowest part as 90 and 70 meters respectively. In addition, the logs display core number, section number and depth.



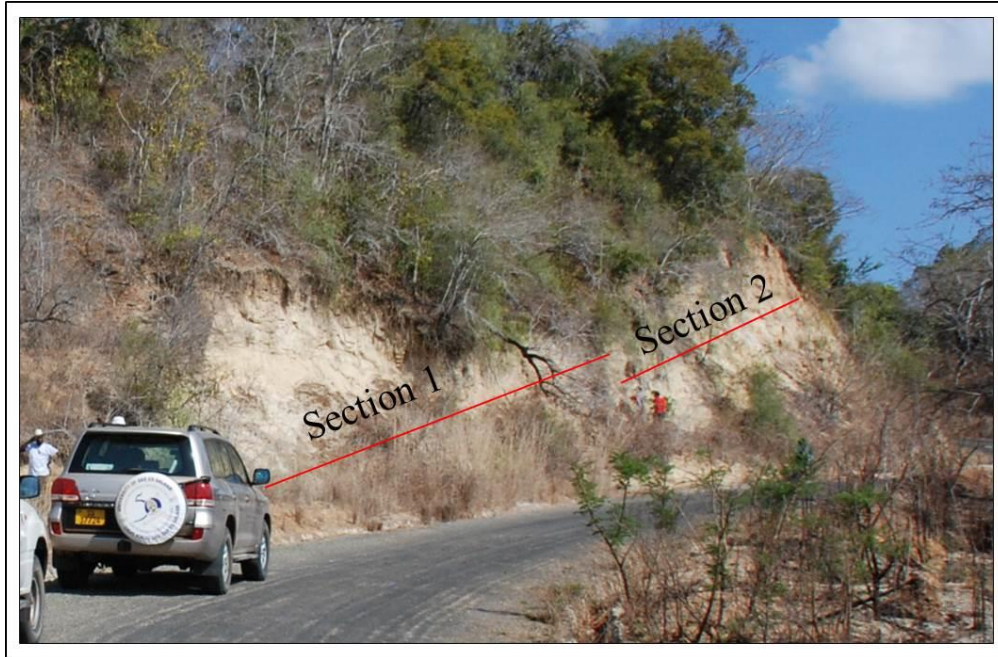
**Figure 3.1:** Example from logged well TDP 7B. Core 45 is divided into three sections of one meter each. Diameter of the cores is 5 cm. Black arrow illustrates right way up. Red box displays a selected sample that would be named 7B/45/1 0-20 cm.

Field samples were named with identification numbers referring to locality – section number - sample number – year of collection. An example from one of the formations would be NG-2-1-13 (NG = Ngoro). The average sample sizes were about 1-2 fist sizes. Due to time restrictions the field participants were divided into two groups, where each group logged different sections of the outcrops. Sedimentary logs from the field are therefore divided into sections (Figure 3.2).

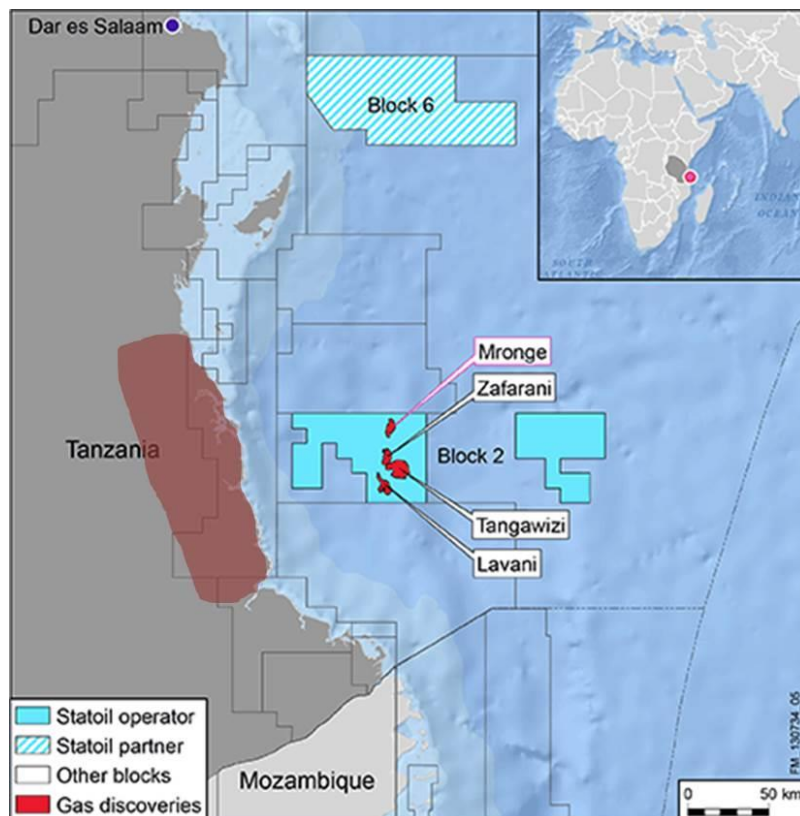
### 3.1.2 Offshore

Since 2007, Statoil has had a production sharing agreement (PSA) for block 2 with TPDC. In 2012 and 2013 Statoil and its partner Exxon Mobile made significant gas discoveries in the Zafarani, Lavani, Tangawizi and Mronge fields in block 2, approximately 80 km off the southern coast of Tanzania (Figure 3.3). Two samples provided by Statoil are briefly discussed in this thesis to look for correlation between onshore and offshore sandstones (Statoil, 2014). The two samples from Block 2 are of Cenomanian age, and are named 2/2/14\_a and 2/2/14\_b, with the sample identification number referring to block2/sample number/year/a or b.





*Figure 3.2: Upper Mitole Mb. outcrop, divided into section 1 and section 2, outlined with red.*



*Figure 3.3: Offshore gas fields outside coastal Tanzania. Mandawa Basin lies directly west from these gas fields.*

### 3.2 Facies description and facies associations

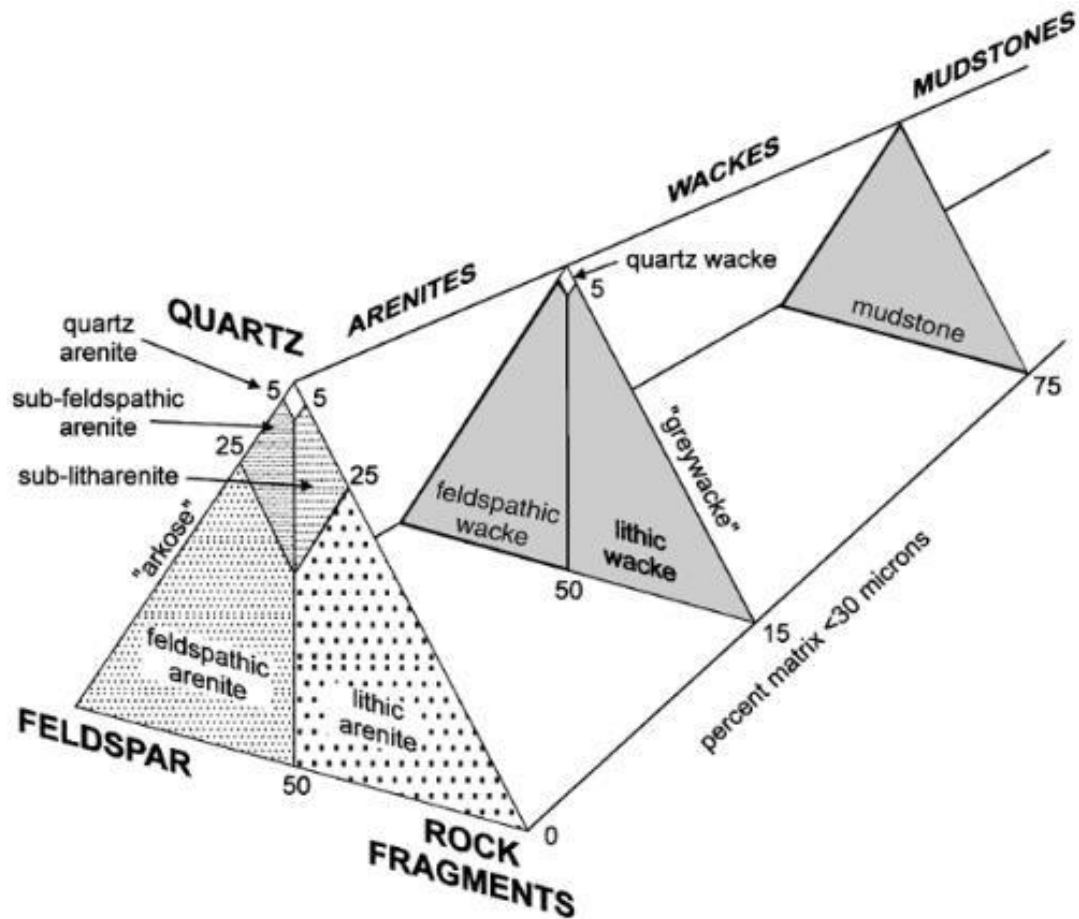
Field observations, sedimentary logs, thin section analysis and photos were used to define sedimentary facies within the sedimentary units. The sedimentary successions are divided into facies and facies associations to interpret the depositional environments of the studied sandstones. Facies are defined as a body of rock, characterized by lithological, physical and biological structures, that is different from the bodies of rock above and below (Dalrymple, 2010). Similar rock intervals are grouped into the same facies. Closely related facies are grouped into facies associations. The facies associations constitute larger bodies of rock that indicate a unique depositional environment.

Facies and facies associations identified in the outcrops were separated from those identified in the cores. This was due to the outcrops being more weathered than the core samples, and a general difference in appearance and depositional environment when comparing the outcrops and cores. The Wentworth grain-size classification (Wentworth, 1922) with various millimeters and phi units was used to classify the sedimentary rocks, ranging from clay to boulder (Table 3.1).

*Table 3.1: The Wentworth grain-size scale for sediments (Wentworth 1992).*

Millimeters	Phi ( $\phi$ ) units	Wentworth size class
> 256	-8	Boulder
16 – 64	-6	Cobble
4 – 16	-4	Pebble
2 – 4	-2	Granule
1 – 2	-1	Very coarse sand
0,50 – 1	0	Coarse sand
0,25 – 0,50	1	Medium sand
0,125 – 0,25	2	Fine sand
0,625 – 0,125	3	Very fine sand
0,0039 – 0,0625	4	Silt
< 0,0039	8	Clay

The sandstones were further classified according to their detrital composition. Arenites are distinguished by wackes by the proportion of detrital matrix. Sandstones containing less than 15% matrix are classified as arenites (Dott Jr, 1964). Sandstones are also classified according to the relative proportion of the three major classes of detrital components; quartz, feldspar and lithic fragments (Figure 3.4).



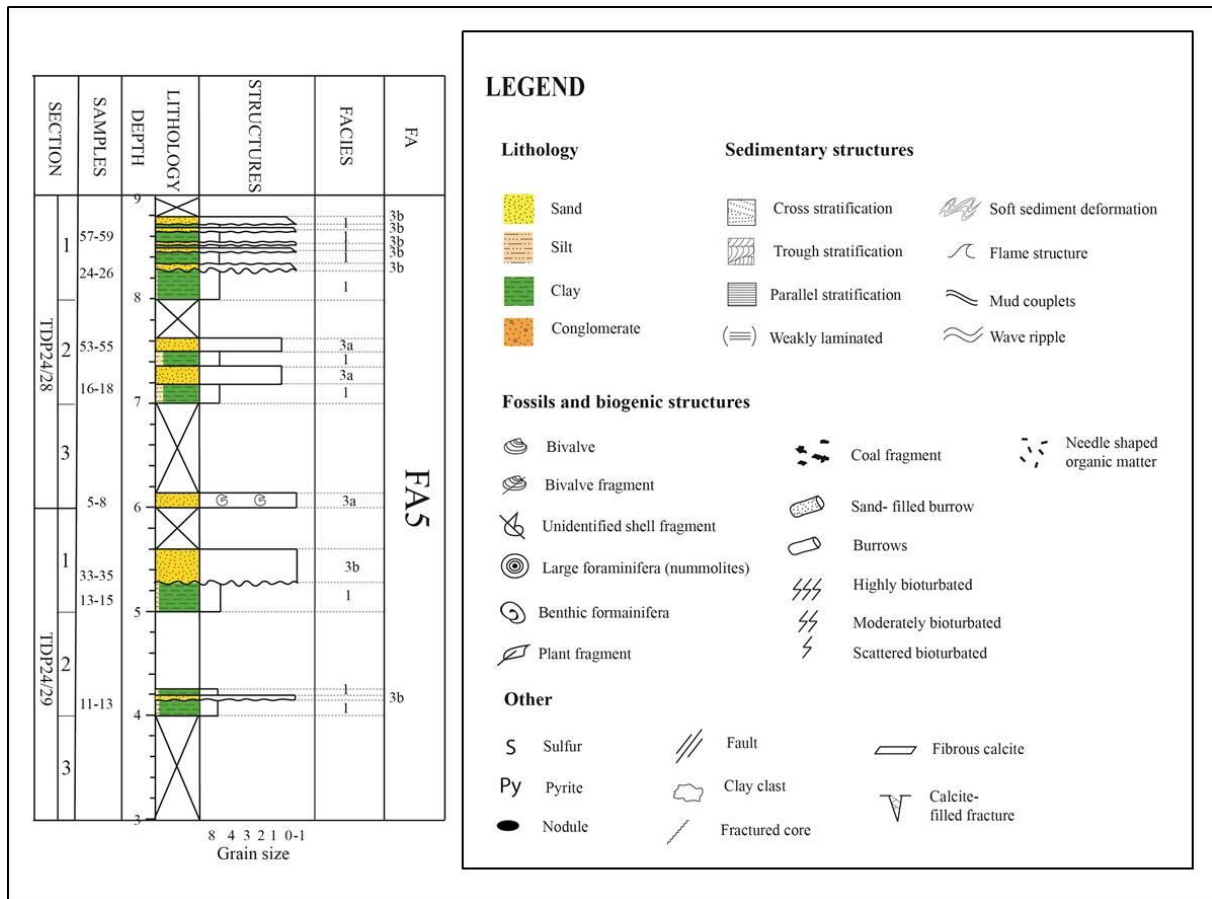
*Figure 3.4: Sand and sandstone classification according to composition. The separation of the three triangles is based on the proportion of the detrital matrix. Arenites: < 15% matrix, Wackes: 15-75 % matrix, and Mudstone: > 75% matrix.*

*Modified by Miall (2003) after Dott (1964).*

### 3.3 Digitalizing of sedimentary logs

All field logs and core logs were digitalized by the author, Kristine Nerbråten and Katrine Fossum in Adobe Illustrator (Figure 3.5). The legend displayed in Figure 3.5 is used in all the sedimentary logs.





**Figure 3.5:** Part of a sedimentary log from cores from well site 24, and the legend used in this thesis on logs from both field outcrops and wells.

### 3.4 Petrographical and mineralogical analysis

Petrological analysis of sandstone samples was performed using optical thin-section observations, scanning electron microscopy (SEM) on selected samples of thin sections and stubs, electron microprobe (EMP) and X-ray diffractometry (XRD) on bulk rock assemblages. Remaining pieces of the studied samples were stored at the Department of Geosciences for future work.

#### 3.4.1 Thin section

A total of 104 samples were selected for thin section preparation from core logging and field work, along with offshore samples from Statoil, Block 2. The samples were impregnated in blue epoxy, glued on glass slides (2,5 cm x 4,5 cm), and polished down to 30µm. 98 samples were prepared by Lars Kirksøther at (IFE Petrosec). Salahaddin Akhavan (UiO) produced 4 thin sections. The thin section analysis comprised detailed observation of 28 samples (Table

3.2). A Nikon Optiphot-Pol petrographic microscope was used to study the thin sections. Optical analysis was conducted to describe rock texture and mineralogy. An attempt to elaborate particular mineral-mineral relations was preformed in order to describe the diagenetic relations. In the optical microscope all thin sections were studied under plane polarized light (ppl) and cross polarized light (xpl) to observe mineral characteristics, such as relief, zoning and twinning.

*Table 3.2: All thin section samples studied in microscope.*

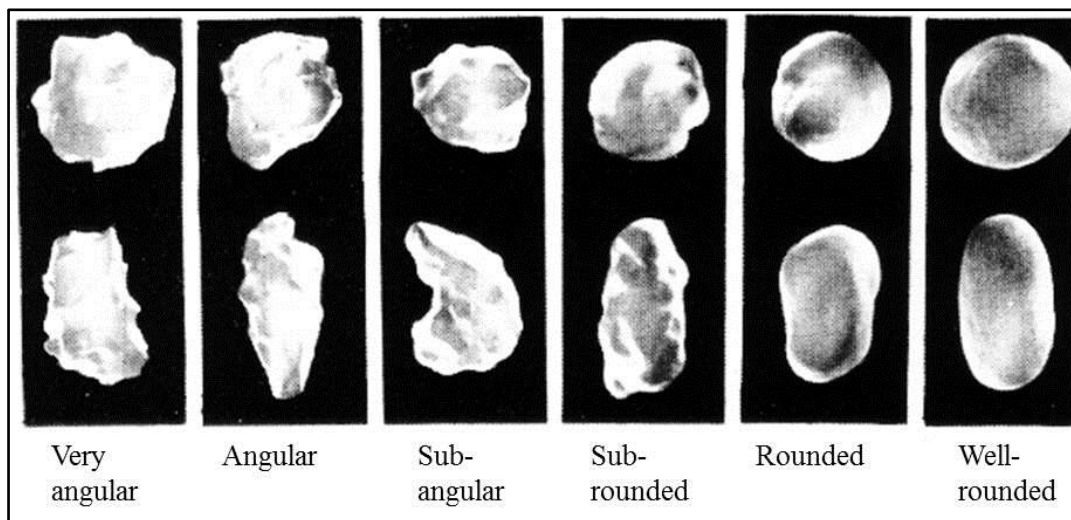
Formation	Sample		Borehole	Sample	
Upper Kipatimu Mb.	MN-2-2-13		24	24/30/1 3-5	
	MN-2-3-13			24/28/3 5-8	
	MN-1-3-13			24/28/1 57-59	
	MN-1-5-13			24/17/3 9-10	
	MN-1-6-13			24/16/3 13-16	
Upper Mitole Mb.	NG-1-1-13				24/13/2 62-64
	NG-1-2-13		21		21/25/1 5-6
	NG-1-5-13				21/24/1 10-12
	NG-2-1-13				21/20/1 88-90
Makonde Fm.	MB-1-4-13				
	MB-1-7-13			21/17/2 56-58	
	MB-2-1-13			21/17/2 82-84	
	MB-2-2-13		Offshore – Cenomanian	2/2/14_a	
	MB-2-4-13		Offshore - Cenomanian	2/2/14_b	

### 3.4.2 Point counting

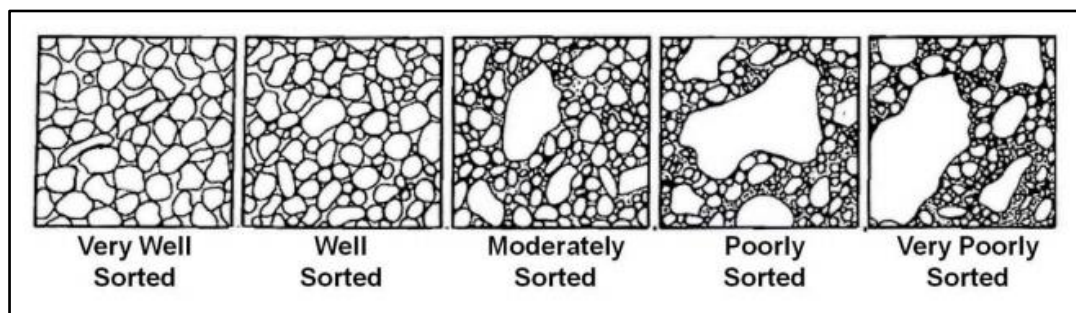
400 point counts were conducted for each slide using a Nikon Labophot-pol petrographic microscope, installed with a Swift Model F automatic point counter with automatic top frame sample holder. All samples counted are presented in Table 3.2. Based on qualitative analysis the mineral groups considered to compose the bulk mineralogy were counted. In addition,

textural features such as sorting, grain size, porosity, permeability, roundness, preservation of grains and grain contacts were noted.

Rounding of detrital grains was determined by the use of Powers' (1953) terminology (Figure 3.6), and the degree of sorting was determined using the classification scheme made by Compton (1962) (Figure 3.7).



*Figure 3.6: Terminology of rounding degree of detrital grains (Powers, 1953).*


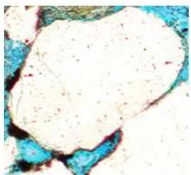
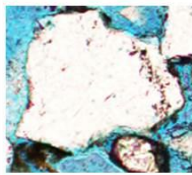
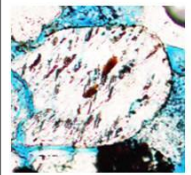
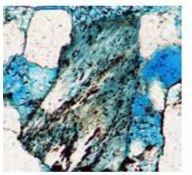
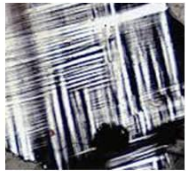
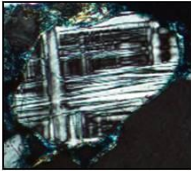
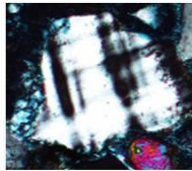
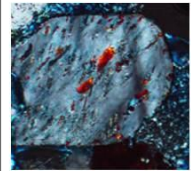
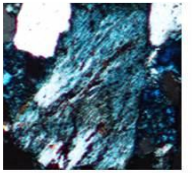


*Figure 3.7: Classification of sorting degree (Compton, 1962).*

Feldspar is classified according to degrees of preservation. Category 1 represents “fresh” feldspar with perfect preservation, category 5 (end member) represents the lowest degree of preservation where the feldspar grain is barely recognizable (Table 3.3).

**Table 3.3:** Preservation of feldspar, ranging from category 1 to 5 are displayed.

Representative examples viewed in both PPL and XPL.

Category	1	2	3	4	5
<b>Description</b>	Fresh, has not been subjected to weathering	Subjected to some weathering. Twins are almost fully preserved	Twins start to look blurry. Grain surface show evidence of etching	Very rough surface. Twins are difficult to recognize	Twins are absent. Only parts of the grain is preserved. Difficult to recognize the mineral.
<b>Example PPL</b>					
<b>Example XPL</b>					

### 3.4.3 XRD - X-ray diffraction analysis

XRD-analysis was carried out at the Department of Geosciences at UiO and is a definitive tool for characterizing mineralogical composition. All core samples were first crushed to rock powder using a “swing-mill”, while field samples were crushed in an agate mortar. The samples were then micronized to rock powder using a *McCrone* micronizer, and subsequently packed into glass sample holders to run in the X-ray diffractometer. The data was collected on a Bruker D8 Advance Diffractometer equipped with a Lynxeye linear PSD detector. It was operated at 40 kV and 40 mA, using Ni-filtered Cu K $\alpha$  radiation.

The use of X-ray diffraction is possible due to the crystal properties of the minerals. Each mineral has a specific unit cell and characteristic distances in the mineral lattice. The spacing of the atomic planes in the mineral lattice is referred to as the *d-spacing*. In addition, each mineral produces specific  $2\theta$  values when x-ray beams are diffracted. The specific signature each mineral produces is then recognized in a diffractogram by using the values of d-spacing,  $2\theta$ -values and intensities (Goldstein et al., 2003). The detection limit of a multi-mixture phase is highly dependent on the mixture itself, and multi-phase mixtures can show many diffraction peaks with some of these peaks overlapping each other. Considering the relatively small step

size ( $0,01^\circ 2\theta$ ), the detection limit is 1-2% for the analyzed samples (Aerts, 2014). Qualitative analysis of bulk material was conducted manually by reading peak positions in the diffractogram, using the d-values in Table 3.4. Further, the analytical software EVA was used with a search and match function to distinguish minor mineral phases in the samples, and semi-quantitative evaluation was conducted by reading the count intensity of target peaks. The counting value for each mineral phase was recalculated to percentage.

**Table 3.4:** Summary of utilized d-values for the qualitative estimation of XRD-bulk samples (Chen, 1977).

<b>Mineral</b>	<b>d- values (Å)</b>
<b>Quartz</b>	4,25
<b>K-feldspar</b>	3,24
<b>Plagioclase</b>	3,19
<b>Mica</b>	10,08
<b>Hornblende</b>	8,4
<b>Mixed layer clay</b>	10-13
<b>Kaolinite</b>	3,58
<b>Chlorite</b>	3,54
<b>Calcite</b>	3,04
<b>Dolomite</b>	2,89
<b>Aragonite</b>	3,39
<b>Pyrite</b>	2,71
<b>Anatase</b>	3,7

Quantitative phase analysis was carried out using the software package Siroquant V2.5. Minerals identified in EVA was entered into a task file in Siroquant, and based on all the peaks from the minerals entered, the software generated a theoretical trace from the minerals using the Rietveld method. Chi-squared values are obtained as a measure of “good fit” between the theoretical and measured traces; errors for the weight percentages of each phase are calculated. In this study chi-values range from 3-5, and are considered as good.

### 3.4.4 SEM – Scanning electron microscope

Key thin sections were examined using a scanning electron microscope (SEM) at UiO. When using the SEM an energy dispersive x-ray spectrum (EDX) is produced, which reflects the elemental composition. The SEM was operated by the author under the supervision of Berit Løken Berg. Thin sections, coated in carbon were used to perform structural and chemical analysis, using backscatter electron imaging (BSE). Comparing elemental composition with known mineral elemental composition results in a precise mineral identification. When identifying the minerals the SEM petrology atlas (Welton, 1984) was used. Surface morphologies of rock samples glued on brass stubs, coated in gold, were studied using secondary electron imaging (SEI). The SEM analysis was conducted on a JEOL JSM-640L, with a LINK INCA Energy 300 (DS) from Oxford instruments.

### 3.4.5 EMP – Electron microprobe analysis

Electron microprobe (EMP) analysis was performed using a Cameca SX100 instrument with an accelerating voltage of 15 kV and a beam current of 10 nA. Peak counting times were 10 s for each element. The EMP was used to try to do quantitative analysis of kaolinite, feldspar, smectite-chlorite coating and dolomite zonation. Detection limits of the analyzed elements are presented in Table 3.5.

The EMP was operated by the author under the supervision of Muriel Marie Laure Embert at UiO.

*Table 3.5: Detection limits for the major element analysis, when analyzing kaolinite, feldspar, smectite-chlorite and dolomite.*

Element	Detection limit (wt%)	Element	Detection limit (wt%)
Si	0,03	Cr	0,05
Al	0,02	Mg	0,03
Ca	0,04	Na	0,03
Fe	0,06	K	0,02
Mn	0,07	Ti	0,03

### **3.4.6 IGV (Intergranular volume)**

IGV is calculated from point counting results, and is an important parameter for measuring compaction in sandstones. IGV varies to a limited degree with sorting and does not vary with particle size. It should be noted that the 2D representation through a thin section gives an apparent variation in grain size. IGV is used to characterize clastic diagenesis and reservoir quality (Ehrenberg, 1995).

$$\text{IGV (\%)} = V_{\text{intergranular porosity}} + V_{\text{intergranular cement}} + V_{\text{detrital matrix}}$$

## 4. Results

During field work in September 2013 three formations from Late Jurassic to Mid Cretaceous age, and two boreholes of Mid Cretaceous age were logged (well site 21 and 24) (Figure 1.1). Sedimentological, petrographical and mineralogical features are presented in the following chapter.

### 4.1 Facies

Based on criteria in chapter 3.2, seven different facies (Table 4.1) were identified from the logged sections in the field outcrops and eight facies (Table 4.2) were identified from the cores. Facies with similar sedimentological appearance are divided into subunits. The following chapters present the main characteristics of the facies.

#### 4.1.1 Field outcrops (Late Jurassic – Mid Cretaceous)

*Table 4.1: Sedimentary facies identified in the field outcrops.*

Facies nr.	Facies	Grain size	Characterization	Figure
<b>A</b>	Silty mudstone	Clay to silt	Silt content: 0-40%. Clay rip-up clasts may occur.	4.1, 4.2, 4.3
<b>B</b>	Massive sandstone	Medium to coarse sand	No apparent bedding, clay rip-up clasts.	4.3, 4.4, 4.5, 4.6
<b>C</b>	Massive sandstone	Fine	No apparent bedding, erosive base, upwards fining.	4.2, 4.3,
<b>D</b>	Conglomerate	Very coarse	Subrounded grains, grain supported conglomerate.	4.3
<b>E1</b>	Laminated siltstone	Silt to very fine sand	Parallel laminated/weakly laminated.	4.2, 4.3, 4.4, 4.6
<b>E2</b>	Laminated/bedded sandstone	Fine to coarse sand	Parallel laminated/bedded. Silt content: 0-20%. Clay rip-up clasts.	4.2, 4.3, 4.4, 4.6
<b>F1</b>	Cross stratified sandy siltstone	Silt to coarse sand	Cross bedded. Occasionally clay rip-up clasts. Often upwards fining sequences.	4.3, 4.2, 4.4, 4.7, 4.8
<b>F2</b>	Cross stratified sandstone	Medium to coarse sand	Highly cross bedded with mud couplets.	4.4, 4.9
<b>G</b>	Trough cross	Fine to very coarse	Trough cross bedded. Occasionally	4.3, 4.10



	stratified sandstone		clay rip-up clasts. Erosive bases.	
--	----------------------	--	------------------------------------	--

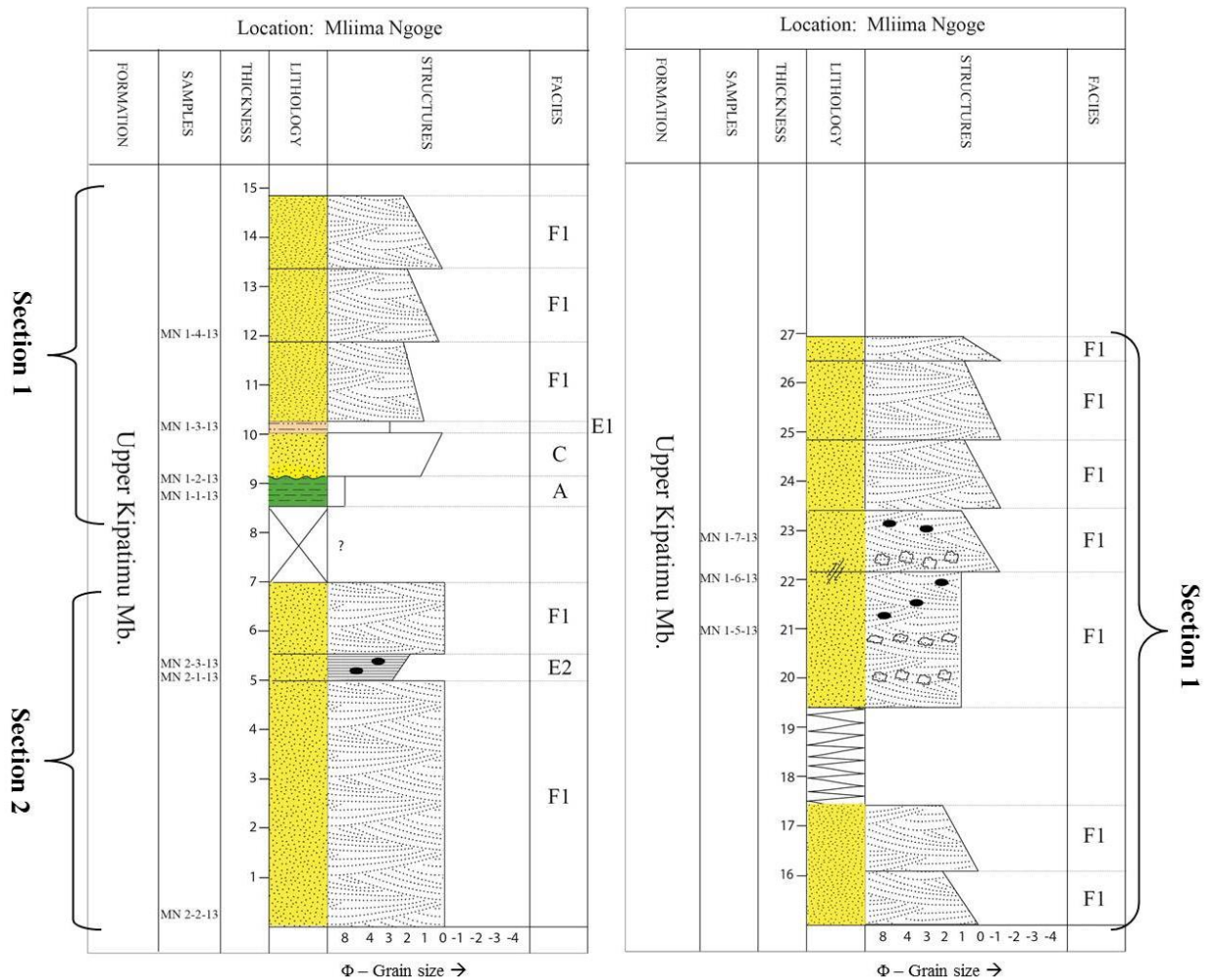
**Facies A. Silty mudstone (Figure 4.1):**

Lack of lamination characterizes this facies and the silt content varies between 0-40% (Table 4.1). The silty mudstone is friable, grey and displays a moderate bioturbation (Figure 4.1).



*Figure 4.1: Friable grey silty mudstone of facies A containing 40% silt, at Mbate (Makonde Fm.).*

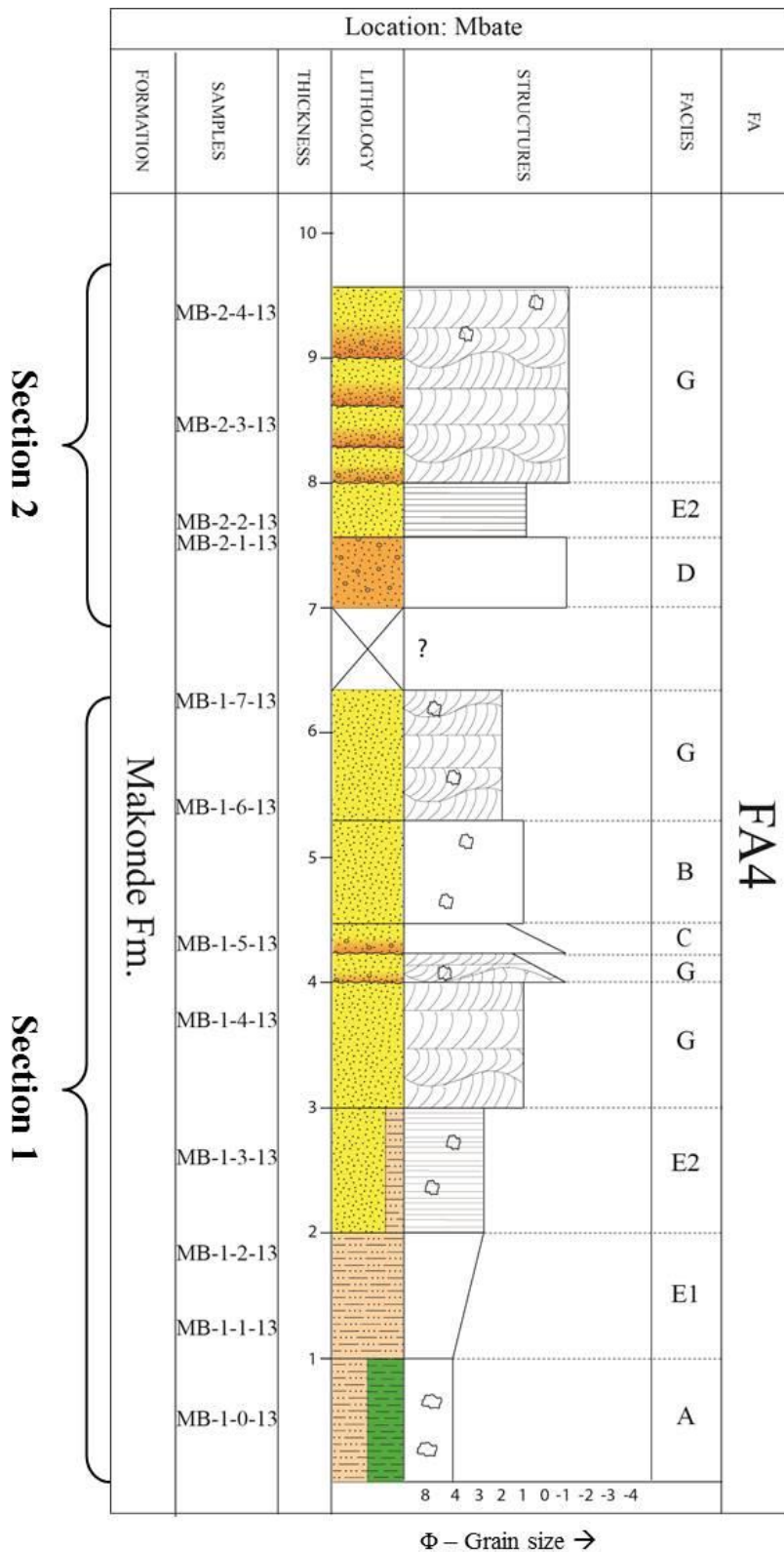
Facies A is present as a 40 cm thick unit in section 1 of Upper Kipatimu Mb. (level 8, 6 – 9, 1 m) (Figure 4.2). The facies is present in section 1 of Makonde Fm. (level 0 – 1 m) as a 1 m thick unit (Figure 4.3). In Makonde Fm. the facies displays a high silt content (40%) and scattered clay rip-up clasts, without any clearcut orientation.



**Figure 4.2:** The Upper Kipatimu Mb. sections, at Mliima Ngoge. Dominated by cross bedded sandstone facies (F1 and F2), with occurrences of mud and siltstone facies (A, E1, E2). Including samples taken in both sections and facies associations (FA 2).

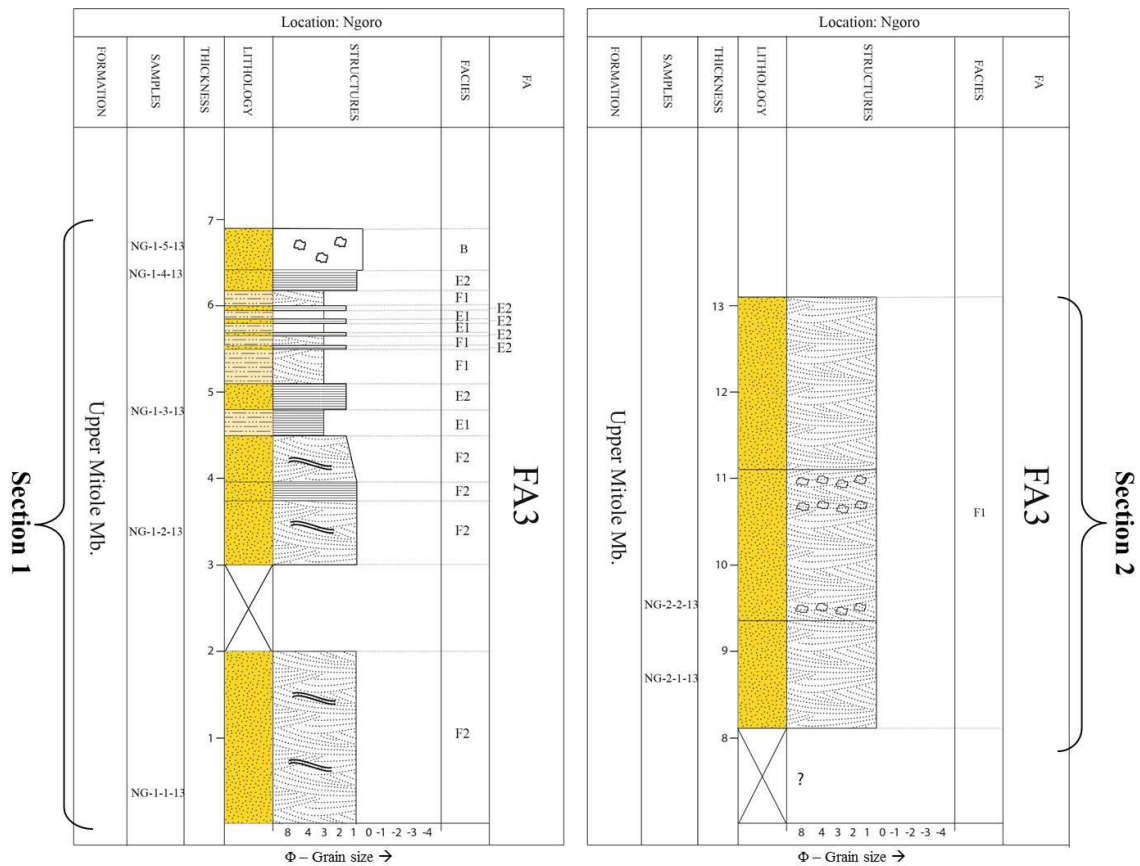
### Facies B. Massive sandstone (Figure 4.5):

Facies B is a medium to coarse massive sandstone, friable and porous with a light yellow/brown color. This facies contains clay rip-up clasts with no preferred orientation (Table 4.2). Facies B is found in section 1 of Upper Mitole Mb. (level 6, 30 – 6, 95) (Figure 4.4) and in section 1 of Makonde Fm. (level 4, 5 – 5, 20 m) (Figure 4.3). The lower boundary is non-erosive in both outcrops.



**Figure 4.3:** The Makonde Fm. sections, at Mbate. Identified facies; A, B, C, D, E1, E2, G and facies association FA4 of the Makonde Fm. is presented. Including samples collected from the sections.





**Figure 4.4:** Logged sections of Upper Mitole Mb, at Ngoro. Both sections are dominated by cross bedded facies F1 and F2. Other facies identified are facies B, E1, E2, F2 and facies association FA3. The collected samples taken from both sections are shown within the samples column.



**Figure 4.5:** Massive sandstone of facies B at Mbate (Makonde Fm.). The facies has a sharp boundary against the underlying trough cross bedded coarse sandstone, which is marked by the red line (facies G).

**Facies C. Massive sandstone:**

Facies C comprises of a upwards fining unit, ranging from very coarse to fine sand, with an erosive lower boundary (Table 4.2). The facies contains rip-up clay clasts without any clearcut orientation. Color is light yellow/brown, similar to facies B (Figure 4.5). This facies is only represented in Makonde Fm. as a 15 cm thick and massive unit (level 4,20 – 4, 40 m) (Figure 4.3).

#### **Facies D. Conglomerate:**

Facies D is composed of very coarse grain-supported conglomerate, with predominantly subrounded grains (Table 4.1). The facies displays a light yellow color, and the composition of the rock is highly porous. Facies D is present in section 2 of Makonde Formation as a 30 cm thick unit (level 7, 0 – 7, 30 m) (Figure 4.3).

#### **Facies E. Laminated silt and sandstone;**

##### **1. Laminated siltstone (Figure 4.6):**

This silt- and sandstone facies varies in grain size from silt to very fine sand (Table 4.1). Facies E1 is characterized by weak lamination in the siltstone units, and strong lamination in the very fine sand units. This facies is present in all three field formations. In Upper Kipatimu Mb. a 20 cm thick unit (level 10 – 10, 2 m) consisting of laminated very fine sand is present in section 2 (Figure 4.2). In section 1 of Upper Mitole Mb. (level 4, 4 – 6 m) facies E1 comprises five units of laminated very fine sand (Figure 4.4). In Makonde Fm. the facies is present as one distinct unit (level 1 – 2 m) in section 1. The facies displays upwards coarsening units ranging from silt to very fine weakly laminated sand (Figure 4.3). The color of facies E1 is light red in Upper Kipatimu Mb., and light yellow in Upper Mitole Mb. and Makonde Fm. (Figure 4.3).

##### **2. Laminated/bedded sandstone (Figure 4.6):**

The sandstone facies E2 consists of fine to coarse sand with plane-parallel laminae or bedding. Silt content varies between 0 – 20% (Table 4.1). This facies is found in all three field formations. In section 2 of Upper Kipatimu Mb. a distinct unit of 30 cm (level 5 – 5, 3 m) displays laminated fine sand (Figure 4.2). In Upper Mitole Mb. six units of bedded fine to coarse sandstone are found in section 1 (level 4, 8 – 6, 3 m), with a thickness of 10 -20 cm (Figure 4.4). In section 1 of Makonde Fm. facies E2 is present as a one meter thick unit (level 2 – 3 m) consisting of very fine sand with lamination (Figure 4.3). Facies E2 contains mud

rip-up clasts, without orientation, in Upper Kipatimu Mb. and Makonde Fm. In Upper Kipatimu Mb. the color is brick red, while in Upper Mitole Mb. and Makonde Fm. the color is light yellow (Figure 4.6). The facies has a sharp contact with the underlying facies in the logged sections.



*Figure 4.6: Laminated sandstone of facies E1 and E2, marked in the figure, at Ngoro (Upper Mitole Mb.). In addition the massive sandstone facies B and cross bedded facies F1 is marked.*

## **Facies F. Cross stratified silt and sandstone;**

### **1. Cross stratified siltstone and sandstone (Figure 4.7):**

Facies F1 consists of cross stratified sandy siltstone, comprising 20 cm – 5 m thick units. The facies displays grain sizes that vary between very fine to coarse sand (Table 4.1). Facies boundaries are erosive with occurrences of clay clasts along the base. Facies F1 is present in both sections of Upper Kipatimu Mb. (Figure 4.2 and 4.7), displaying several upwards fining units with grain sizes varying from very fine to very coarse sand. Foresets are tangential and the color is brick red. In Upper Mitole Mb. the facies is present in both sections (Figure 4.4), consisting of units with thickness varying from 10 – 30 cm, the color of these units are light yellow.





**Figure 4.7:** *Cross stratified coarse sandstone of facies F1, planar foresets, brick red color. Upper Kipatimu Mb. at Mlia Ngoge.*

The units of Upper Mitole Mb. consist of fine sand within section 1, and coarse sand within section 2 (Figure 4.8). Facies F2 display cross bedding with sigmoidal foresets and double drapes in section 2 .



**Figure 4.8:** *Cross bedded coarse sandstone of facies F1, yellow color, sigmoidal foresets, and double drapes. Section 2 of Upper Mitole Mb. at Ngoro.*

## 2. Cross stratified sandstone (Figure 4.9):

This facies dominates section 1 of Upper Mitole Mb. (level 0 – 4,5 m) (Figure 4.4). Facies F2 comprises grain sizes that vary from medium to coarse sand. This facies is highly cross bedded, with several double mud coplets (Figure 4.9 B) (Table 4.1). Foresets are sigmoidal and the thickness of the foreset beds are variable (Figure 4.9 A).



**Figure 4.9:** A) Cross stratified sandstone of facies F2, light yellow color. Section 1 of Upper Mitole Mb. at Ngoro. B) Double mud coplets within facies F2. Section 1 of Upper Mitole Mb. at Ngoro.

## Facies G. Trough cross stratified sandstone (Figure 4.10):

Facies G is characterized by highly trough cross bedded porous sandstone, with occasional clay rip up clasts, and erosive boundaries towards the underlying facies (Figure 4.10) (Table 4.1). This facies displays several upwards fining sequences. The basal layer of these upwards fining sequences consist of coarse grained supported conglomerate, which grades over to fine sandstone. Facies G is identified in both sections of Makonde Fm. (Figure 4.3).





*Figure 4.10: Facies G, porous trough cross stratified coarse sandstone, yellow/brown color, at Mbate (Makonde Fm.).*

#### 4.1.2 Facies description – cores from well sites 24 and 21

*Table 4.2: Sedimentary facies identified in the studied cores.*

Facies nr.	Facies	Grain size	Characterization	Figure
1	Claystone	Clay	No apparent lamination. Varying degree of bioturbation.	4.11, 4.12, 4.13
2	Sandy siltstone	Silt to fine sand	Varying degree of bioturbation. Some shell and coal fragments.	4.12, 4.13
3a	Moderately sorted sandstone	Very fine to coarse	Moderately sorted, varying silt content between 0 – 40%.	4.12, 4.13, 4.14
3b	Sandstone	Fine to very coarse	Occasionally erosive beds. Clay rip-up clasts. Upwards fining sequences.	4.12, 4.13, 4.15
4	Laminated clay- and siltstone	Clay to very fine sand	Weakly parallel laminated/ parallel laminated. Scattered bioturbation.	4.12, 4.13, 4.16
5	Inverse graded siltstone	Silt to very fine sand	Upwards coarsening sequences.	4.12, 4.17
6	Soft sediment deformed silt- and claystone	Very fine to medium sand	Soft sediment deformation and water escape structures. Some coal and shell fragments.	4.12, 4.13, 4.18
7	Cross stratified	Very fine to	Cross stratified. Upwards fining	

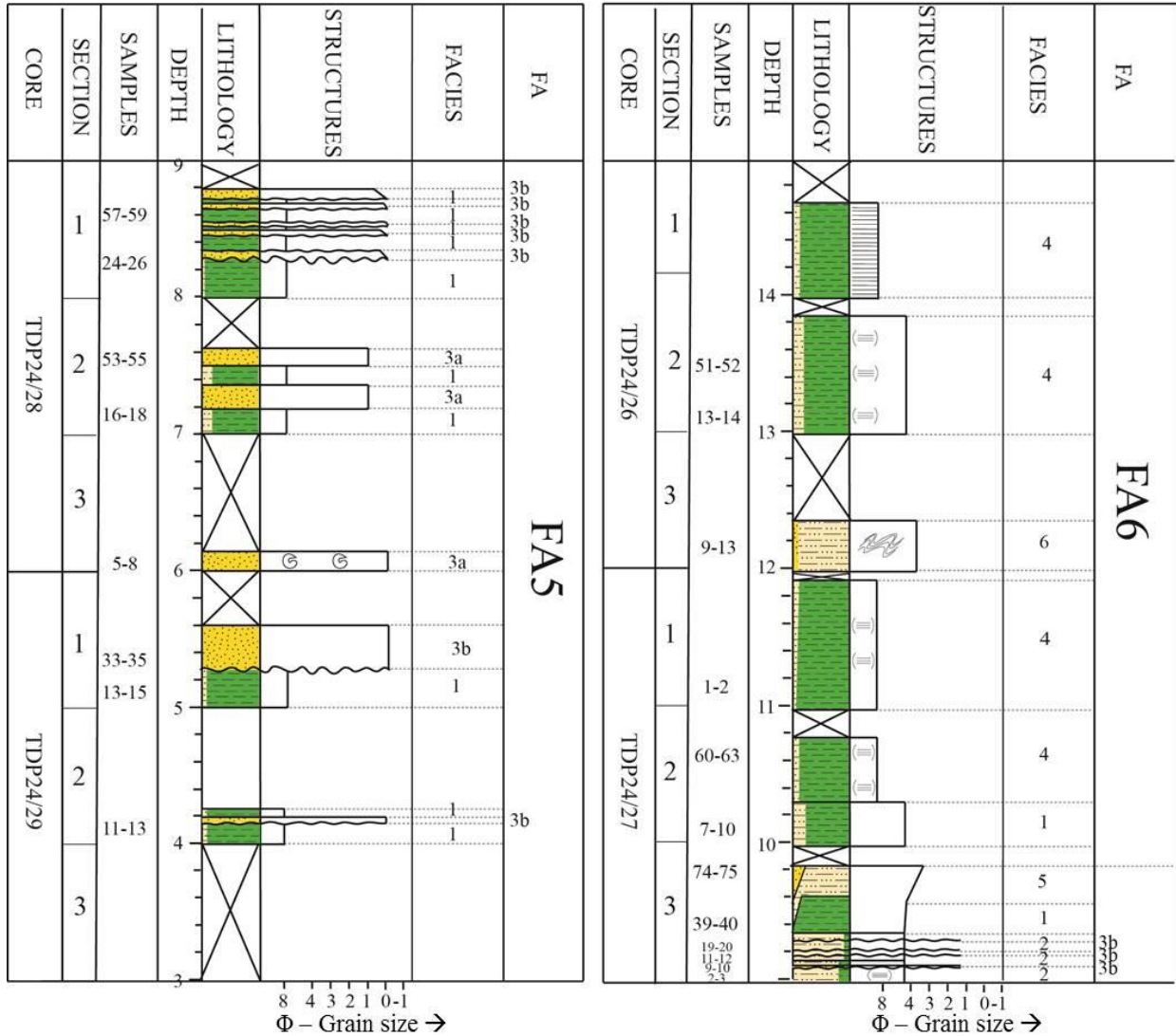
	sandstone	coarse sand	sequences.	
8	Shell rich siltstone	Silt to very fine sand	Abundant shell and shell fragments	

**F1. Claystone (Figure 4.11):**

F1 is characterized by structureless claystone, with a grey to greenish black color. A few intervals are observed having weak lamination (Figure 4.11 A). The silt content varies from 0% up to 40%, and bioturbation varies from sparsely to moderate. In cores from well site 24 (Albian – Turonian) F1 dominates an interval of 22 m (level 31 – 53 m) (Appendix A), in addition the facies appears as small intervals (10-70 cm in thickness) throughout the core (Figure 4.12). In cores from well site 21 (Cenomanian – Coniacian) this clay facies dominates 22 m of the core (level 29-51 m) (Appendix B), further the facies appears frequently as small units (10 – 60 cm in thickness) throughout the core (Figure 4.11 B and 4.13).



**Figure 4.11:** A) Greenish/grey slightly laminated claystone of facies F1 (core 16, well site 24). B) Dark grey-black structureless claystone of facies F1 (core 15, well site 21).

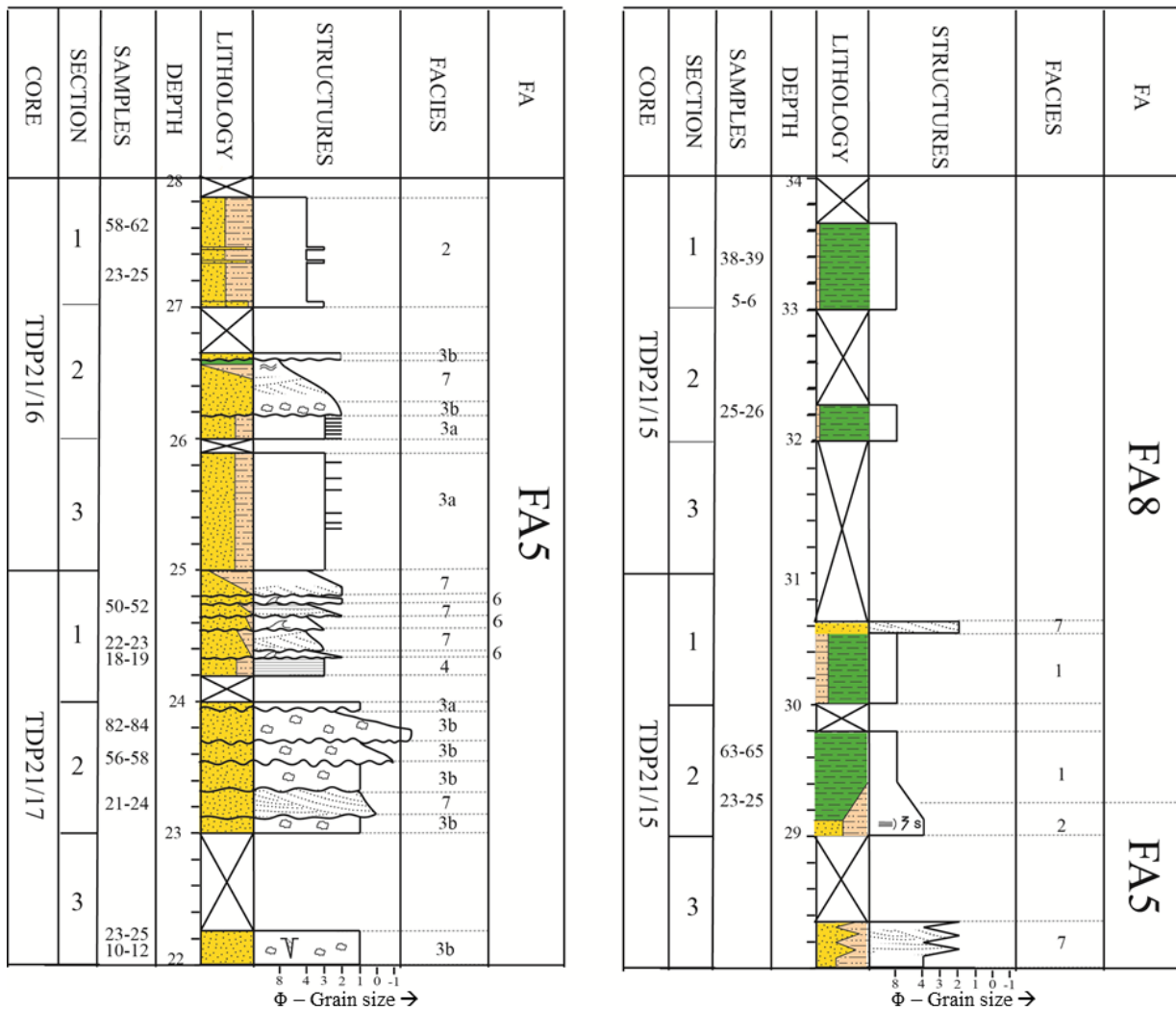


**Figure 4.12:** Core 29 – 27 (level 3 – 15 m) from well site 24. Displaying several facies; 1, 2, 3a, 3b, 4, 5, 6 within the sand dominated facies association FA5 and the silt dominated facies association FA6. Samples collected are marked in the samples column.

## F2. Sandy Siltstone:

Facies F2 consists of greenish grey sandy siltstone, with occasional shell and coal fragments. The clay and sand content varies between 0 – 40%. Facies 2 often displays high to moderate bioturbation. Bioturbation is absent in units containing higher amounts of clay. This facies dominates the upper part of cores from well site 24, comprising a 14 m thick interval (level 60 – 84 m), in addition F2 occurs as small intervals (10 – 80 cm thick) throughout the core (Figure 4.12) (Appendix A). In cores from well site 21, F2 frequently appears as 5 – 70 cm thick units (Figure 4.13) (Appendix B).





**Figure 4.13:** Example from core 17-15 (level 22-31 m), well site 21. Facies identified are F1, 2, 3a, 3b, 4, 6, 7 within facies associations FA5 and FA6. Samples collected are marked in the sample-column.

### F3. Moderately sorted sandstone:

**F3a. (Figure 4.14):** This facies comprises very fine to coarse sandstone with varying silt content from 0% up to 40%. Facies 3a is characterized by light white/grey consolidated sand (Figure 4.14 A and B), and appears to often be interbedded with claystone facies 1 (Figure 4.12). In general bioturbation is absent, but moderate bioturbation is observed in some units. Unidentified fossil are observed. In cores from well site 24 this facies is frequent and present throughout the cores as small intervals (2 – 60 cm thick) (Figure 4.14 A) (Appendix A), cross lamination occur. In cores from well site 21 this facies appears frequently throughout the core,

as small intervals of 2 cm – 90 cm in thickness (Figure 4.14 B) (Appendix B). Some units are parallel laminated and display vertical bioturbation, and coal fragments are observed.



**Figure 4.14:** A) Moderately sorted sandstone of F3a, interbedded within clay of F1 (core 17, well site 24) B) Sandstone facies 3a, moderately sorted, light grey, consolidated (core 24, well site 21).

### **F3b. Normal graded sandstone (Figure 4.15):**

F3b comprises fine to very coarse white/grey sand. The facies characterized by clay rip-up clasts and upwards fining sequences often found with erosive bases. This facies is displayed as eight relatively small units (2 – 20 cm thick) in the lower part of the cores from well site 24 (level 8 – 9, 5 m) (Figure 4.12). F3b displays some cross lamination. In cores from well site 21, F3b is identified in level 16 – 27 m as intervals of 10 – 30 cm in thickness (Figure 4.13). Shell fragments are observed within the facies (Figure 4.15).

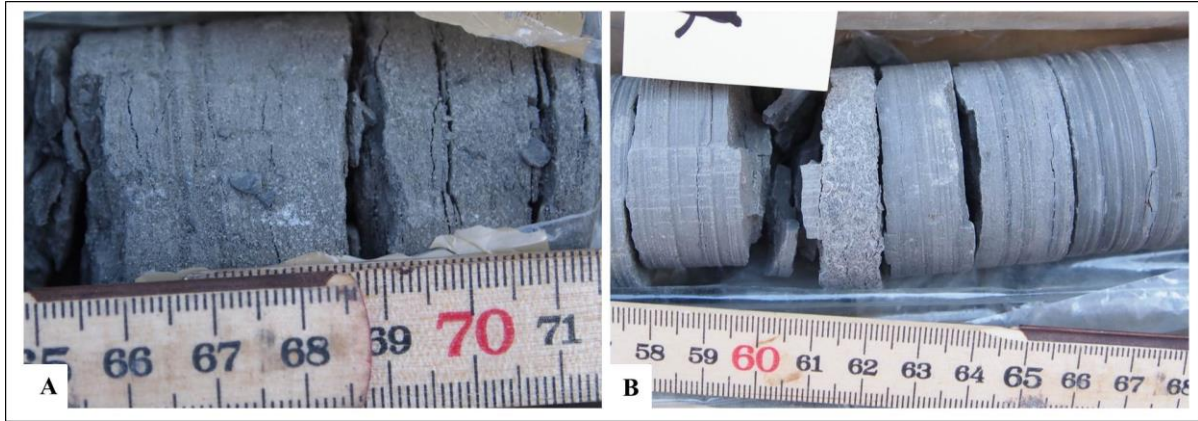


*Figure 4.15: Normal graded sandstone of facies F3b, containing rounded clay rip-up clasts and small white shell fragments (core 17, well site 21).*

#### **F4. Laminated clay- and siltstone (Figure 4.16):**

This facies is characterized by parallel laminated clay- and siltstone. The clay dominated units display varying silt content between 0 – 15% (Figure 4.16 A). Units with high silt content (> 40%) are classified as siltstones (Figure 4.16 B). The silty units contain scattered bioturbation. In cores from well site 24, units of 20 – 85 cm in thickness frequently occur (Figure 4.12) (Appendix A). Calcite veins parallel to the lamination is observed. In cores from well site 21 this facies is present as two distinct units. The first unit is 2,5 m thick (level 42 – 44, 5 m), and consists of weakly laminated homogenous clay. The second unit is 70 cm thick (level 59 – 59,7 m) displaying parallel lamination, where an alternation between consolidated dark clay and weakly consolidated light grey clay is observed (Appendix B).





**Figure 4.16:** A) Laminated clay of facies 4, dark grey color (core 25, well site 24). B) Laminated siltstone of facies 4, light grey (core 23, well site 24).

**F5. Inverse graded siltstone (Figure 4.17):**

F5 is characterized by upwards coarsening sequences, grading from clay to very fine sand (Figure 4.17). Silt content varies from 0% up to 50%. This facies is present in cores from well site 24 at level 53 – 57 m, consisting of units 10 – 70 cm in thickness (Figure 4.12) (Appendix A).

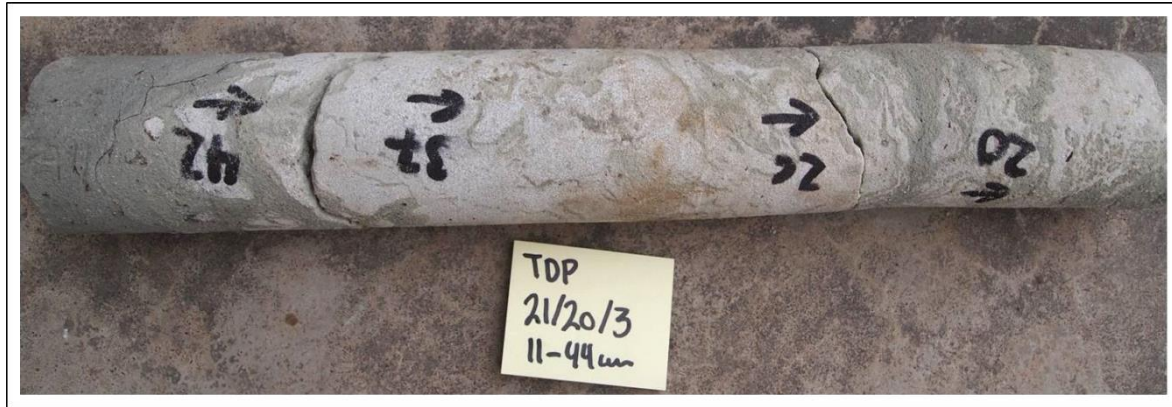


**Figure 4.17:** Inverse graded siltstone of facies 5 (borehole 24, section 13). Red arrow shows stratigraphic right way up.

**F6. Soft sediment deformed silt-and siltstone (Figure 4.18):**

This facies comprises very fine to medium sized sandstone, characterized by soft sediment deformation and water escape structures. Some coal and shell fragments are observed. Appears as one distinct unit in borehole 24 (20 cm thick) at 12 m depth (Figure 4.12)

(Appendix A). In borehole 21 facies F6 is the dominant facies in the lower part (3 – 19 m) of the core, thickness varies between 5 – 100 cm (Figure 4.13) (Appendix B). The facies displays variation between greenish grey colored clay and whitish grey sand (Figure 4.18).



*Figure 4.18: Facies 6, soft sediment deformed sandstone (section 20, borehole 21). Greenish grey clay displays soft sediment structure within whitish grey sandstone.*

#### **F7. Cross stratified sandstone:**

F7 is characterized by light grey cross laminated very fine to medium sand. Silt content varies from 0% up to 20%. Occasionally erosive bases and upwards fining sequences are observed. This facies is present in cores from well site 21 (level 23 – 31 m) as units of 5-30 cm in thickness (Figure 4.13) (Appendix B).

#### **F8. Coquina siltstone:**

This facies is comprised of silt to very fine sand, characterized by abundant shells and shell fragments. The facies classifies as a coquina layer. F8 appears as one distinct unit at the uppermost part of core 1 (level 72, 3 – 72, 8 m), well site 21 (Appendix B).

## **4.2 Facies associations and sedimentological description**

Based on facies descriptions (Table 1.2 and 2.2) three facies associations from field outcrops and four facies associations from the cores were identified. The facies associations are numbered FA1-8. Definition and identification of the facies associations were done in collaboration with Kristine Nerbråten (master thesis UiO, 2014). FA1 is not presented in this thesis, as it represents an older stratigraphic unit, but interpretations of the FA1 can be found



in the thesis of Nerbråten (2014). Sedimentological description and facies associations are presented in the following chapters.

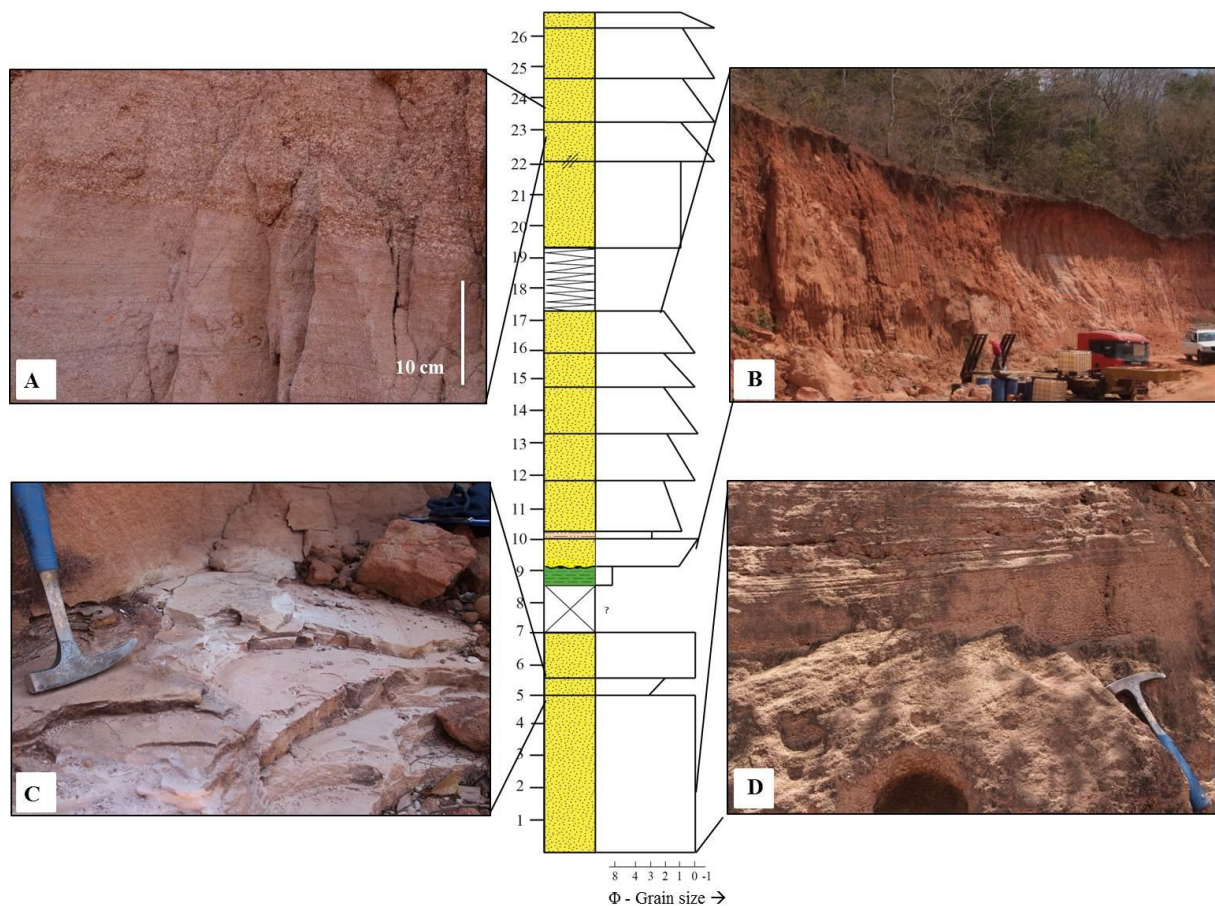
#### 4.2.1 Facies associations – outcrops

*Table 4.3: Facies associations of the studied field outcrops, based on facies presented in Table 4.1*

<b>Facies association</b>	<b>Facies</b>	<b>Figure</b>
<b>FA2</b>	A,C,E1,E2,F1,F2	4.2
<b>FA3</b>	B,E1,E2,G1,G2	4.4
<b>FA4</b>	A,B,C,D,E1,E2,H	4.3

#### **FA2 - Upper Kipatimu Mb. (Kimmeridgian – Tithonian) (Figure 4.19)**

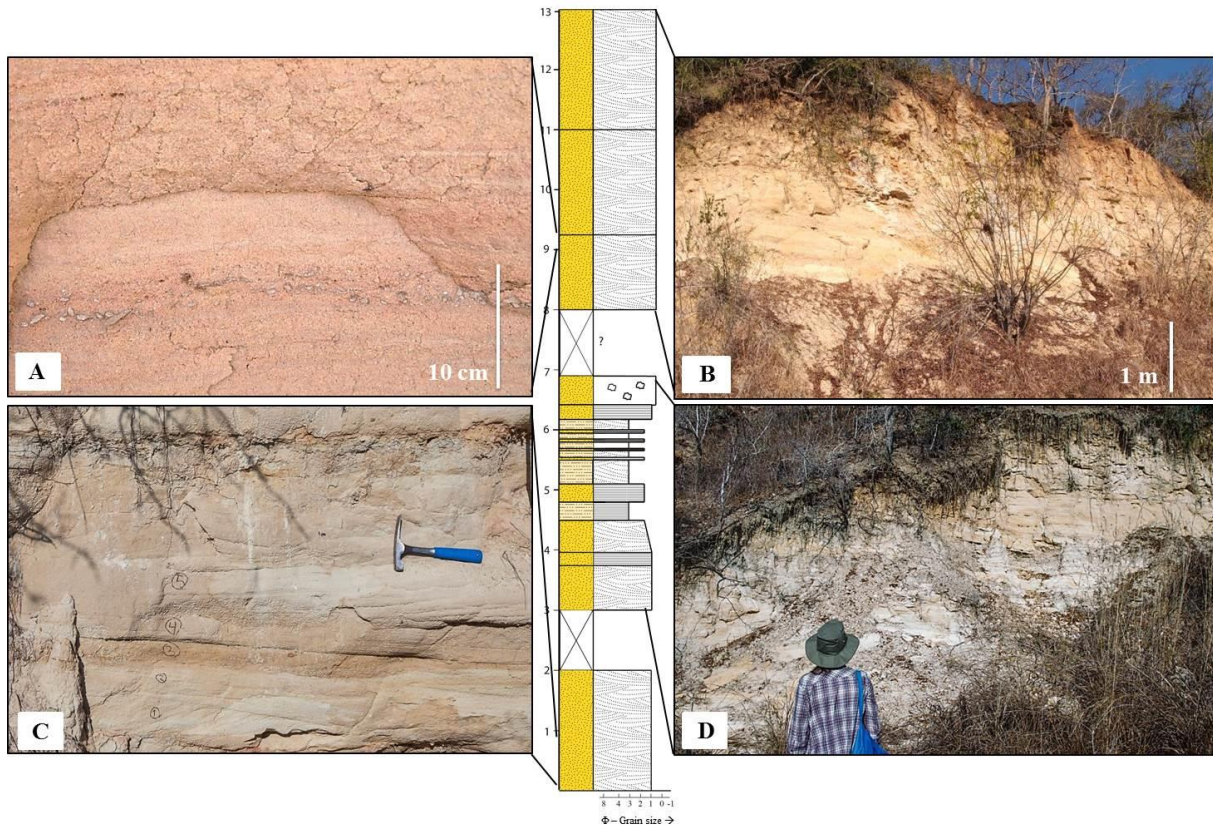
This sandstone formation dominates the northern part of the Mandawa Basin (Figure 2.3). The two logged sections of Upper Kipatimu Mb. measures 23 m at Mliima Ngoge, and the makes up the FA2 facies association (Figure 4.2). A disruption in section 1 (at level 17,2 m) is caused by a fault of unknown displacement. Section 2 was found 289 m westward of section 1. It lies stratigraphically beneath section 1 and is thus put as the first section in the log (Figure 4.2). The FA2 facies association is dominated by the cross bedded coarse sandstone of facies F1 (Table 4.3) (Figure 4.19). Facies F1 displays several upwards fining sequences in section 2 (level 10, 2 – 27 m). Clay and siltstone facies (A, E1, E2) are present (levels; 5 – 5,3 m, 8, 3 – 9, 2 m and 10 – 10, 2 m) as small units (20 – 30 cm thick) in between the cross bedded sandstone. The upper unit of section 1 (level 19, 1 – 27 m) displays the coarsest grain size fraction, consisting of very coarse grained sandstone. The FA2 facies association is slightly upwards coarsening, with mud and siltstone facies present in the lower part of the association (Figure 4.19).



**Figure 4.19:** Facies association FA2, Upper Kipatimu Mb., at Mlima Ngoge. FA2 is presented with the simplified log of Upper Kipatimu Mb., in the middle part of the figure. A) Facies F1, cross bedded sandstone. B) Overview of the location at Mlima Ngoge, consisting of cross bedded sandstone facies F1. C) Parallel laminated sandstone of facies E2. D) Cross bedded sandstone facies F1, lower most part of the log.

### **FA3 Upper Mitole Mb. (Kimmeridgian – Berriasian) (Figure 4.20)**

Upper Mitole Mb. sandstone dominates the western part of Mandawa Basin (Figure 2.3). Two sections of the sandstone member were logged at the Ngoro location, measuring 12 m (Figure 4.4). These two sections are interpreted to be the FA3 facies association (Figure 4.20). The lower part of section 1 (level 0 – 4,3 m) is dominated by cross bedded coarse sandstone with double mud drapes (facies F2) (Figure 4.20). The upper part of section 1 (level 4,3 – 6,8 m) consists of alternating beds of very fine cross bedded sandstone (facies F1 and F2) and bedded coarse sandstone (facies E1 and E2). Section 2 (level 8 – 13 m) is dominated by cross bedded coarse sandstone with mud rip-up clasts (facies F1) (Figure 4.20). The FA3 facies association is generally upwards coarsening from very fine to very coarse sand, and upwards thickening.



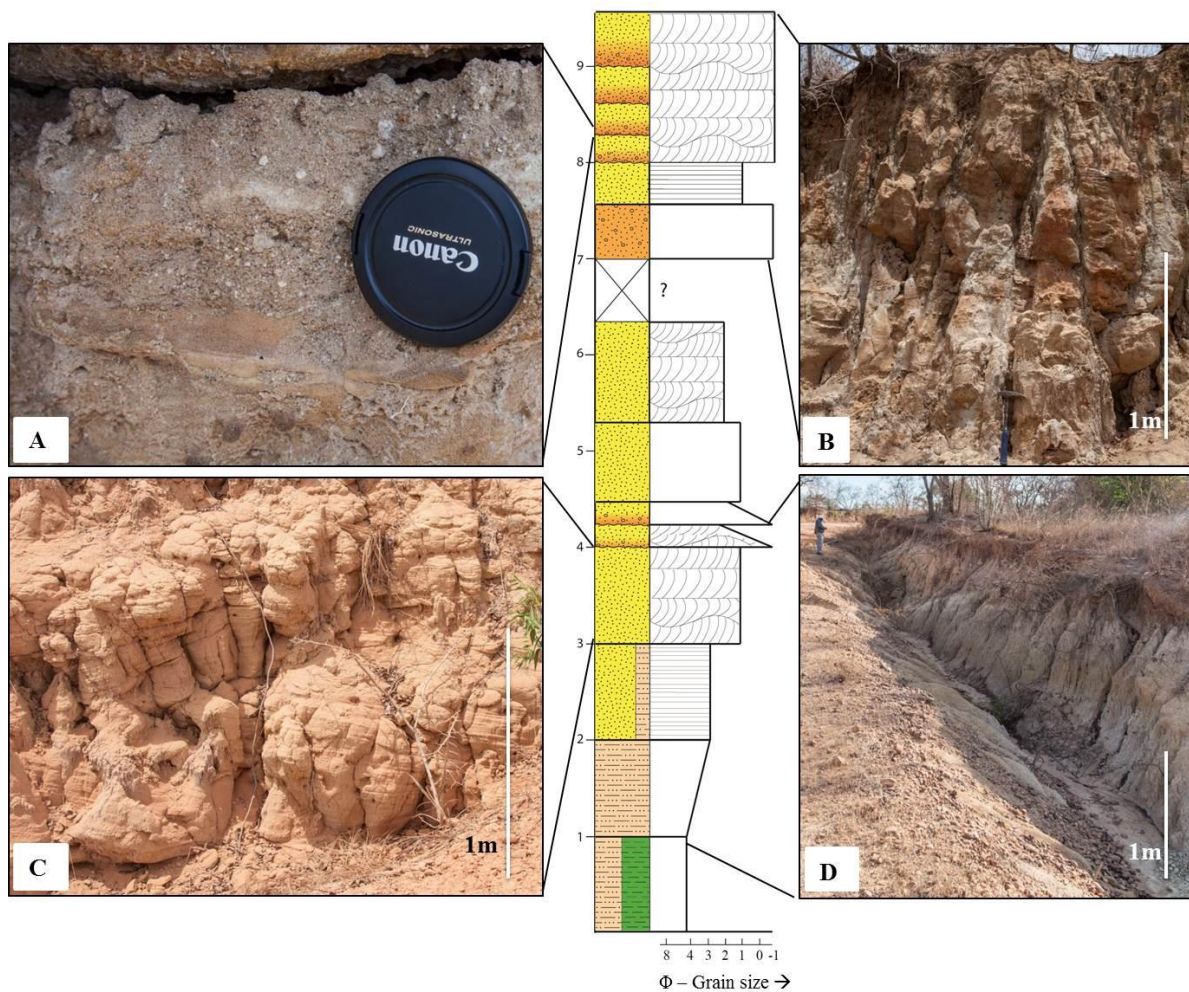
**Figure 4.20:** Overview of FA3, Upper Mitole Mb., at Mlima Ngoge. Middle part of the figure displays the simplified log of Upper Mitole Mb. A) Mud clasts band in cross bedded coarse sandstone of facies F1. B) Overview of section 2 (level 8 – 13 m). Consisting of cross bedded sandstone facies F1. C) Cross bedded sandstone facies F2. D) Overview of section 1 (level 3 -7,2m), consisting of laminated sandstone facies E1 and E2, interbedded within facies F1.

#### **FA4 – Makonde Fm. (Aptian – Albian) (Figure 4.21)**

Makonde Fm. dominates the central part of the basin (Figure 2.3). Two sections of the Makonde Fm. were logged at Mbate (Figure 1.1). The thickness between the two logged sections is unknown, but they are located approximately 1 km apart. The two sections are merged together, measuring 9 m in total thickness, and represent the FA4 facies association (Figure 4.3). The first two meters of section 1 (level 0 – 2 m) consist of clay and silt (facies A and E1). The rest of section 1 (level 2 – 6,3 m) consist of trough cross bedded, parallel laminated, and massive sandstone facies (B, C, D, E2, H). Section 2 (level 7 – 9,3 m) is dominated by coarse sandstone and pebbly conglomerates (facies D, E2, G). In general the FA4 association is upwards coarsening from silt and clays, to very coarse conglomerates. FA4



is dominated by trough cross bedded sandstone, containing upwards fining sequences with erosive bases (Figure 4.21).



**Figure 4.21:** Facies association FA3, Makonde Fm., at Mbate. Middle part of the figure displays the simplified log. A) Basal layer of conglomerate within facies G (level 8, 20 – 30 m). B) Overview of second logged section of Makonde Fm. consisting of conglomerate, laminated sandstone and trough cross bedded sandstone (facies D, E2 and G). C) Trough cross bedded sandstone of facies G (level 3 – 4, 2 m). D) Section 1 of Makonde Fm. outcrop (level 1 – 4, 3 m).

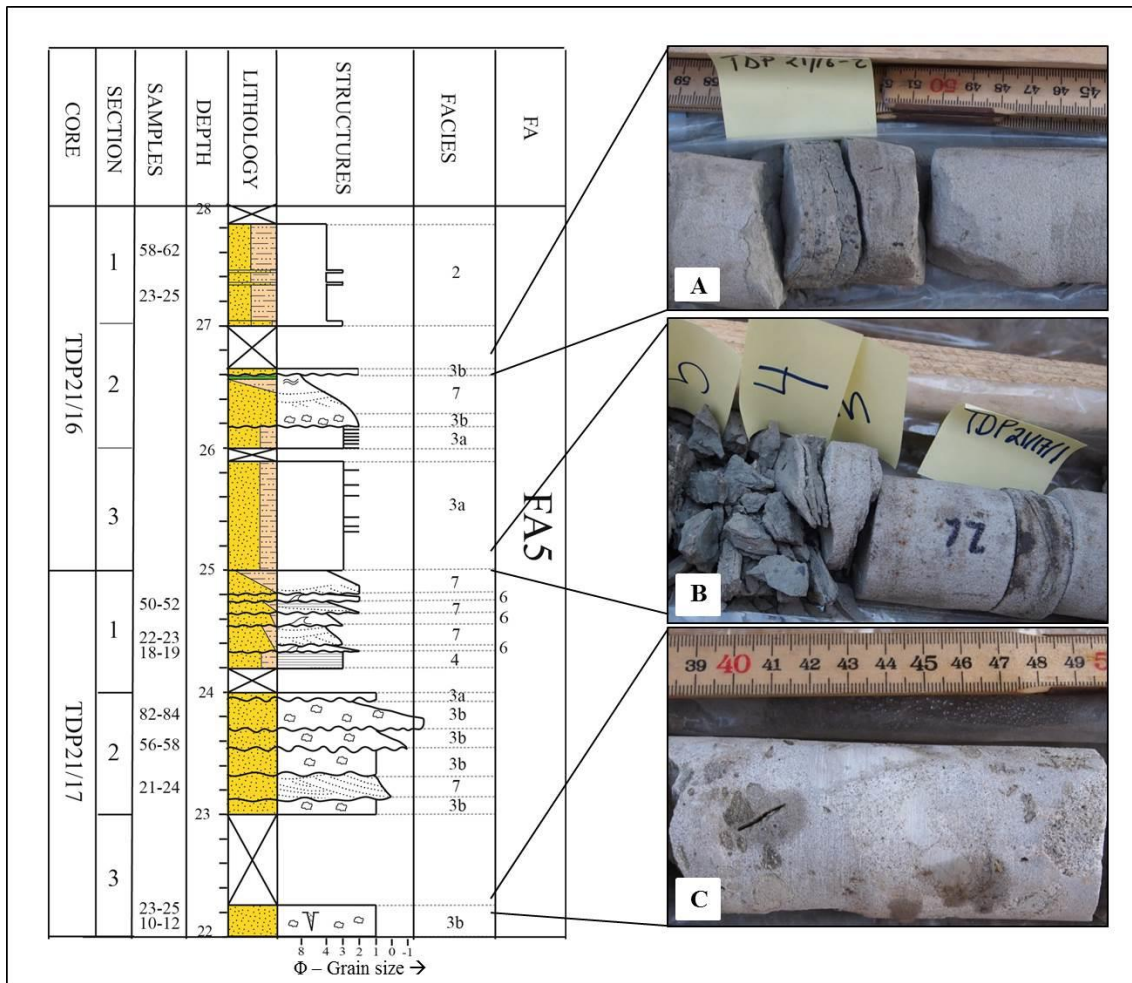
## 4.2.2 Facies associations – cores

*Table 4.4: Facies associations of the studied cores, based on facies presented in Table 4.2.*

<b>Facies association</b>	<b>Facies</b>	<b>Figure</b>
<b>FA5</b>	1, 2, 3a, 3b, 4, 5, 6, 7, 8	4.22
<b>FA6</b>	1, 2, 3a, 4, 6	4.23
<b>FA7</b>	1, 2, 3a, 3b, 4, 5, 7, 8, 9	4.24
<b>FA8</b>	1, 4, 7	-

### **FA5: Sedimentological description**

This silt and sandstone facies association is identified in cores from well site 24 and 21. FA5 is dominated by medium to very coarse grained grey sandstone of facies F3a, F3b and F7 (Figure 4.22), interbedded with greenish grey silt and clay (facies 1, 4, 6, 7) (Table 4.4). In cores from well site 24 the first ten meters (level 0-10 m) are dominated by FA5 (Appendix A). The 8 first meters (level 0-8 m) of FA5 is dominated by coarse sandstone intervals of 10 – 30 cm in thickness, interbedded with clay facies FA1. The uppermost part (level 8-10 m) of FA5 is dominated by minor sandstone beds (2-5 cm) that have sharp, irregular basal contacts, interbedded with claystone and siltstone facies F1 and F2. In cores from well site 21 FA5 is the lowermost facies association (level 0 – 29,1 m) (Appendix B). The first 19 m (level 0-19 m) is dominated by light grey silt and sandstone soft sediment deformed sandstone of facies F6, and sandstone facies F3a and 3b. The uppermost part of FA5 (level 19 – 29,1 m) is dominated by sandstone facies F3a and F3b, displaying massive- to normal graded sandstone beds (10 – 40 cm in thickness) with erosive basal layers, consisting of basal matrix supported conglomerates and mud-rip up clasts.

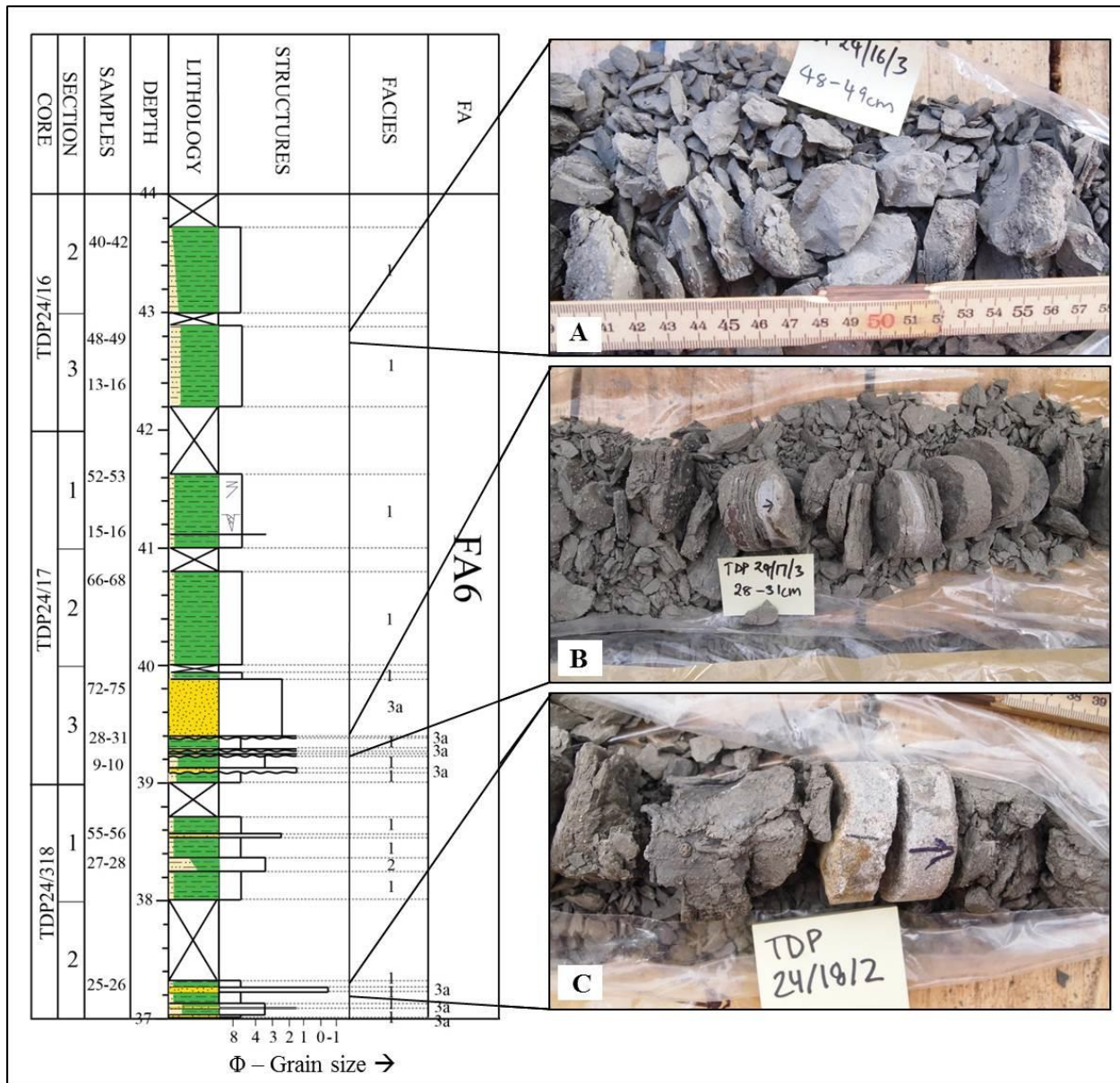


**Figure 4.22:** FA5 displayed by cores 16 and 17, well site 21. A) Normal graded grey sandstone of facies 3b. B) Cross stratified fine grained grey sandstone of facies 7, grading in to siltstone. C) Normal graded medium grained grey sandstone of facies 3b, containing clay rip-up clasts.

### FA6 – Sedimentological description

This clay and siltstones association is dominated by dark grey clay facies F1 and F2, interbedded with homogenous sandstone units (2 – 6 cm in thickness) of facies F3a (Figure 4.23) (Table 4.4). FA6 is present in core 24, where it constitutes 35,3 m of the core, making FA6 the dominant facies association. The underlying facies association FA5 is observed to have a gradational transition to FA6 (Appendix A). The first 30 m of FA6 (level 10-40 m) is dominated by facies F1 and interbedded with facies F2, F4, F3a. The last 13 m of FA5 exclusively consists of F1. Based on these observations FA5 is upwards fining in grain size, and upwards thickening with respect to the dominant facies F1.

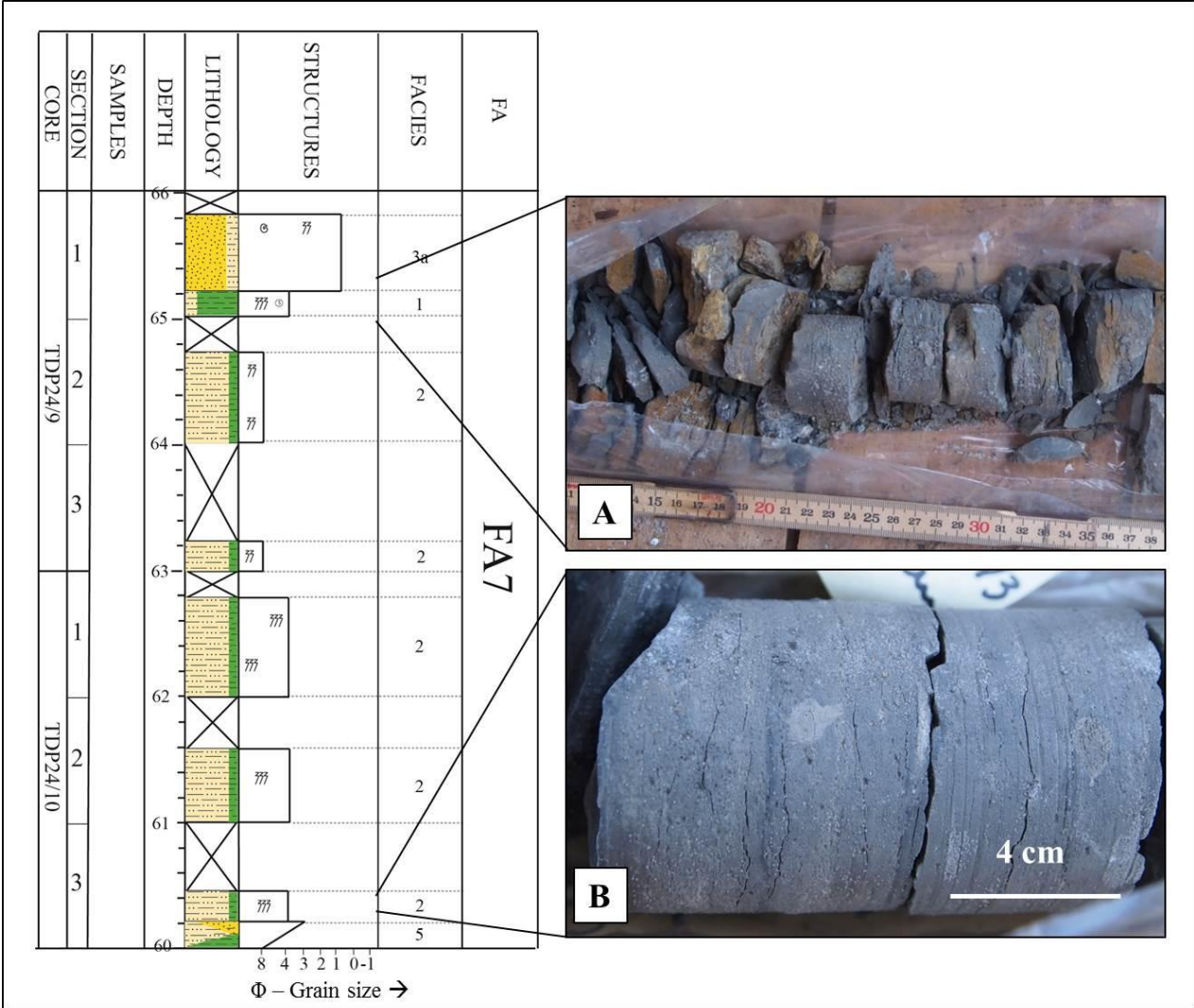




**Figure 4.23:** FA6 displayed by cores 18, 17 and 16, well site 24. A) Grey claystone of facies F1. B) Dark grey claystone of facies F1, interbedded with light grey sandstone facies 3a. C) Dark grey claystone of facies F1, interbedded with light grey sandstone of facies F3a.

**FA7:** Siltstone association dominated by grey siltstone of facies F2, with small intervals of clay and sand (facies F1, F3a, F5) (Figure 4.24) (Table 4.4). In core 24 this is the topmost facies association present (level 52,6 – 90m) (Appendix A). The first 4 m (level) consist of upwards fining facies F5. While the remaining part of the facies association consist of siltstone facies F2 and clay stone faices F1 with some intervals of sandstone facies F3a. Core 24 displays an upwards fining trend. FA7 lies above FA6, and the transition between the two associaitons is abrupt. In borehole 21 the association stretches from level 50-73m (23 m thick)

and are dominated by claystone facies F1 (level 50,4 – 58,1) interbedded siltstone facies F2. sandstone facies F3b and F4 (level 58,1 – 73 m). FA7 lies above FA8 and display a gradational transition (Appendix B.).



**Figure 4.24:** FA7 represented by cores 9 and 10, well site 24. A) Dark grey claystone of facies F1. The claystone is somewhat brown due to flow of oxidizing fluids. B) Bioturbated grey siltstone of facies F2.

**FA8:** This clay association is present in cores from site 21, stretches from 29-50m (32 m in thickness) and is dominated by clay facies F1 (Table 4.4). One unit (10 cm thick) of facies F7 is present in the lower part of the facies (level 30, 48 – 30, 5 m). The transition between the underlying FA5 association is abrupt (Appendix B)

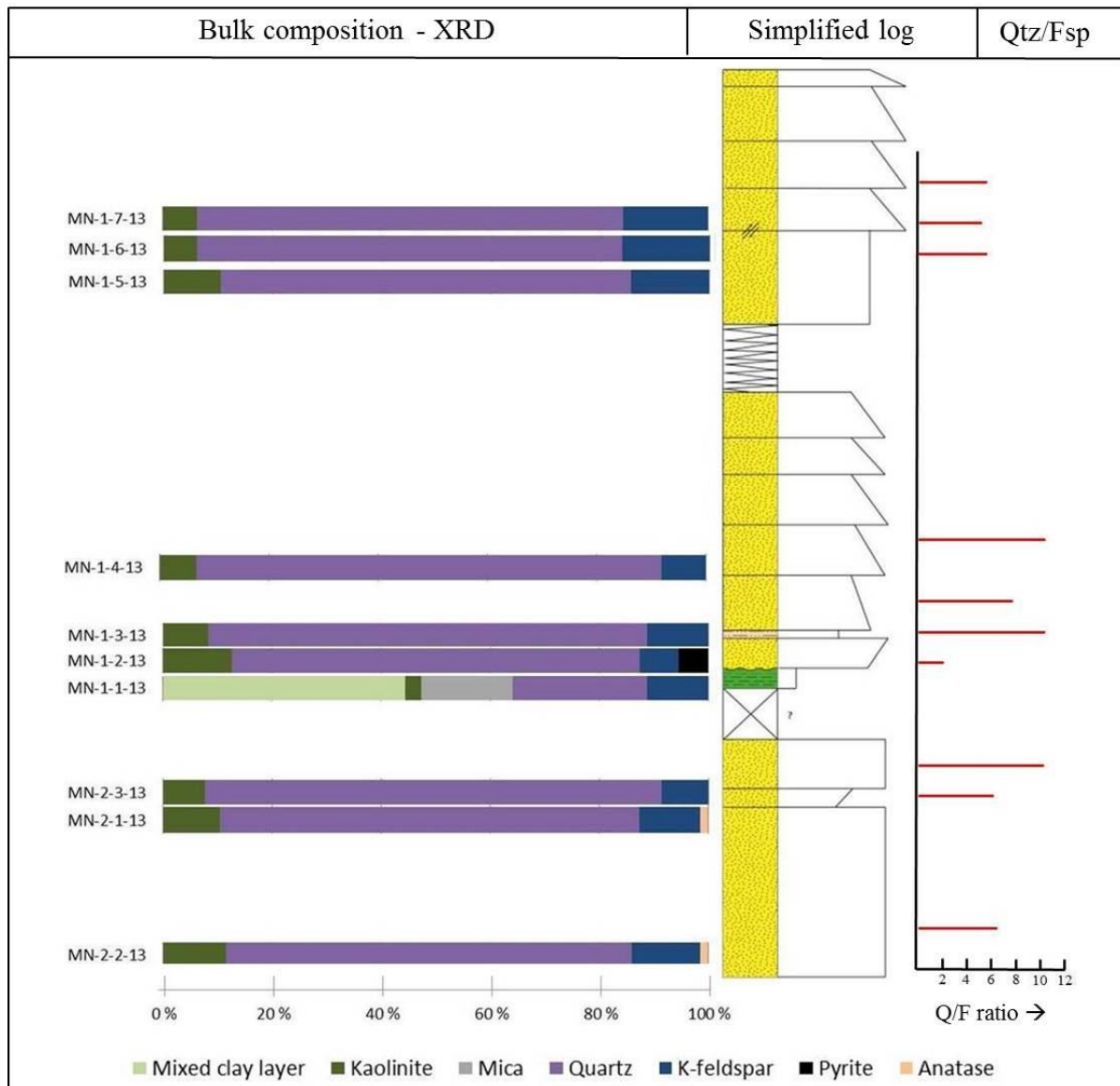


### 4.3 Petrographic description

#### 4.3.1 Upper Kipatimu Mb. (Kimmeridgian - Tithonian)

#### XRD results

Ten samples of the Upper Kipatimu Mb. were analyzed by XRD (Figure 4.25).



*Figure 4.25: Quantitative XRD results and quartz/feldspar ratio presented with the simplified log of Upper Kipatimu Mb, at Mlima Ngoge, indicating where the analyzed samples were taken in the logged sections.*

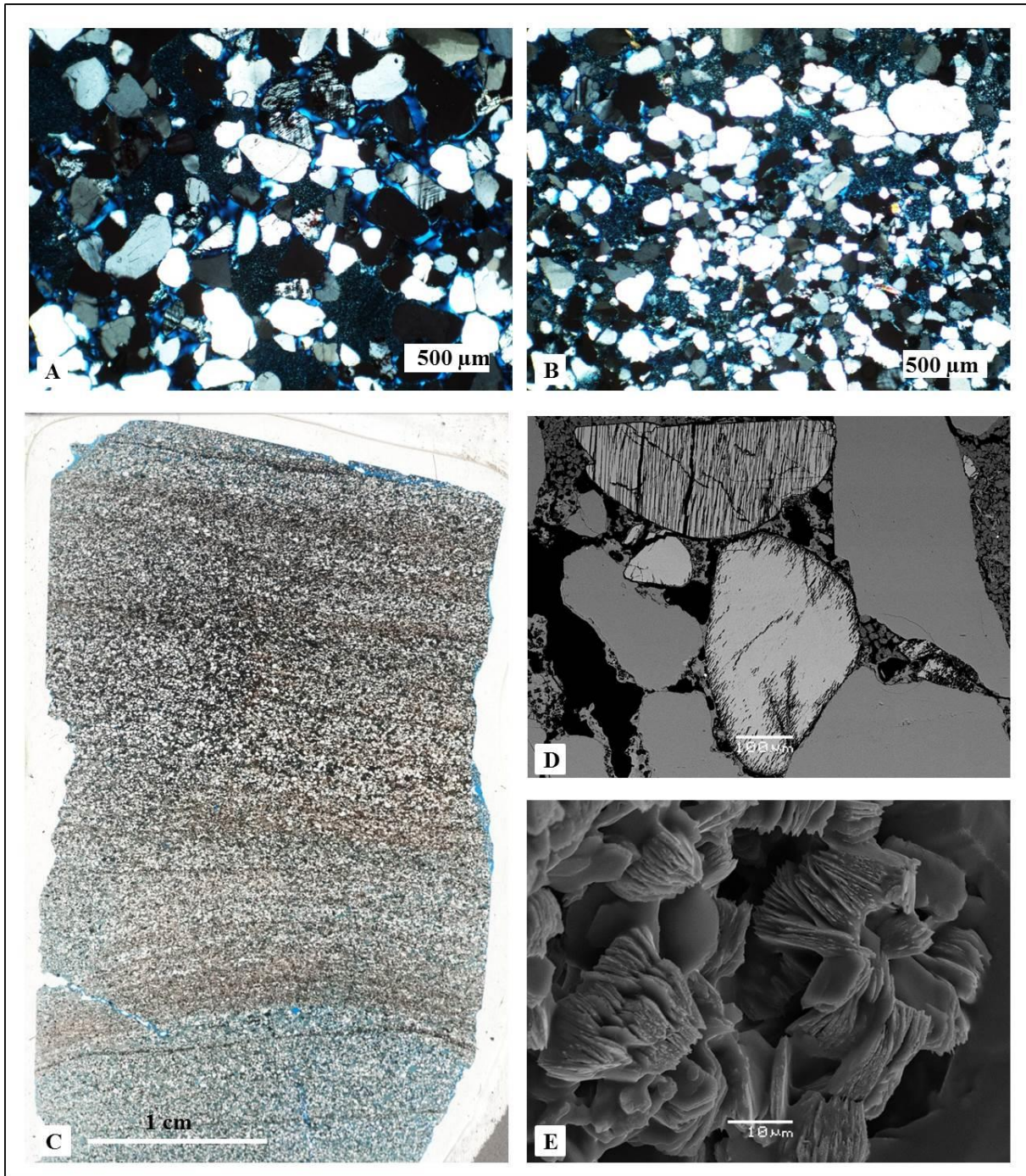
The samples analyzed from Upper Kipatimu Mb. consist primarily of quartz with contents up to 85,10%. Feldspar constitutes up to 16,1%, comprising K-feldspar. Kaolinite is present in all

the samples, with an average value of 8,3%. Other minerals present are pyrite in sample MN-1-2-13 with 5,5%, and anatase in two samples (MN-2-2-13 and MN-2-1-13) with values up to 1,5%. Within the clay sample (MN-1-1-13) a mixed clay layer predominates with 44,4% (Appendix D). The mixed clay layer may consist of smectite, kaolinite, illite, chlorite and vermiculate as described by Mahmic (2014) who studied clays within the Mandawa Basin.

### **Petrographic and mineralogical description**

Five thin sections of sandstone from Upper Kipatimu Mb. were studied in the optical microscope and point counted. Lithic grains are rare and the sandstone classifies as arkosic sandstone (Appendix E). All sandstone samples are grain supported, with abundant pore filling authigenic kaolinite cement and low degree of bioturbation (Figure 4.26 D, E). Grain size ranges from fine to coarse. Grain contacts are mainly tangential and long, some convex-concave contacts are observed. The samples are weakly to moderately compacted.

The majority of grains are subrounded, but some angularity is observed (Figure 4.26 A, B and D). The samples display a sorting ranging from moderately well to poor (Figure 4.26 A and B). Feldspar preservation displays mainly a variation between category 4 and 5 (Table 3.3), few feldspar grains are moderately preserved and display a weathering grade of 3 (Figure 4.26 D). Point counting proved monocrystalline quartz as the most abundant mineral with amounts up to 56,8%, where quartz grains with undulatory character make up 4,4-14,6% of the quartz fraction. Pore filling kaolinite is present with values up to 20% (Figure 4.26 E). A complete table of point counting results is presented in Appendix C.

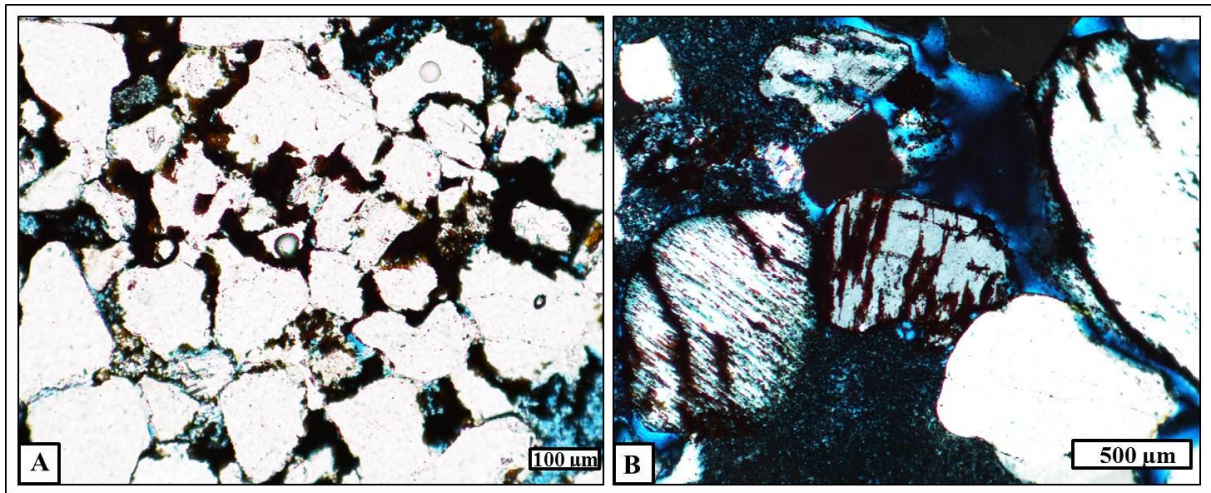


**Figure 4.26:** A) Thin section micrograph displaying well sorted coarse sandstone B) Thin section micrograph displaying poorly sorted coarse sandstone C) Scanned thin section of Upper Kipatimu Mb., sample displaying fine lamination. D) SEM image of weathered feldspar E) Pore filling kaolinite.

Quartz/feldspar ratios vary mainly between 4 and 10. The Upper Kipatimu Mb. sandstone display total porosity values between 5 and 21%. Primary intergranular porosity dominates the samples. Secondary porosity, recognized as dissolved feldspar grains, microcracks and



corroded framework minerals make up 2-6% of the porosity present. All the samples contain Fe-oxide with values ranging between 1,2 and 4,2% (Figure 4.27 A and B).



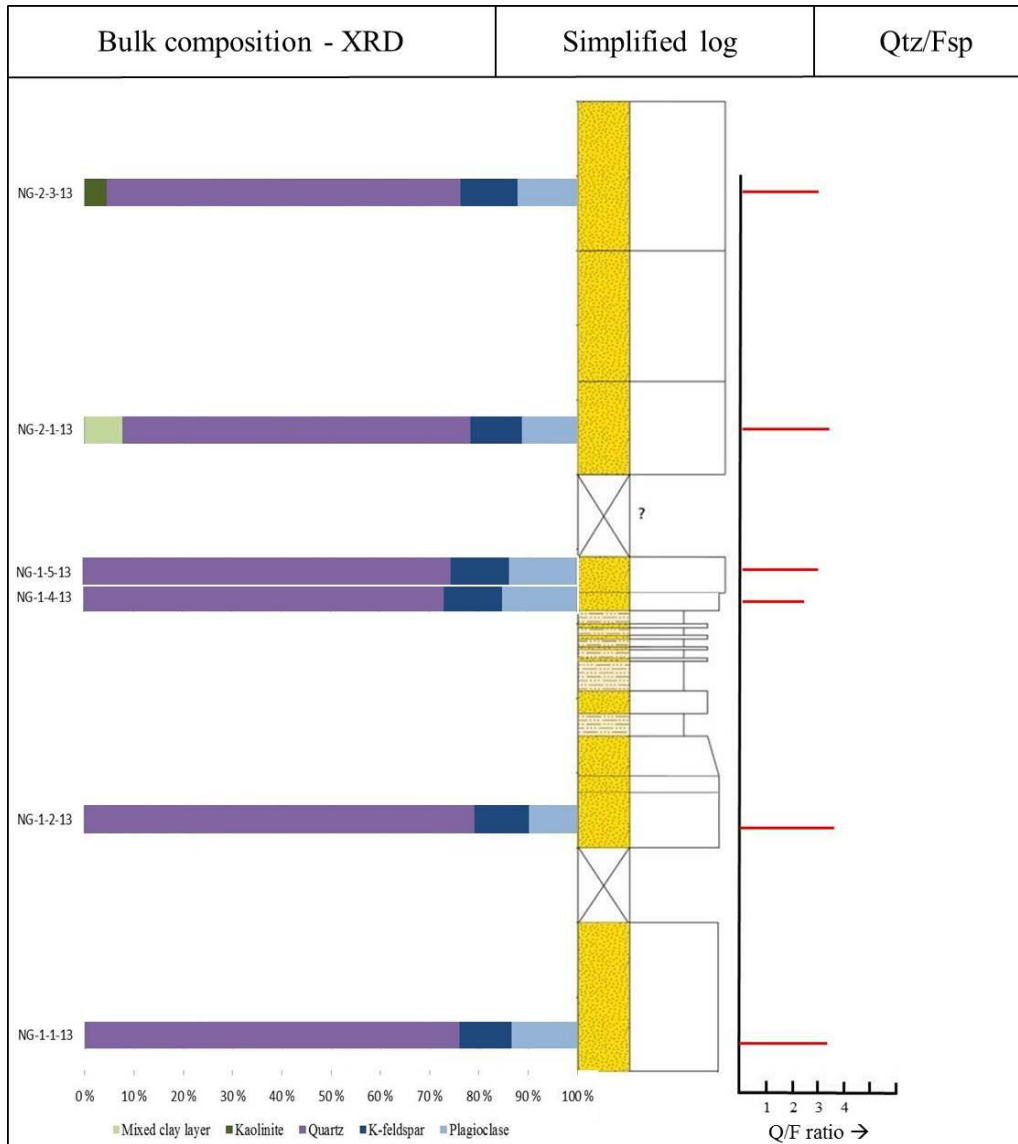
*Figure 4.27: A) Pore filling Fe-oxide B) Fe-oxide within micro fractures of K-feldspar and quartz grains.*

SEM revealed that feldspar and muscovite are partially altered to clay. Within sample MN-2-1-13 light microscope revealed lamination of heavy minerals (Figure 4.26 C.). SEM analysis showed that the heavy minerals mainly consist of zircon, rutile and anatase. Small amounts of pore filling smectite that looked detrital in origin were observed in several of the samples. Relations between the different diagenetic minerals present were studied in SEM. Authigenic clay minerals, such as kaolinite, illite and smectite, occur in close association with partially dissolved feldspars and mica. Smectite and kaolinite fill in the lines and pores created after dissolution of feldspar and mica. Kaolinite occurs as well developed booklets, consisting of stacked pseudo-hexagonal plates. The authigenic kaolinite commonly fills the intergranular pores (Figure 4.26 D and 4.26 B). In addition, kaolinite intergrowing with detrital muscovite was observed. The kaolinite within the muscovite grains looks more dense and detrital in morphology compared to the authigenic booklet kaolinite. In addition, the kaolinite seems to have expanded the detrital muscovite. Perthitic feldspars are common and display selective leaching of albite lamella (4.21 D and 4.22 B). The Fe-oxide occurs as porefill within primary intergranular pores, within the secondary pores created by feldspar dissolution and within grain microcracks. The Fe-oxide appears to be one of the later emplaced diagenetic minerals (Figure 4.27 A and B).

### 4.3.2 Upper Mitole Mb. (Kimmeridgian – Berriasian)

#### XRD results

The mineralogical compositions of six samples from Upper Mitole Mb. was analyzed by XRD (Figure 4.28).



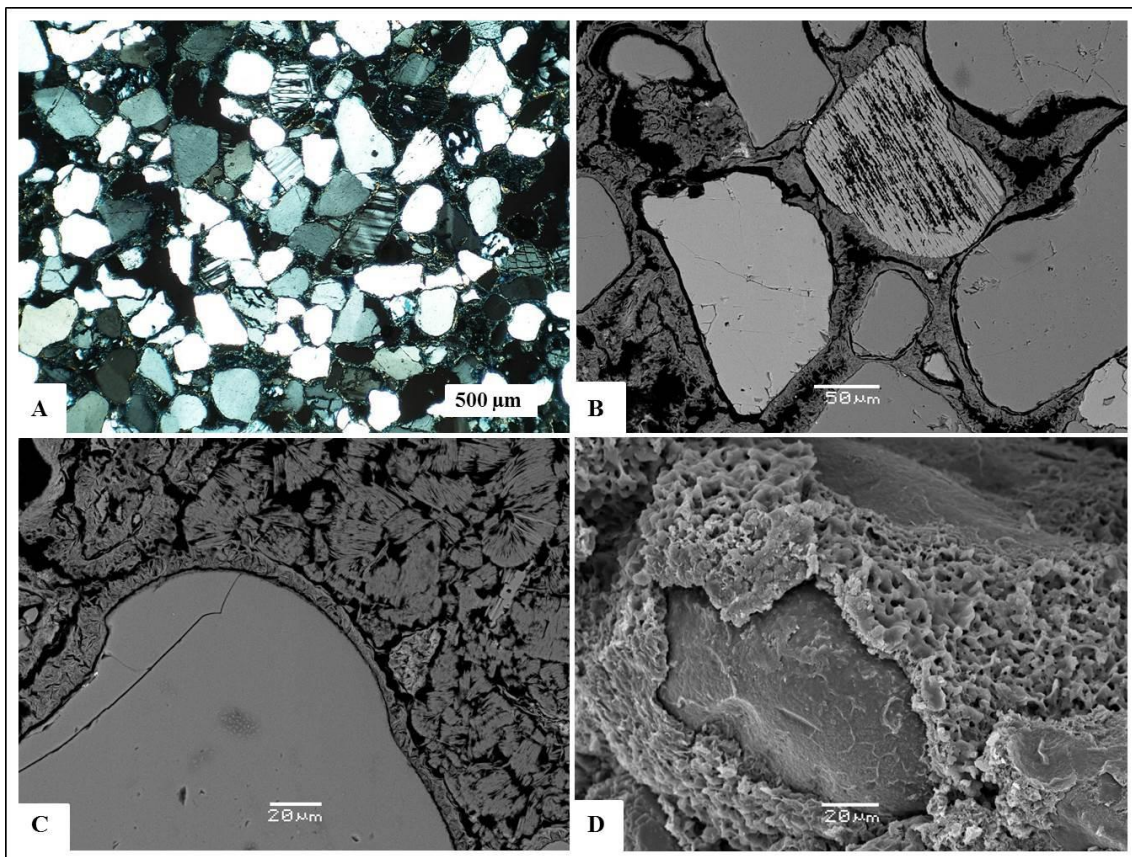
**Figure 4.28:** Quantitative XRD results and quartz/feldspar ratios presented with the simplified log of Upper Mitole Mb., at Ngoro, indicating where the analyzed samples were taken in the logged sections mineralogical content. The right part illustrates the quartz/feldspar ratio within the analyzed samples.

Quartz is the main component in all the samples with amounts up to 79,1%. The feldspars display values up to 27,1%; subdivided into plagioclase (up to 15,2%) and K-feldspar (up to

11, 9%). Sample MN-1-3-13 contains mixed layer clay (up to 7,7%), and sample NG-2-3-13 contain 4,5% kaolinite (Appendix D). Quartz/feldspar ratio varies between 2, 5 and 4 (Figure 4.28), and the plagioclase/k-feldspar ratio between 0, 8 and 1, 3.

### **Petrographic and mineralogical description**

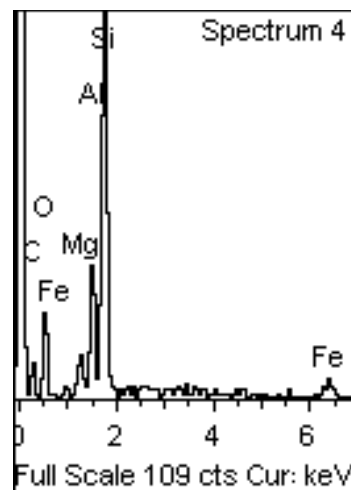
Four thin samples from Upper Mitole Mb. were studied in the optical microscope and point counted. The sandstone is classified as arkosic (Appendix E). All samples are grain supported, display low degree of bioturbation and contain pore filling kaolinite and smectite-chlorite coatings (Figure 4.29 A, B, C, D). Grains are moderately packed with mainly tangential and long contacts, though some concave-convex contacts were observed. The samples display weak to moderate compaction.



**Figure 4.29:** A) Micrograph of coarse moderately sorted sand B) SEM image of thin section showing smectite-chlorite coating C) SEM image of thin section showing smectite-chlorite coating and pore filling kaolinite D) SEM image of rock sample place on stub, showing smectite-chlorite coating around quartz grain.

Grain shapes vary from moderately well rounded to subangular, and sorting ranges from well to moderate. Monocrystalline quartz is the most abundant mineral with values up to 54,6%, while quartz grains with undulatory character display values up to 12,5%. All grains have apparent radial smectite-chlorite coating, where point counting revealed values ranging between 11,5 and 13,2%. Feldspar preservation varies between categories 3-5 (Table 3.3), some feldspars display moderate preservation while others are completely weathered. Locally small amounts of pore filling kaolinite (up to 4,5%) are observed. Point counted total porosity varies between 11 and 26%, where primary intergranular porosity dominates. In addition, microporosity was observed within the authigenic clay coating. Secondary porosity makes up about 2-7 % of the samples, consisting of dissolved feldspar grains, corroded framework grains, microcracks, shrinkage voids and clay rims. In addition, chert and heavy minerals were observed in the samples.

SEM analyses revealed a coating whose energy dispersive spectra seem to resemble a mix of smectite and chlorite. The coating has grown perpendicular to the host grain surfaces, forming an isopachous rim of cement. The morphology of the coating resembles a smectite, appearing to be tangentially attached to the detrital surface and curl upwards away from the surface with arandom orientation. Coating seems to be recrystallized and somewhat rough at the outer rims. At grain contacts the coating is minimized or absent (Figure 4. 29 D).



**Figure 4.30:** Representative energy dispersive spectrum of analyzed grain coating containing Si, Al, Mg and Fe. Sample 2-1-13, Upper Mitole Mb.

The relation between diagenetic minerals was also studied in the SEM. Smectite-chlorite coating seems to predate the observed kaolinite, thus being the primary diagenetic mineral.

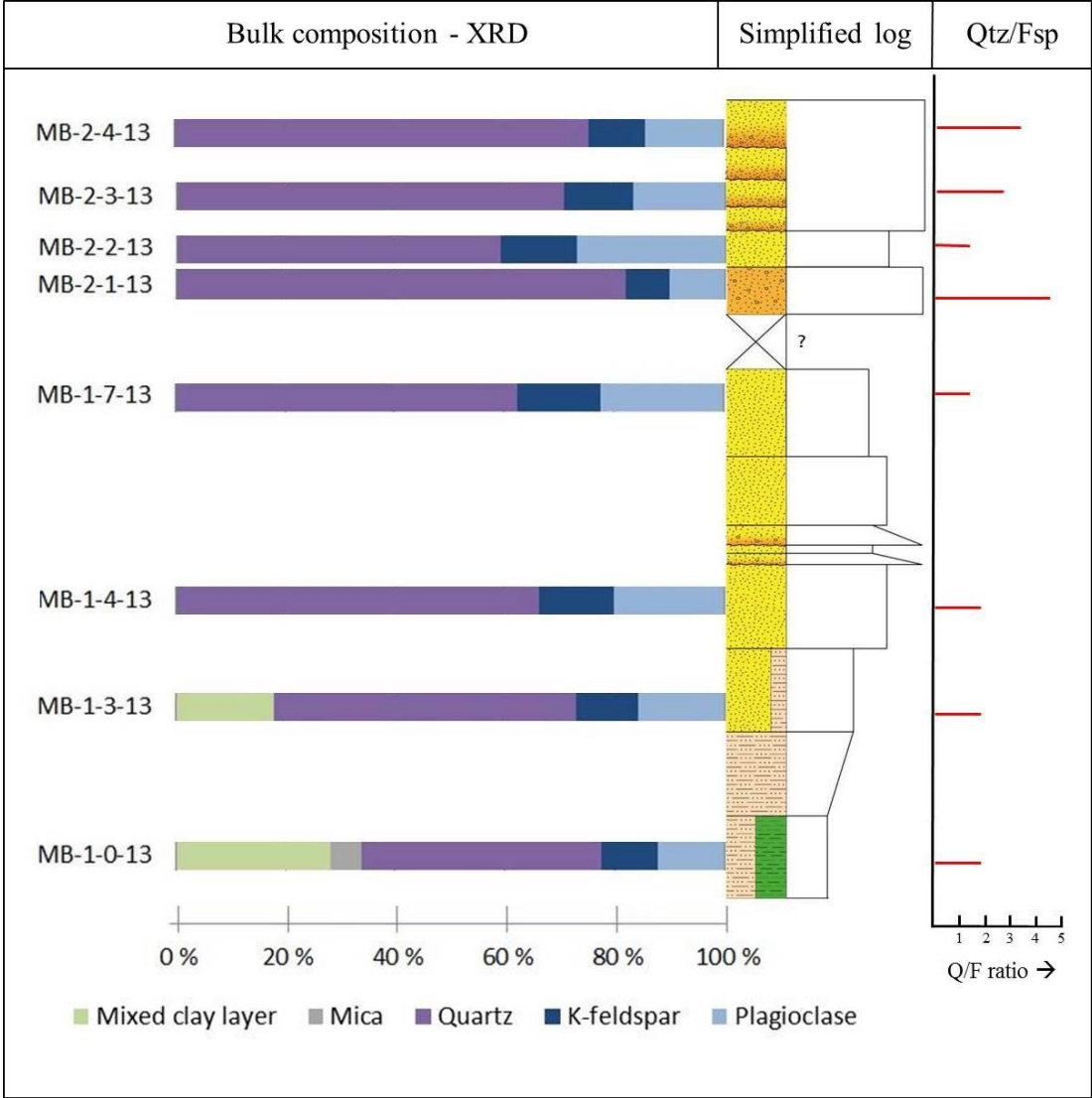


Highly weathered feldspar grains display smectite-chlorite coating. Altered feldspars and micas are commonly associated with kaolinite.

**4.3.3 Makonde Fm. (Aptian – Albian)**

**XRD results**

Eight of the samples from Makonde Fm. were analyzed by XRD.



*Figure 4.31: Quantitative XRD results and quartz/feldspar ratios presented with the simplified log of Makonde Fm. at Mbate, indicating where the analyzed samples were taken in the logged sections.*

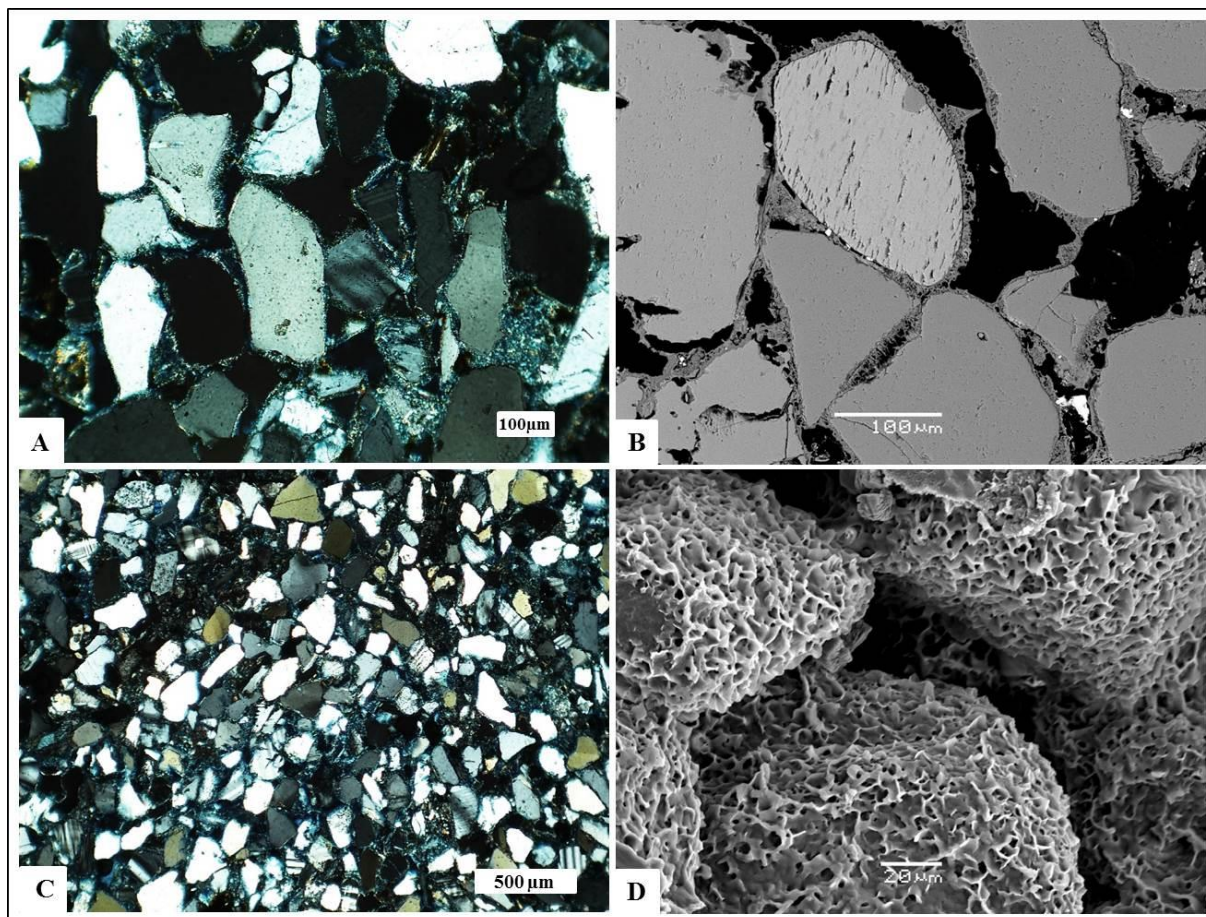
Sandstone samples display quartz content with values up to 82,0%. Feldspar content varies from 18,0-40,9%, with plagioclase being the most abundant feldspar mineral with values up



to 27,0%. K-feldspar is present with amounts up to 15,10% (Appendix D). The quartz/feldspar ratio ranges from 1 up to 5 (Figure 4.31), and the plagioclase feldspar ratio between 1, 2 – 1, 9. Clay sample MB-1-0-13 contains mixed layer clay (28,3%) and mica (5,6%). The mixed clay layer may consist of smectite, kaolinite, illite, chlorite and vermiculate as described by Mahmic (2014) who studied clays within the Mandawa Basin.

### **Petrographic and mineralogical description**

The sandstone samples consist of subrounded and subangular grains (Figure 4.32 A and B). Grain contacts are mainly tangential and long, some concave-convex are observed. Sorting varies between well to poor (Figure 4.32 A and C); the coarser samples have the poorest sorting. The samples are all classified as arkosic sandstones (Appendix F). Feldspar preservation mainly classifies as category 3, in addition observations of feldspar that classifies as category and 2, 4 or 5 is present (Table 3.3). Monocrystalline quartz makes up the dominant mineral phase with values up to 58,2%. Where quartz grains with undulatory character varies between 5,2 and 10,8%. The quartz/feldspar ratio vary between 2 and 5. Other minerals observed are chert, biotite, muscovite and heavy minerals. Elongated minerals in the moderately compacted samples tend to be bended between framework grains. Primary porosity is the dominant porosity type in the samples. Total porosity values lie between 14 and 27%. Secondary porosity is present as dissolved feldspar grains, microcracks, shrinkage voids and clay rims, and make up 3-6% of the total porosity. In addition, microporosity is observed within the authigenic clay coatings.



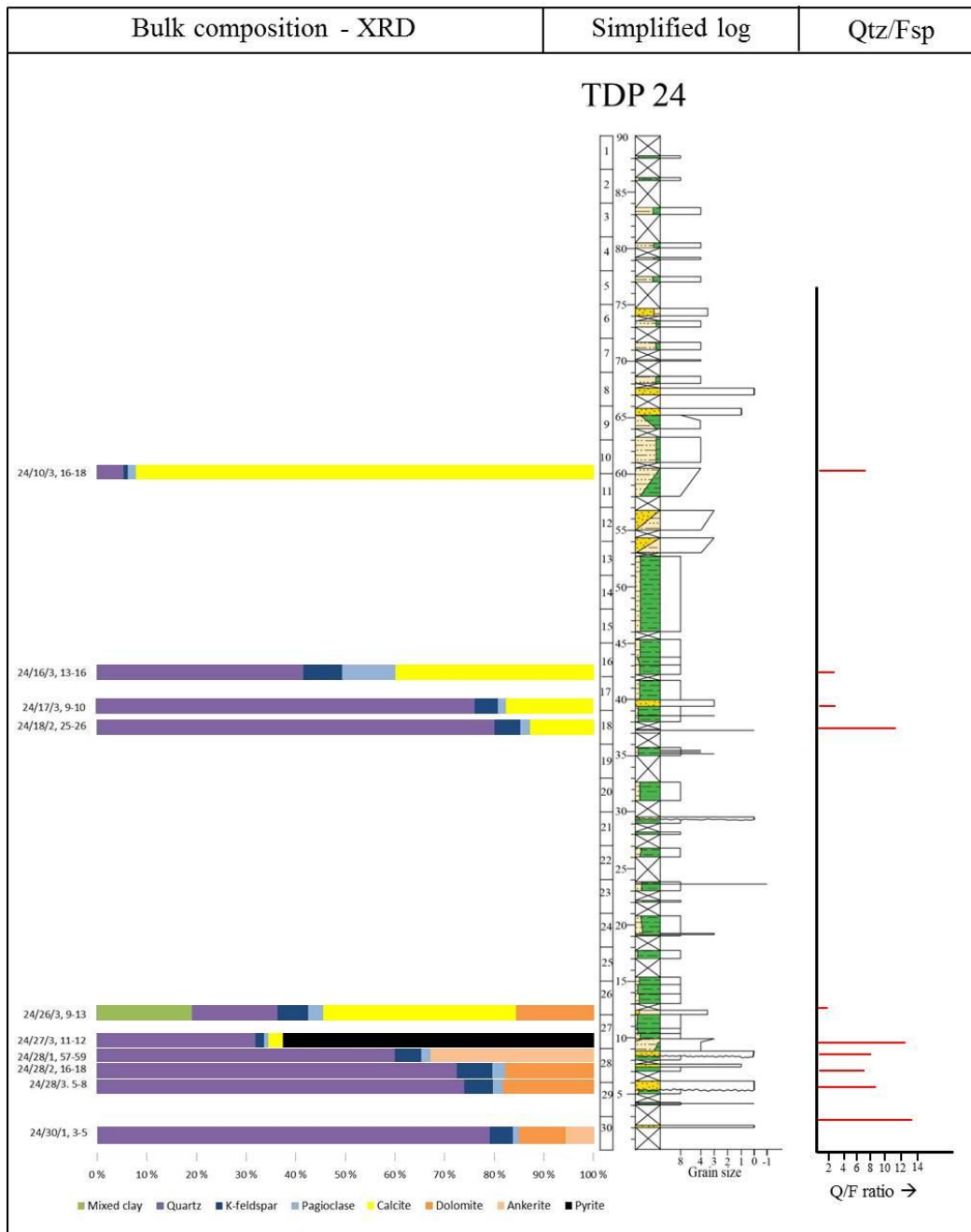
**Figure 4.32:** A) Micrograph of moderately sorted medium sized sandstone. B) SEM image of thin section showing subangular/angular feldspar and quartz grains with smectite-chlorite coating. C) Micrograph of moderately sorted medium sized sandstone D) SEM image of rock mounted on stub, showing smectite-chlorite coating on subangular grains.

SEM revealed the clay coating to be smectite-chlorite. The smectite-chlorite coating was observed to be tangentially attached to the detrital surface of the grains, and appears to curl away from this surface with a random orientation (Figure 4.32 D). The smectite appears recrystallized and rough at the edges, where the honeycomb structure is somewhat diminished. The coatings are absent or minor at grain contacts (Figure 4.32.B). SEM energy dispersive spectrum is similar to the analyzed grain coating in Upper Mitole Fm. (Figure 4.30). Partially altered feldspar was observed with kaolinite. In addition, smectite precipitation occurs within dissolved feldspar grains. Authigenic kaolinite appears to have formed later in the diagenetic process compared to the smectite-chlorite coating.

#### 4.3.4 Well site 24 (Albian – Turonian)

##### XRD results

Eleven samples of cores from well site 24 were analyzed by XRD.



*Figure 4.33: Quantitative XRD results and quartz/feldspar ratios presented with the simplified log of core 24, indicating where the analyzed samples were taken in the logged sections*

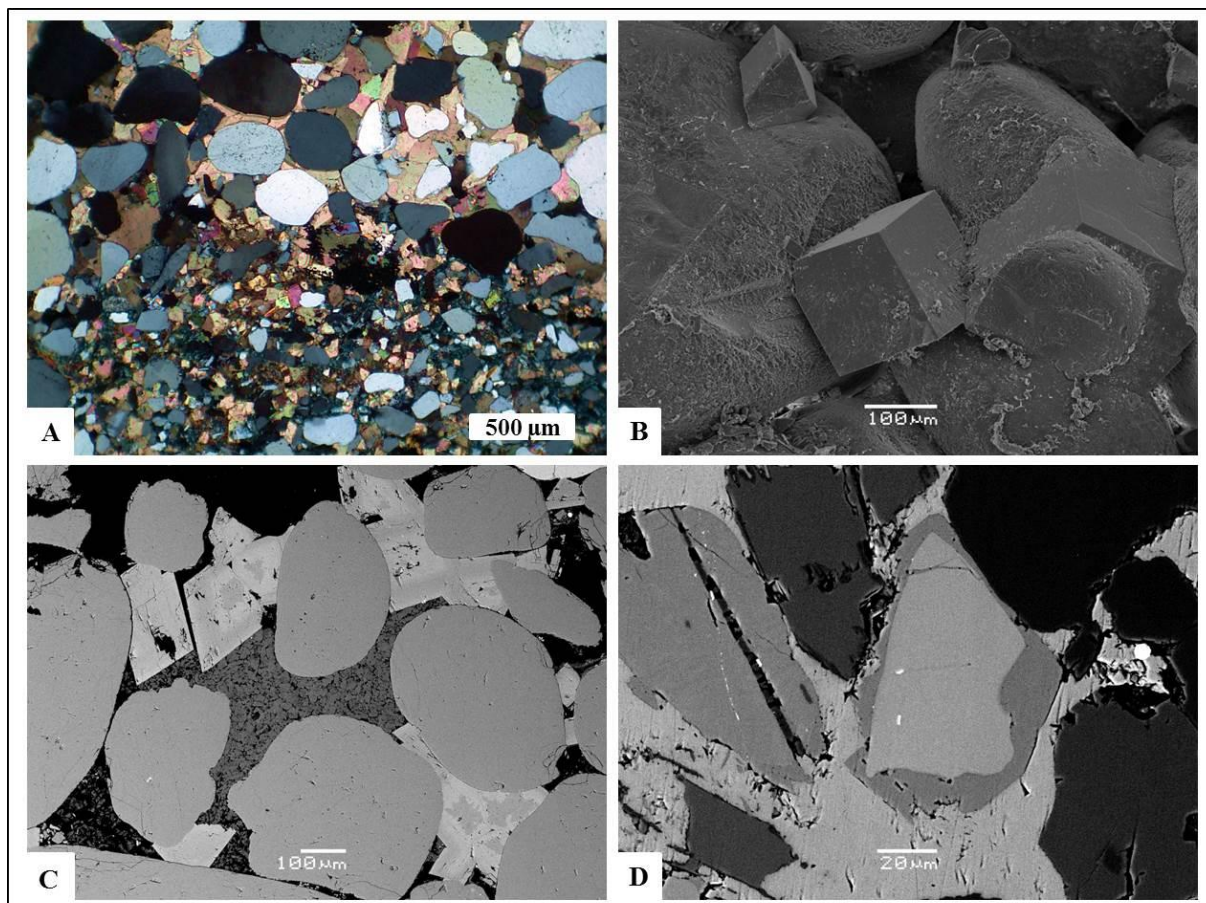
Quartz and carbonate cement make up the main constituents in the sandstone samples, where average quartz content is 49,3% and average carbonate content is 30,6%. The carbonate fraction can be subdivided into calcite (up to 92,1%), dolomite (up to 18,3%) and ankerite (up to 32,9%). One sample (24/27/3) is dominated by pyrite (62,6 %). Average feldspar content is 7,7%, where plagioclase makes up 2,8% and K-feldspar makes up 4,9% (Appendix D). The quartz/feldspar ratio varies between 2 and 15 (Figure 4.33).

### **Petrographic and mineralogical description**

Five sandstone samples were studied and point counted, and all samples classify as arkosic sandstone (Appendix F). The sandstones mainly consist of subrounded and subangular grains, and display a weak to moderate compaction. The majority of the sandstone samples are grain supported sand. Sample 24/16/3 is matrix supported by carbonate cement. Grain size varies from medium to coarse grained sand. Elongated grains have no preferred orientation and are bent between framework grains. The grain contacts are mainly tangential and long, with a few observations of concave-convex contacts. Monocrystalline quartz is the predominant mineral with values up to 71%, while quartz grains with undulatory character display values up to 17%. The feldspar weathering classifies mainly as category 4 (Table 3.3). Total porosity varies between 0,5-20%. In the case of high porosities, primary intergranular porosity is the main porosity type. Secondary porosity is present in minor amounts (2-4%) consisting of dissolved feldspar, dissolved carbonate cement and microcracks.

SEM revealed prominent zonation in void filling dolomite crystals in sample 24/30/01 3-5 cm (Figure 4.34 B and C). Dolomite crystals are present as individual rhombs that are concentrically zoned. The zonation is easily seen in SEM due to color variations between dark and light zonation. The number of zonation within the crystals range from 2 to 4. The SEM analysis did not detect any differences in the composition within the zonation. In sample 24/17/3 9-10 framboidal pyrite and minor amounts of porefilling barite were observed as late diagenetic minerals.





**Figure 4.34:** A) Micrograph of well sorted carbonate cemented sandstone, with lamination. B) SEM image of rock mounted on stud, displaying rounded quartz grains and rhombic dolomite. C) SEM image of rounded quartz grains, dolomite with zonation and pore filling kaolinite D) K-feldspar overgrowth that displays euhedral crystal shape. Detrital core is light grey, while overgrowth is darker grey.

Clay minerals analyzed in SEM are pore filling glauconite, and some smectite within dissolved plagioclase.

K-feldspar overgrowth is a minor diagenetic mineral observed, displaying euhedral crystal shapes and a darker color compared to the detrital core. No compositional variation was detected by the SEM analyses between detrital and authigenic K-feldspar. The K-feldspar overgrowths are surrounded by calcite cement.

Carbonate cement is the major diagenetic cement present, preserving much of the intergranular volume. Dolomite and ankerite often occur as isolated rhombs, and appear to have formed later than the calcite. In samples where calcite and dolomite/ankerite are present, the calcite appears to predate the dolomite and ankerite. Dissolution of feldspar and

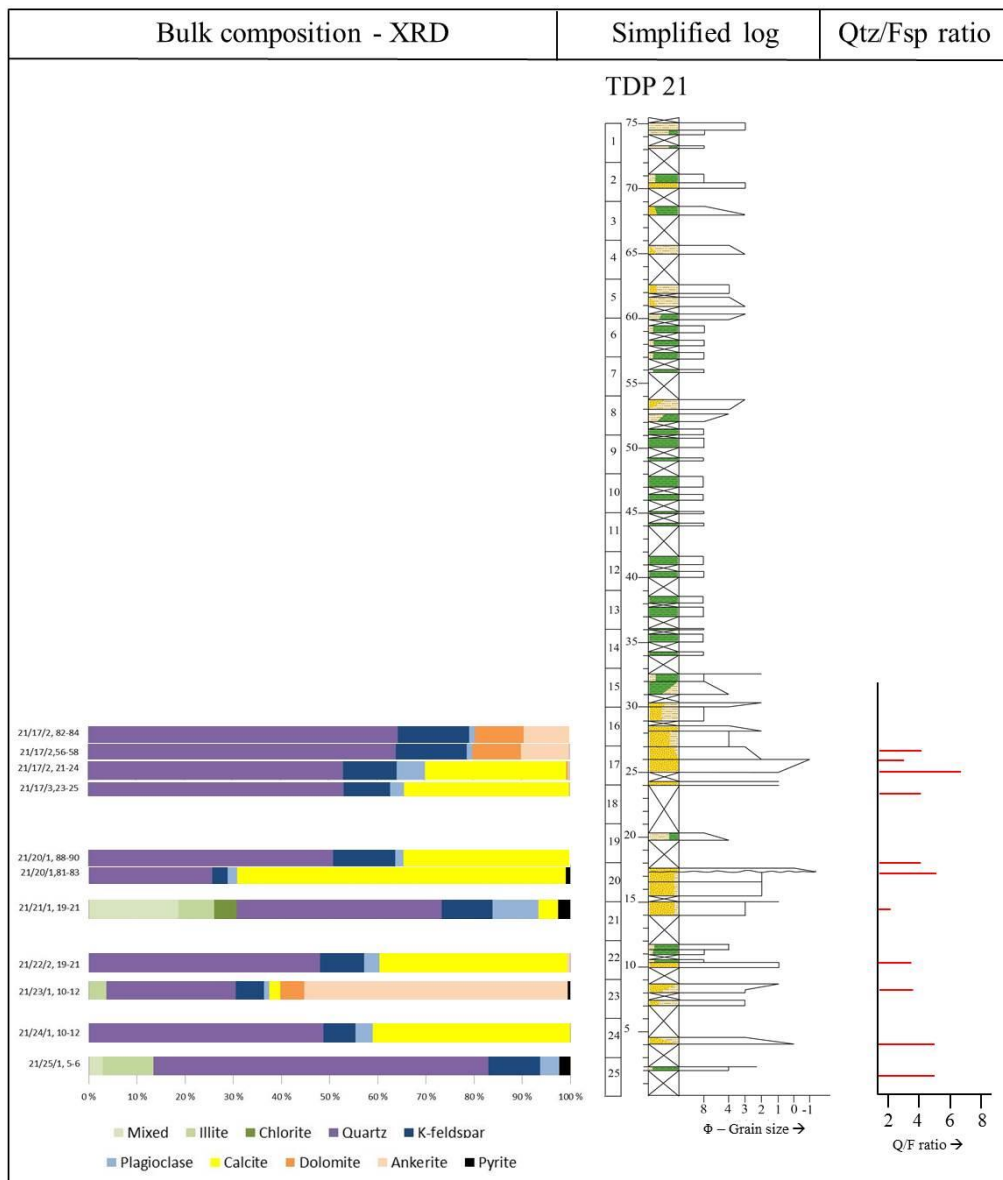


development of secondary porosity postdates the calcite cementation. Minor amounts of kaolinite are associated with dissolved k-feldspar.

#### 4.3.5 Well site 21 (Cenomanian – Coniacian)

##### XRD results

Ten samples were analyzed by XRD.



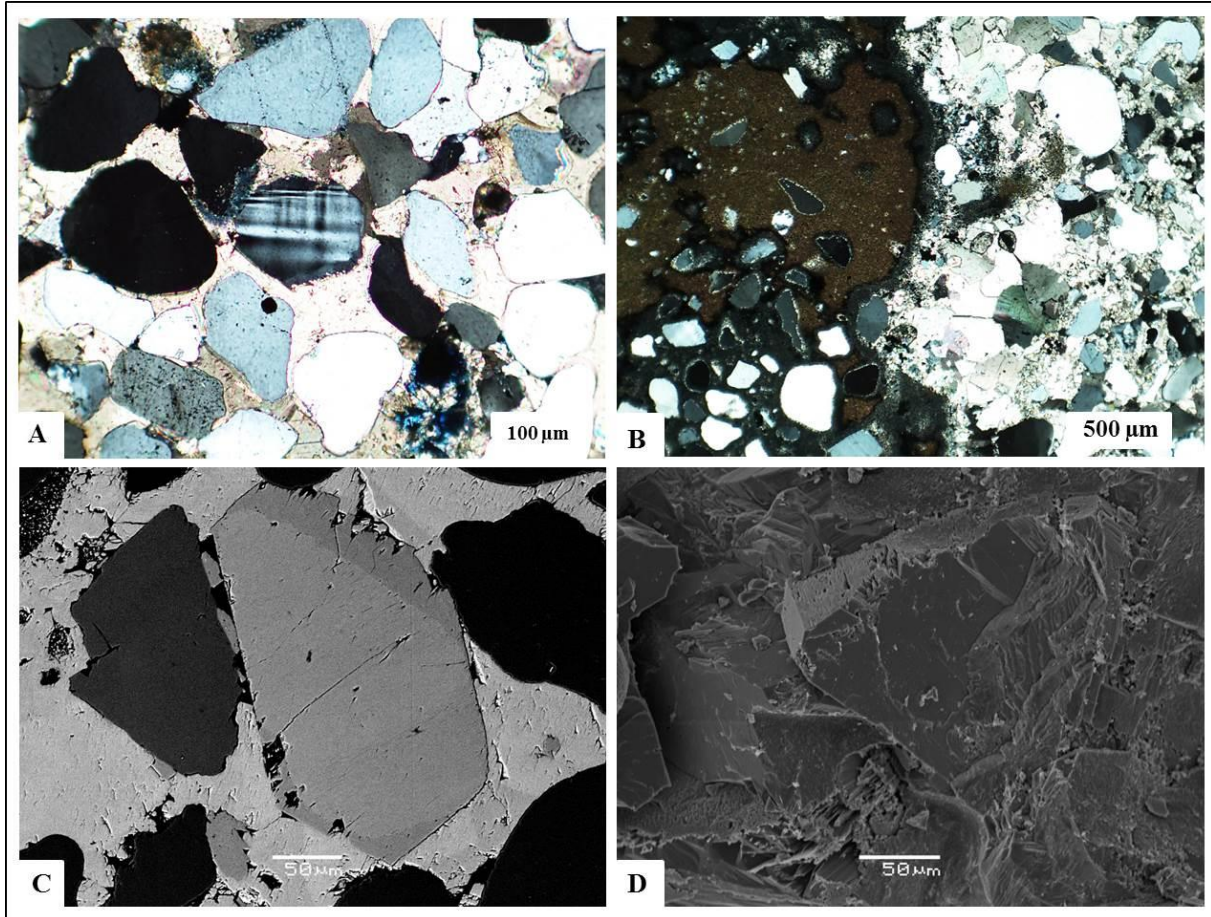
**Figure 4.35:** Quantitative XRD results and quartz/feldspar ratios presented with the simplified log of core 21, indicating where the analyzed samples were taken in the logged sections

Quartz is the dominant mineral in the samples with an average value of 49,3%. The sandstone samples are carbonate cemented with an average content of 34,0%, consisting of calcite with exception of two ankerite and dolomite dominated samples (21/23/1 and 21/17/2). The feldspar content has an average value of 12,6%; subdivided into plagioclase (3,5%) and K-feldspar (9,1%) (Appendix D). The quartz/feldspar ratio varies between 2 and 8. (Figure 4.35 C).

### **Petrographic and mineralogical description**

Six sandstone samples were point counted and studied using optical microscope. All samples classify as arkosic sandstone (Appendix F). The samples consist of mostly subrounded grains with some subangular grains. The samples are mostly weakly compacted, and display mostly tangential grain contacts, with a few long contacts observed (Figure 4.36 A and B). The average grain size is medium. Total porosity values vary between 5 and 30%, where primary porosity is the dominant. Secondary porosity represents minor amounts (2-4%), consisting of dissolved feldspar, dissolved carbonate cement and microcracks. The sandstones are dominated by monocrystalline quartz with values up to 58,5%, where quartz grains with undulatory extinction display values up to 26%. Chert is also present with 0,2%. Some pore filling kaolinite present in the samples. Feldspar preservation classifies mostly as a category 3 (Table 3.3). A complete table of point counting results can be found in Appendix C.

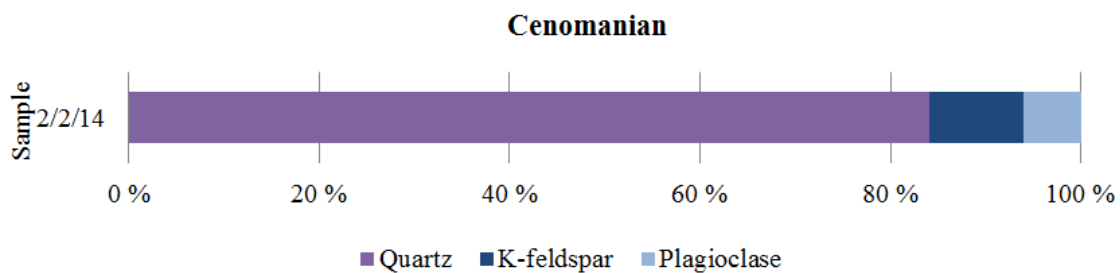
Digenetic K-feldspar overgrowths on detrital K-feldspars were revealed in light microscope and by SEM analysis (Figure 4.36 C and D). SEM studied showed that the K-feldspar overgrowth varying between fully enclosure on the detrital core, displaying euhedral crystal forms, and as a saw-tooth like edge not fully enclosed. The grain-overgrowth contact is clean, and the overgrowth is surrounded by calcite cement. Several of the K-feldspar overgrowths display rough and dissolved overgrowth, indicating that K-feldspar overgrowth predates the calcite cement. In addition, small amounts of pore filling smectite/illite and framboidal pyrite were observed, appearing to predate the carbonate cement. Dissolved K-feldspar displays smectite and seems to be connected to authigenic kaolinite. In addition, a detrital smectite matrix and pore lining clay were identified by SEM analysis in sample 21/5/1. This samples does not contain any carbonate cement.



**Figure 4.36:** A) Micrograph of moderately compacted sandstone displaying medium sized moderately well sorted sandstone B) Micrograph of fine grained sandstone with clay clasts. C) SEM image of thin section showing K-feldspar with overgrowth. Darker rim displays the authigenic k-feldspar overgrowth D) SEM image of stub, showing K-feldspar with euhedral overgrowth.

#### 4.3.6 Offshore samples

XRD results of sandstone sample 2/2/14\_a, of Cenomanian age.



**Figure 4.37:** Quantitative XRD results of the two analyzed offshore sandstone samples 2/2/14\_a.

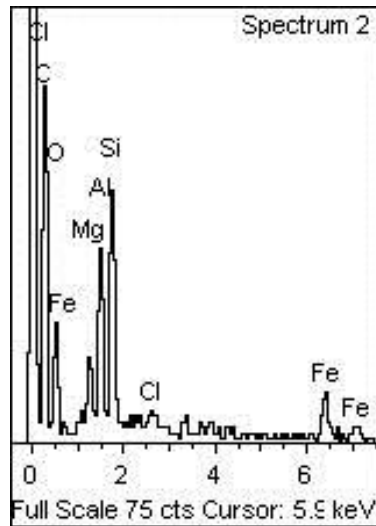
Quartz is the predominant mineral in sample 2/2/14\_a comprising 84,1% of the bulk mineralogy. The feldspars make up 15,9%; subdivided into K-feldspar (9,9%) and plagioclase (6%) (Figure 4.37) . The quartz/feldspar ratio is 5,2, and the plagioclase/feldspar ratio is 0,6.

### **Petrographic and mineralogical description**

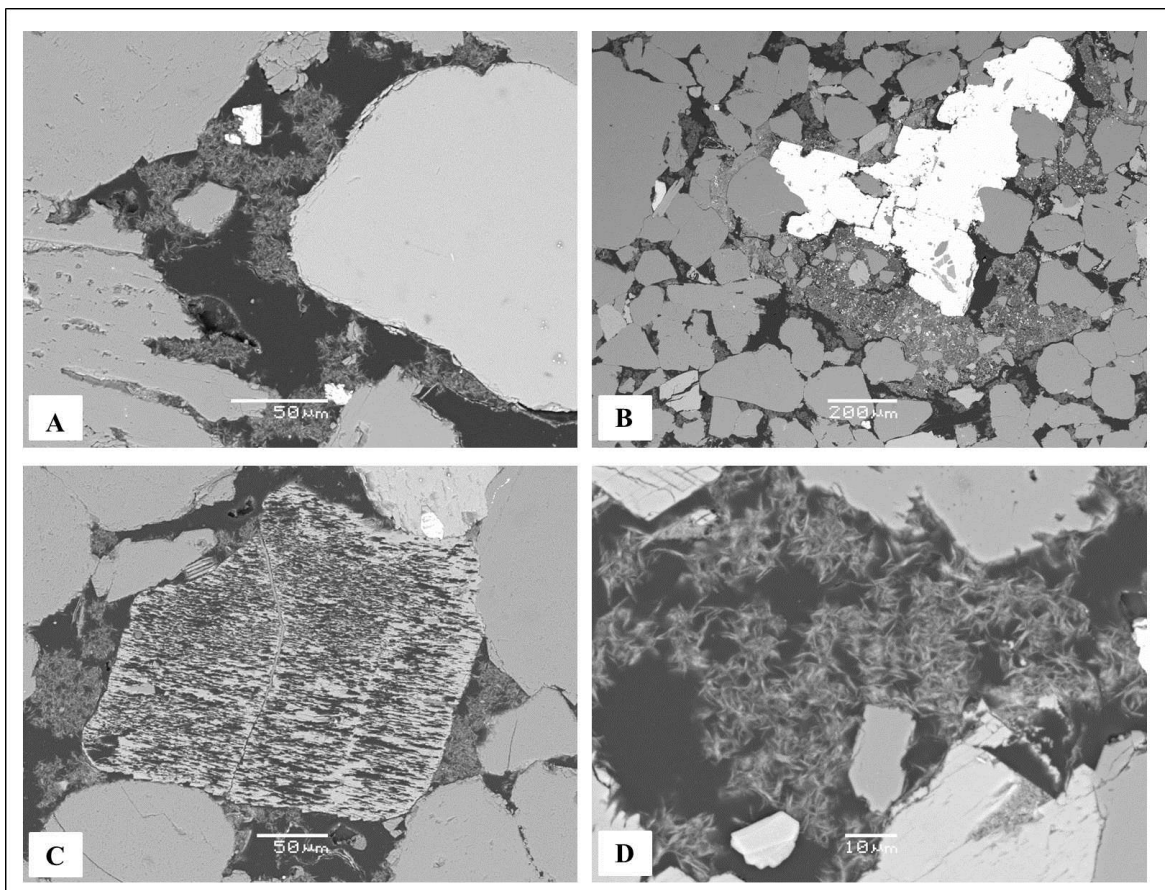
Two thin section samples (2/2/14\_a and 2/2/14\_b) of offshore Tanzania were studied in the optical microscope and point counted. Both samples are grain supported and contain up to 5% matrix. Grain contacts are mainly tangential and straight, but concave-convex contacts were observed. The samples display moderate compaction, and elongated grains are bent between framework grains. Sample 2/2/14\_a is well sorted with subrounded to subangular grains, while sample 2/2/14\_b is moderately sorted with subrounded and subangular grains. Both samples consist of coarse grained sand. Monocrystalline quartz is the most abundant mineral with up to 83%. Quartz undulatory character comprises 17,8% of the quartz composition. Feldspar preservation displays variation between category 3-5, with the majority of the feldspar grains classified as category 4. Minor amounts of calcite cement were observed, making up 1,1% of the mineral composition. Intergranular primary porosity is up to 21,5% of the sample. Minor amounts of secondary moldic porosity, caused by feldspar dissolution, are observed in both samples. The sandstones are classified as arkoses (Appendix G).

SEM analysis of sample 2/2/14\_a revealed a pore filling clay with an energy dispersive spectrum resembling a mixed smectite-chlorite composition (Figure 38). The energy dispersive spectrum displays significant Si, Al and Mg tops, with minor Fe and Cl tops.

Morphology of the pore filling clay is needle like and fibrous, displaying an authigenic origin (Figure 4.39 A,C and D). The fibrous morphology resembles chlorite. Small amounts of local pore filling pyrite, calcite cement and glauconite was observed in the SEM study (Figure 4.39 D). Pore filling authigenic clay seems superimposed by pyrite and calcite. Pore filling calcite cement is partly dissolved and replaced by authigenic clay.



**Figure 4.38:** Representative SEM energy dispersive spectrum of analyzed pore filling clay, displaying significant Si, Al and Mg tops. In addition, Fe and Cl tops are recognized.



**Figure 4.39:** Micrograph SEM back scatter images of thin sections, sample 2/2/14\_a, Block 2. A) Pore filling authigenic clay. B) Pore filling pyrite (white) and glauconite. C) Dissolved feldspar with preservation grade 5. D) Fibrous pore filling authigenic clay.



The calculated IGV of the two samples, 2/2/14\_a and 2/2/14\_b are 22,7% and 33,3% respectively (Table 4.5)

**Table 4.5:** The calculated IGV of the two samples, 2/2/14\_a and 2/2/14\_b are 22,7% and 33,3% respectively (Table 4.5)

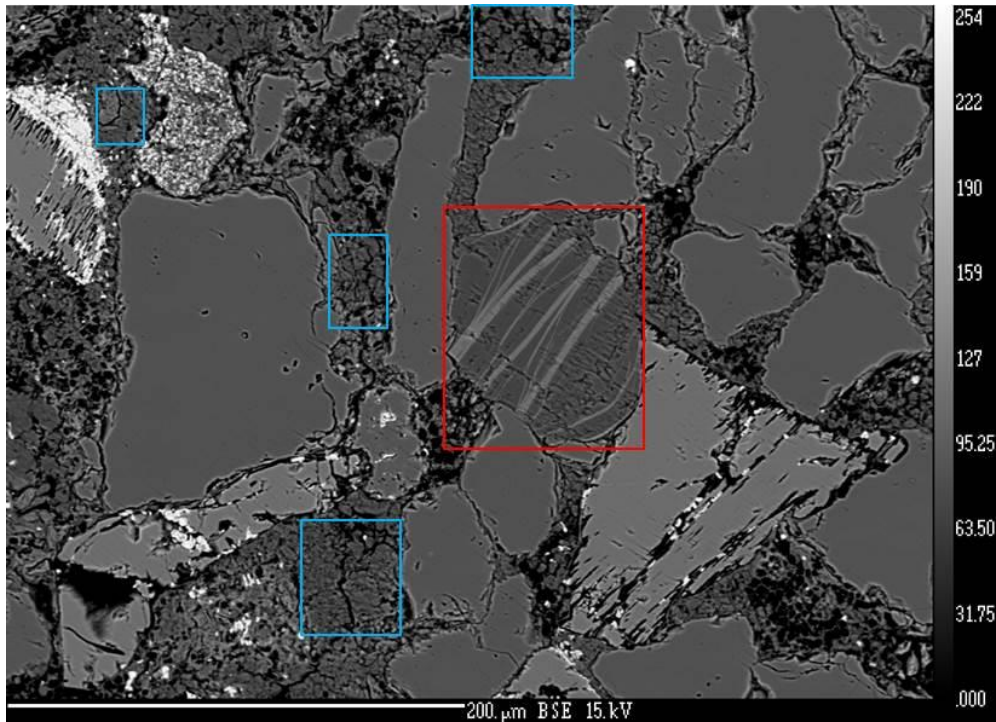
Sample	Porosity	IGV
2/2/2_a	18	22,7
2/2/2_b	21,5	33,3

## 4.4 EMP – Electron Micro Probe

### 4.4.1 Kaolinite

In Upper Kipatimu Mb. two types of kaolinite were observed within sample MN-2-1-13 by SEM analysis. The two samples differ in morphology and are thought to be (1) Authigenic pore filling kaolinite, displaying booklets and (2) detrital dense kaolinite intergrowing within muscovite (Figure 4.40). Both types of kaolinite were analyzed using EMP and six of the analyzed grains are presented in Table 4.6. A full table of analysis can be found in Appendix J.

The analyzed samples show a rather uniform composition of both authigenic and the inferred detrital kaolinite. Minor differences appear in the SiO<sub>2</sub> and Al<sub>2</sub>O<sub>3</sub> content. Authigenic kaolinite has slightly more SiO<sub>2</sub> and less Al<sub>2</sub>O<sub>3</sub> than the detrital grains



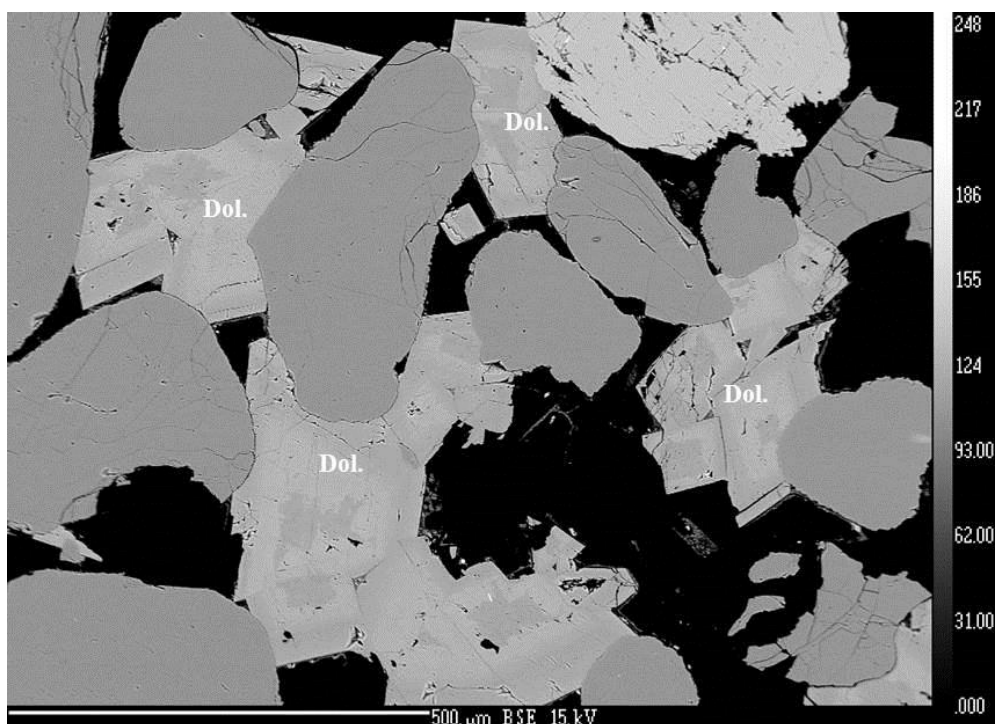
**Figure 4.40:** EMP micrograph of analyzed kaolinite (red box), sample MN-2-1-13. Displaying detrital kaolinite within muscovite, this kaolinite is more dense in appearance and looks detrital compared to the pore filling kaolinite around (blue boxes).

**Table 4.6:** Six representative EMP analysis of detrital and authigenic kaolinite, in wt%.

Analyzed	Sample	SiO <sub>2</sub>	Al <sub>2</sub> O <sub>3</sub>	CaO	FeO	MnO	Cr <sub>2</sub> O <sub>3</sub>	MgO	Na <sub>2</sub> O	K <sub>2</sub> O	TiO <sub>2</sub>	Tot.
<b>1. Authigenic</b>	MN-2-1-13	50,07	34,05	0,03	0,64	0	-0,01	0,15	0,03	0,18	-0,02	85,12
<b>2. Authigenic</b>	MN-2-1-13	48,70	35,45	0,03	0,66	0,01	0,01	0,15	0,01	0,10	0,01	85,13
<b>3. Authigenic</b>	MN-2-1-13	48,18	36,02	0,09	0,91	0,01	0,01	0,31	0,03	0,39	0,09	86,06
<b>4. Detrital</b>	MN-2-1-13	45,98	37,46	0,03	0,82	-0,01	-0,01	0,04	0,04	0,05	0,02	84,42
<b>5. Detrital</b>	MN-2-1-13	46,05	38,21	-0,03	0,13	0,04	0,04	0,02	0,01	0,02	-0,02	84,48
<b>6. Detrital</b>	MN-2-1-13	45,97	37,28	0	0,38	-0,001	-0,02	0,18	0,04	0,82	0,01	84,66

#### 4.4.2 Dolomite zonation

Dolomite zonation from sample 24/30/01 3-5 (core 30, well site 24) was analyzed under the EMP to disclose possible elemental differences between dark and light zonation within single dolomite crystals (Figure 4.41). Table 4.7 displays four representative measurements from EMP. 27 EMP analysis were done on dolomite crystals and the additional 23 analysis can be found in Appendix I.



*Figure 4.41: Zonation in dolomite, sample 24/30/1. Darker and lighter zones were analyzed by EMP (Table 4.7).*

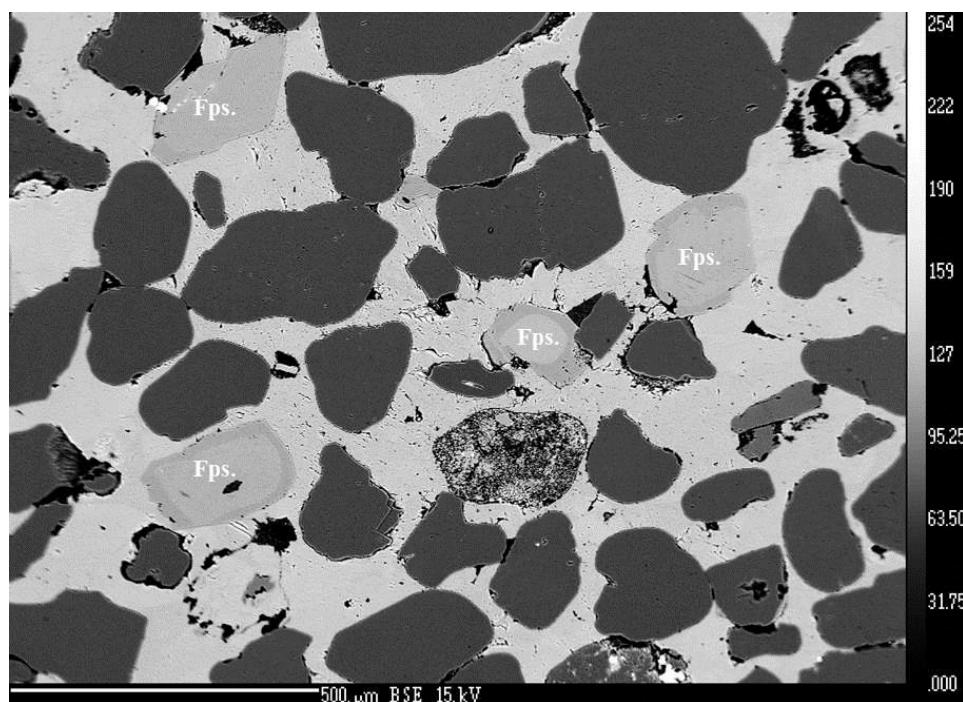
*Table 4.7: Four representative analysis of dolomite zonations, in wt%.*

Analyzed	Sample	CaO	FeO	MnO	MgO	SrO	SiO <sub>2</sub>	Total
<b>Dark</b>	24/30/1	30,3	3,0	0,3	17,8	-0,1	0,10	51,5
<b>Dark</b>	24/30/1	29,9	2,9	0,4	17,3	-0,1	0,04	50,4
<b>Light</b>	24/30/2	32,1	3,4	0,4	15,6	-0,2	0,02	51,4
<b>Light</b>	24/30/1	31,7	3,8	0,4	15,5	-0,1	0,02	51,4

The central parts of the dolomites tend to be darker in color, and from EMP analysis the darker zones were shown to have higher values of Mg, while the lighter zones have slightly higher values of CaO and FeO.

#### 4.4.3 Feldspar overgrowth

In sample 21/24/1 the feldspar overgrowth was the most apparent (Figure 4.42). EMP analysis was used to disclose differences in elements between the detrital core and the authigenic overgrowth. Table 4.8 displays three representative samples from three analyzed feldspar grains. The remaining analysis is presented in Appendix I.



**Figure 4.42:** Feldspar overgrowth from sample 21/24/1 (core 24, well site 21).

*Detrital parts are lighter, overgrowths display a darker outer rim.*

**Table 4.8:** Six representative EMP analyses of light detrital feldspar cores, and dark authigenic feldspar overgrowths in wt%, sample 21/24/1.

Analyzed	Sample	SiO <sub>2</sub>	Al <sub>2</sub> O <sub>3</sub>	CaO	FeO	MnO	Na <sub>2</sub> O	K <sub>2</sub> O	BaO	Total
<b>1. Core</b>	21/24/01	64,5	18,7	-0,05	0,02	-0,02	0,1	15,5	0,7	100
<b>2. Core</b>	21/24/01	63,8	18,5	-0,01	0,03	-0,03	0,8	15,6	1,3	100
<b>3. Core</b>	21/24/01	63,7	18,8	0,1	-0,03	-0,04	1,5	14,6	1,3	100
<b>4. Overgrowth</b>	21/24/01	65,1	18,4	0,02	0,03	-0,03	0,04	16,8	0,01	100
<b>5. Overgrowth</b>	21/24/01	65,4	18,5	0,01	0,02	-0,02	0,02	16,6	0,2	100
<b>6. Overgrowth</b>	21/24/01	64,6	18,5	0,07	-0,01	0,03	0,06	17,0	0,01	100

Elemental differences between detrital core and authigenic feldspar are minor in the regards to the amount of SiO<sub>2</sub> and Al<sub>2</sub>O<sub>3</sub>. Detrital grains, however, are enriched in Na<sub>2</sub>O and BaO, while the overgrowths display higher K<sub>2</sub>O concentrations.

#### **4.4.4 Smectite-chlorite coating**

Microprobe analyses of smectite-chlorite coatings were done on one sample from Upper Mitole Fm. and one sample from Makonde Fm. The oxide total values range between 50,6 and 85,8. It was not possible to obtain analyses whose oxide totals were close to what they should be for a smectite-chlorite (i.e. 85-88%). The EMP results did not collaborate well with SEM analysis. The poor results are thought to be due to a factor of microporosity within the smectite-chlorite crystals, and the laser beam not hitting the exact point of the clay. One example of this is the coating having high Si values, indicating that the beam also hit the quartz grains in most of the analyses. The EMP results of the coatings will not be discussed further.

#### **4.5 Porosity and IGV (Intergranular volume)**

To achieve better knowledge of sandstone porosity, point counting and area measurements were conducted. Area measurements were done in SEM lab on thin sections. These measurements are only 2D. But are a first approach giving a rough idea of the porosity



present. 5 area measurements on each selected sandstone sample were done. Area measurements were executed on the most prominent reservoir sandstone samples, and the results are presented in Tables 4.10 and 4.12, together with point counted porosities. IGV was calculated for all the samples and listed in Tables 4.9 and 4.11, together with point counted porosities.

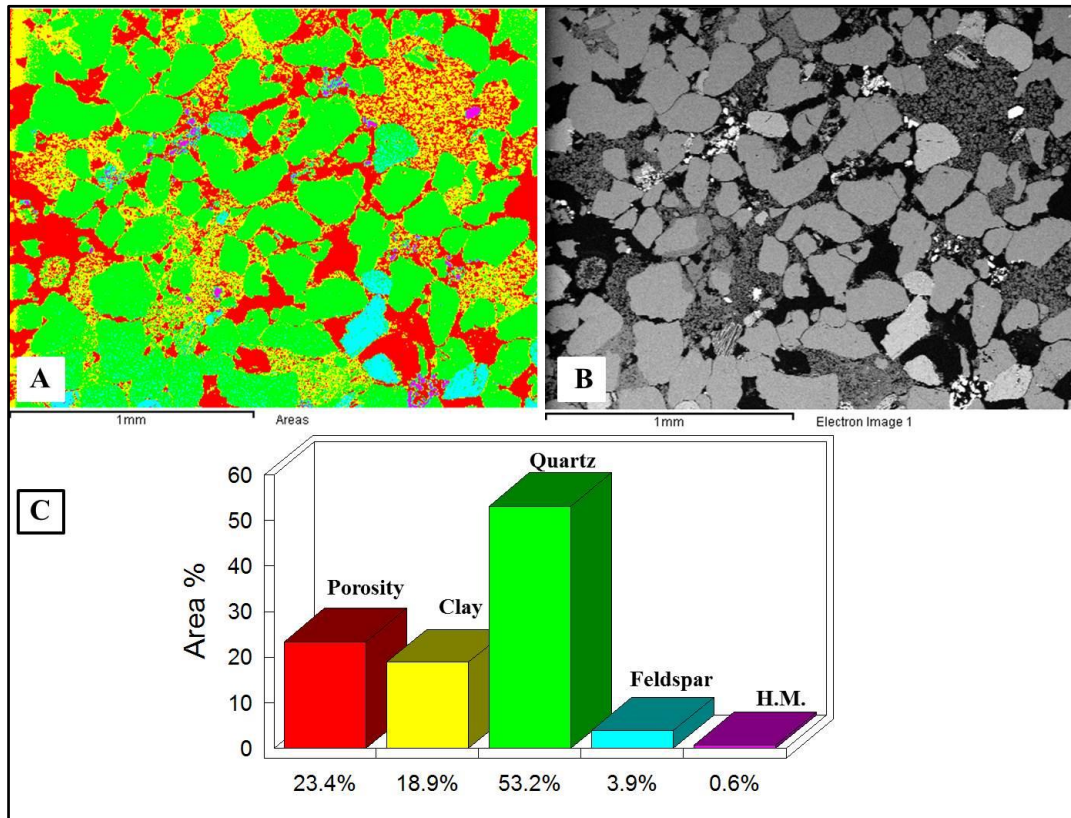
### Upper Kipatimu Mb. (Kimmeridgian – Tithonian)

Point counted porosity from Upper Kipatimu Mb. varies from 5,5% to 21,5%, with an average of 11,3% (Table 4.9).

*Table 4.9: Point counted porosity and calculated IGV of the studied samples from Upper Kipatimu Mb.*

Formation	Sample	Porosity %	IGV %
Kipatimu	MN-1-6-13	8,7	39,4
Kipatimu	MN-1-5-13	21,5	36,4
Kipatimu	MN-1-3-13	13,5	37,9
Kipatimu	MN-2-1-13	7,5	41,4
Kipatimu	MN-2-3-13	5,5	37,5
Kipatimu	<b>Average</b>	<b>11,3</b>	<b>37,6</b>
Mitole	NG-1-2-13	26,7	41,4
Mitole	NG-1-5-13	21,2	41,7
Mitole	NG-1-1-13	19	38,4
Mitole	NG-2-1-13	11	33,8
Mitole	<b>Average</b>	<b>19,5</b>	<b>38,8</b>
Makonde	MB-2-2-13	16,5	31,7
Makonde	MB-2-1-13	14,7	35,8
Makonde	MB-2-4-13	27,2	34,7
Makonde	MB-1-7-13	14,7	37,9
Makonde	MB-1-4-13	19,2	44,3
Makonde	<b>Average</b>	<b>18,5</b>	<b>36,8</b>

Area measurements from sample MN-1-5-13, showed porosities between 22,0% and 22,7% making up an average of 25,2% (Table 4.10). Figure 4.43 illustrates one area measurement with a porosity of 23,4% (red color), clay content of 18,9% (yellow color), quartz (53, 2%), feldspar (3, 9%) and heavy minerals 0,6% (purple).



**Figure 4.43:** Porosity analysis of sample MN-1-3-13. A) Micrograph image from SEM, with color indexes. B) Micrograph image from SEM, backscatter. C) Area measurement results from sample MN-1-5.13. With the color indexes; red areas are pores, yellow are clays, green is quartz, blue is feldspar, purple is heavy minerals.

Porosity values obtained by area measurements of sample MN-1-5-13 are presented in Table 4.10.

**Table 4.10:** Area measurement results from sample MN-1-5-13, Upper Kipatimu Mb.

Sample	Porosity %	Sample	Porosity %	Sample	Porosity %
MN-1-5-13	26,8	NG-1-1-13	19,5	MB-2-2-13	9,6
MN-1-5-13	27,7	NG-1-1-13	17,5	MB-2-2-13	23,3
MN-1-5-13	26,0	NG-1-1-13	21,9	MB-2-2-13	22,8

<b>MN-1-5-13</b>	23,4	<b>NG-1-1-13</b>	20,2	<b>MB-2-2-13</b>	20,9
<b>MN-1-5-13</b>	22	<b>NG-1-1-13</b>	17,7	<b>MB-2-2-13</b>	17,6
<b>Average</b>	25,18	<b>Average</b>	19,7	<b>Average</b>	18,8

### **Upper Mitole Mb. (Kimmeridgian – Berriasian)**

Point counting of key samples from Upper Mitole Mb. displays an average porosity of 19,5%. The calculated IGV varies from 33 to 41% within the analyzed samples (Table 4.9). Sample NG-1-1-13 has a porosity of 19% and is a representative sample from the Upper Mitole Mb. outcrops (Table 4.9). From area measurements the values range between 12,9% and 21,9%, with an average porosity of 19,7% (Table 4.10).

### **Makonde Fm. (Aptian – Albian)**

The average porosity from point counting analysis is 18,5% in the Makonde Fm. Calculated IGV varies from 31 to 44%, with an average of 36 % (Table 4.9). Sample MB-2-2-13 displayed a porosity of 16,5% from point counting (Table 4.9). The values obtained from the area measurements vary from 9,6-23,3%, with an average of 18,8% (Table 4.10).

### **Drill hole 24 (Albian – Turonian)**

Point counting of the samples from borehole 24 displays a large variation in porosity from 0,5 up to 17,7%, where the samples with low porosities are carbonate cemented (Table 4.11).

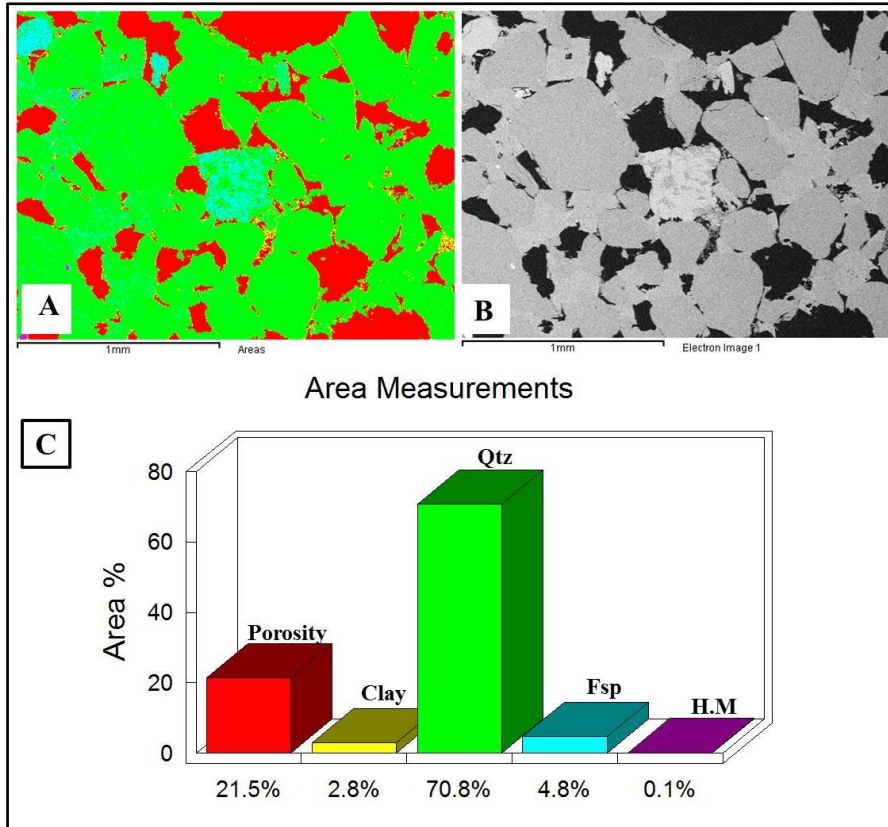
The results of point counting of sample 24/28/3 5-8 displays a porosity of 16%, while area measurements of these samples display an average porosity of 23,4% (Table 11 and 12, Figure 4.44). Area measurements of sample 24/28/3, show porosities between 22,0%-22,7% making up an average of 25,2% (Table 4.12). Figure 4.44 illustrates one area measurement with a porosity of 23,4% (red color), clay content of 18,9% (yellow color), quartz (53, 2%), feldspar (3, 9%) and heavy minerals 0,6% (purple).

**Table 4.11:** Point counted porosity and calculated IGV from analyzed samples in cores from well site 24.

Sample	Porosity %	IGV %
24/17/3 9-10	2,2	28,5
24/16/3 13-16	8	40,5
24/28/3 5-8	16	30,9
24/28/1 57-59	0,5	33,2
24/13/2 62-64	4,5	42,9
24/30/1 3-5	17,7	26,7
<b>Average</b>	8,15	33,7
Sample	Porosity %	IGV %
21/17/2 82-84	25,7	37,2
21/17/2 56-58	1,2	39,4
21/24/1 10-12	1,2	41,1
21/25/1 5-6	21,2	40,2
21/20/1 88-90	4,5	44,5
21/17/3 23-25	1,7	47,6
<b>Average</b>	9,25	41,7

### **Borehole 21 (Cenomanian – Coniacian)**

Average point counted porosity values from key samples from the cores from well site 21 vary between 1,2% and 25,7% (Table 4.11), where samples with low porosity are carbonate cemented. Area measurements of sample 21/35/1 5-6 display porosity values ranging from 26,7% and up to 34,1%. Average porosity in this sample is 29,5% (Table 4.12).



**Figure 4.44:** Porosity analysis of sample 24/28/3. A) Micrograph image from SEM, with color indexes. B) Micrograph image from SEM, backscatter. C) Area measurement results from sample 24/28/3. With the color indexes; red areas are pores, yellow are clays, green is quartz, blue is feldspar, purple is heavy minerals.

**Table 4.12:** Results of SEM area measurements of sample 24/28/3 5-8.

Sample	Porosity %	Sample	Porosity %
24/28/3 5-8	21,5	21/35/1 5-6	28,7
24/28/3 5-8	21,6	21/35/1 5-6	25,4
24/28/3 5-8	26	21/35/1 5-6	32,5
24/28/3 5-8	31,1	21/35/1 5-6	34,1
24/28/3 5-8	17	21/35/1 5-6	26,7
<b>Average</b>	23,4	<b>Average</b>	29,48



## **5. Discussion**

### **5.1 Facies associations and depositional environment**

The facies associations described from logged field outcrops (FA2, FA3, FA4) comprises Upper Kipatimu Mb., Upper Mitole Mb and Makonde Fm. of Late Jurassic – Mid Cretaceous age. The facies associations identified in the cores from well sites 24 and 21 comprise facies associations FA5, FA6, FA7 and FA8 of Mid-Cretaceous – Late Cretaceous age. The cores from well sites 24 and 21 are equivalent in time with the Kihuluhulu Fm. (Figure 4.2). Mandawa Basin was experienced several regressive and transgressive phases throughout Upper Jurassic to Pleistocene (Hudson, 2011).

#### **5.1.1 FA2 - Upper Kipatimu Mb.**

The FA2 facies association, identified within the Upper Kipatimu Mb., is dominated by the red sandstone facies F1 (Table 4.3) (Figure 4.2 and 4.19). The sandstone is highly cross bedded with planar foresets, and consists of several upwards fining sequences with erosive bases. Upper Kipatimu Mb. is interpreted as fluvial channel deposits by Hudson (2011). A fluvial depositional environment is also suggested for FA2 in this study.

Channelized deposits are observed in FA2 and contain several upwards fining sequences. These sequences indicate a decrease in stream power from an initial high energy erosive phase, and leads to the interpretation of migrating channels (Collinson, 1986). Further, the thickness of these upwards fining sequences varies from 20 cm to 5 m, with grain sizes varying from fine to very coarse. Variations in both thickness and grain size most likely reflect differences in channel slope and channel curvature (Allen, 1970). The fluvial style is interpreted to be a braided river system, dominated by permeable coarse-grained sand and gravel as discussed by Morad et al. (2010). Meteoric waters can circulate more easily through coarse grained sands of better connected braided deposits compared to meandering systems (Nelson, 1994).

Within the FA2 facies association, a 30 cm parallel laminated unit of facies E2 stands out (Figure 4.2). The facies contains a distinct lamination that comprises a segregation of grain size and heavy and light minerals (Figure 4.26 C). The basal layer in these laminations is apparent due to concentration of zircon, apatite and anatase. Both the mineralogical and

textural differences enhance each lamina, which is observed by bands of dark colored heavy minerals alternating with light colored quartz-rich lamina. This type of evenly laminated sand can be obtained from bed flow during wave backwash at beaches (Clifton, 1969). This separation of heavy and light minerals is also observed and discussed in braided rivers systems by Hjellbakk (1997). He discusses this feature in planar horizontally stratified sandstone facies, as a result of hydrodynamic sorting, thus supporting the theory of these deposits originating from a braided high energy fluvial system. In addition, no marine fossils are observed in the sandstone, reinforcing the theory of an alluvial depositional environment.

The color of the FA5 (Upper Kipatimu Mb.) sandstones is brick red due to a high abundance of ferric iron (Figure 4.19). Oxidized iron is observed as grain coating, pore filling cement and as infill of micro fractures in feldspar and quartz grains. These types of red beds may form in several environments; arid, desert conditions or seasonal climates. The red color is produced when the iron is taken in to solution through decomposition of ferromagnesian minerals and oxidized to  $Fe^{3+}$  (Morton and Hallsworth, 1999, Besly and Turner, 1983). In desert deposits the grain sizes range between 200-300  $\mu m$ , while Upper Kipatimu Mb. sandstones displays grain size variations from fine to very coarse sand. Further the majority of the sandstone samples can be classified as moderate sorted and with subangular shape, which are inconsistent with prominent features of desert deposits (Laming, 1966). These observations consequently favor that these Upper Kipatimu Mb. beds originate from channelized fluvial processes.

### **5.1.2 FA3 - Upper Mitole Mb.**

FA3 is found within the two logged sections of Upper Mitole Mb., at Ngoro (Figure 4.4). The association is characterized by coarse, cross bedded sandstone, with sigmoidal and planar foresets (facies F1 and F2) (Figure 4.20) (Table 4.3), and tidal bundles with mud couplets. The Upper Mitole Mb. is interpreted as fluvio-deltaic deposits by Hudson (2011). In this study a sub tidal channel environment is proposed for the FA3 facies association.

Cross bedded sandstone with tidal bundles bounded by mud couplets are primary sedimentary structures associated with dominant tidal currents (Smith, 1988, Visser, 1980). A mud couplet is characteristic of the subtidal zone, displaying two slack water stages during a flood-ebb cycle (Nio and Yang, 1991).

Further, this association displays several intervals of parallel laminated fine sandstone (facies E1 and E2). These thin sand laminae can be associated subordinate tidal flow (Smith, 1988). Reactivation surfaces of the foresets within the cross bedded units are observed, which can be produced by unidirectional flow (De Mowbray and Visser, 1984). The first 6 m of Upper Mitole Mb. (level 0 – 6) (Figure 4.20) are slightly upwards fining, while the upper part of section 1 and the whole section 2 (level 6 – 13 m) is upwards coarsening. This upwards coarsening trend could indicate a progradational tidal channel with a higher sedimentary input and higher energy, resulting in upwards coarsening and thickening units. This interpretation, of Upper Mitole being a progradating tidal channel, is further supported by the observations made by Hudson (2011).

### **5.1.3 FA4 - Makonde Fm.**

The FA5 facies association was studied at Mbate (Figure 1.1) and consists of two logged sections of Makonde Fm (Figure 4.3). The FA4 facies association is dominated by fine to very coarse sandstone (facies B, H, E2) (Figure 4.21). Sand and siltstone facies (A and E1) is present in the lowermost part of section 1 (1-2 m). Sandstone with cross stratification and clay-rip up clasts are predominant structures within this association. These observations are typical features of channelized deposits, and are interpreted to be deposited by a terminal distributary channel. The parallel laminated beds composing of fine sand (0-1 m) , unlike the coarse trough cross stratified beds, are interpreted to be mouth bar deposits interbedded with the terminal distributary channel deposits (Olariu and Bhattacharya, 2006). The trough cross stratification could represents dune migration of lower flow regime (Brierley, 1989).

The depositional environment of FA4 sandstone is interpreted to be more subaqueous in origin, than the sandstones of FA2 facies association. This is due to the color of FA4 being light yellow/grey, and not brick red as the sandstone of Upper Kipatimu Mb. Still, some features indicates a partial subaerial exposure, as the presence of red Fe-oxide staining.

The presence of the mud facies (A1) within FA4 may indicate an overbank deposit where the depositional rate is slower due to diminishing flow, or by overbank flooding of an adjacent active channel (Elliot, 1986). The rip-up clasts are thought to be eroded from low-energy deposits and redeposited in high energy environments. Erosion of floddplain deposits, facies A, are common in fluvial channel deposits as described by Morad (2010).

The Makonde sandstone is in general upwards coarsening and may display progradational channel fill deposit (Van Heerden and Roberts, 1988).

#### **5.1.4 Well site 24 (Albian – Turonian)**

The cored sections from well site 24 are interpreted to consist of three facies associations; (1) FA5; (2) FA6; (3) FA7. The lowermost cores (level 0 – 10 m) consist of sandstone association FA5. Further up the clay association FA6 dominates (level 10 – 53 m) the cores. The upper cores are interpreted as the FA7 association (level 53- 90 m). The detailed log with the facies associations is presented in Appendix A.

##### **FA5 (Kihuluhulu Fm.)**

This silt and sandstone association is dominated by sparsely bioturbated sandstone of facies F3a and F3b, interbedded with claystone facies F1 (Figure 4.22, Table 4.4). The bases of the different sandstone units display a variation between erosional and sharp bases towards the underlying clay- and siltstones. The characteristic cm- to dm-thick sandstone beds within FA5 are decreasing in thickness upwards, and the sandstone beds are interpreted to be higher energy events that might be turbidites. Turbiditic currents form when sediments overstep and are liquefied. The liquefied currents move downslope, where sediments within the flow are supported by the upward-moving component of fluid turbulence. Sediments within the turbiditic current fall out of suspension when the current strength decreases (Lowe, 1976). Further, the FA5 facies association is slightly upwards fining, shifting from coarse and very coarse sandstone (F3a and F3b) to siltstone facies (F2). The claystone and siltstone beds interbedded with the sandstones may have been deposited as background sedimentation. An upper slope environment is proposed for FA5, where the sandy intervals are interpreted to represent higher energy events (Pearson et al., 2004, Jiménez Berrocoso et al., 2010). A similar depositional environment is described by Hill (1984) in the Nova Scotian upper continental slope.

##### **FA6 (Kihuluhulu Fm)**

The FA6 facies association is dominated by dark silt and clay of facies F1, F2 and F4 (Figure 4.23) (Table 4.4). The sediments within FA6 are characterized by few sedimentary structures, but irregular beds of scarce lamination occur. FA6 appears to have a gradational transition from the underlying FA5 association. The structureless claystone and siltstones may represent

a more proximal position, possibly on the quite outer continental shelf, compared to FA5. The mud dominated sediments could be deposited from suspension from sediments higher up in the water column, or sediments in suspension derived from turbulent plumes (Mulder and Alexander, 2001). Further, the wispy laminations and lack of bioturbation could reflect an oxygen depleted environment (Ekdale, 1984). Based on the lack of sedimentary structures, and the overall fine grained sedimentation in FA6 could represent deposition in an outer shelf environment below storm wave base, as discussed by Jiménez et al. (2010). The association could also represent an upper slope environment, since sediment supply and energy conditions on the shelf break are highly variable. The alteration between clay, silt and sand within FA5 could also relate to different current intensities on the upper slope, and the sedimentation could reflect either suspended or resedimentated material from the shelf (Piper et al., 1976).

#### **FA7 (Kihuluhulu Fm.)**

The FA7 facies association is dominated by siltstone facies F2, with irregular interruptions by clay facies F1 and sandstone of facies F3a (Table 4.4) (Figure 4.24). Interruptions by the sandy intervals are interpreted to originate from higher energy transportation, and may indicate that bottom currents were relatively common (Pattison, 2005). FA7 is located on top of silt- and claystone association FA6, and a transition from darker colored clay and silt to a lighter colored siltstone is observed. FA7 displays bioturbation, frequent sandstone beds and a general coarser grain size than the underlying facies association. This could also indicate that the depositional environment was shifting towards a more distal position towards the upper slope, but with a lower energy environment compared to FA5 (Jiménez Berrocoso et al., 2010). Upper slope environments with similar facies of bioturbated silt and fine sandstones are described by several authors (Piper et al., 1976, Hill, 1984). The finer sediments on the upper slope could represent rapid hemipelagic sedimentation fed by sediment thrown in suspension by turbiditic currents (Hill, 1984).

#### **5.1.5 Well site 21 (Cenomanian – Coniacian)**

The cored sections from well site 21 are interpreted to consist of three facies associations: FA5, FA7 and FA8. The lowermost association (level 0 – 29 m) is interpreted to be the FA5 association. Further up, clay association FA8 dominates with a thickness of 21,5 m (level 29 –



53 m). The upper cores are interpreted as the FA7 association (level 53- 73 m). The complete detailed log of the cores from well site 21 is presented in Appendix B.

#### **FA5 (Kihuluhulu Fm.)**

This sandstone association is described in chapter 5.1.5. Cores from well site 21 FA5 consists mainly of sandstone facies F3a, F3b, F6 and F7, and the sandstone units are often upwards fining and contain clay rip-up clasts. Further, irregular clay- and siltstone beds of facies F1 and F2 are interbedded within the dominant sandstone facies. There are several units within core 21 that could represent parts of Bouma sequences. A complete Bouma sequence is normally not observed in field studies (Shanmugam, 1997). In this study, especially one 30 cm thick unit stands out within core 17. The unit display massive coarse sandstone with a basal lag, normal grading and an erosive base. This unit could represent the A-layer within a Bouma sequence. Continuing upward in the unit parallel laminated fine sandstone is present, which could represent the B-layer. Following the B-layer a cross laminated fine sand unit grades over to wavy lamination and ends up in structureless mud, which could represent the C- and E-layers, respectively. This 30 cm thick sandstone bed could represent a more or less complete Bouma sequence (Bouma, 2004, Lowe, 1976). The FA5 association is interpreted to represent a transgressive phase, mainly due to the association being upwards coarsening. In addition the sandy beds within FA5 are thicker than the sandstone units within FA5 in core 24. This could reflect that the turbiditic currents were larger in cores from well site 21, and that the sediment supply was higher at the time of depositions. This type of interpretation was discussed by Piper et al. (1976), who described facies within a slope environment.

#### **FA8 (Kihuluhulu Fm.)**

The FA8 facies association is dominated by dark grey claystone of facies F1 (Table 4.4). The clay is structureless, but there are some intervals that are poorly laminated. The clay intervals with sparse bioturbation could be interpreted as shelf muds (Johnson and Baldwin, 1986). The clay within this facies association is suggested to have been deposited in a restricted oxygen environment. Observations of the mud being dark grey/black and the development of weak laminations could infer that few bottom dwellers were present (Myrow, 1990, Morris, 1979). The few laminated intervals could perhaps indicate periods of relatively high sediment supply, where bioturbation did not destroy the sedimentary structures (Hill, 1984). Jiménez et al. (2010) interpreted the deposits to derive from a shelf environment with low energy, and

deposition below the storm wave base. An outer shelf environment is proposed for the FA8 association in this study, where the mud facies could have been deposited in the low energy environments. Crockett and Nittrouer (2004) described a sandy inner shelf, where mud facies dominated the outer part of continental shelf, where the energies were low.

### **FA7 (Kihuluhulu Fm.)**

FA7 displays variation between bioturbated mud- and siltstone of facies F1, F2, F4 and F8. This facies association is located on top of the clay dominated facies association FA8, and a sharp transition between the two associations is observed. As discussed earlier in chapter 5.1.4, bottom currents and events of higher energy are a possible explanation for the frequent silt and sandstone layers. The presence of mud facies could be explained by longer periods of lower energy, where deposition of suspended particles was the main background sedimentation. An upper slope environment is proposed by Jiménez (2010), which fits well with the interpretation of FA7 done in this study. FA7 appears more distal compared to the underlying FA8 facies association.

## **5.2 Petrography and diagenetic history**

Sediments and sedimentary rocks are mixtures of mineral grains and rock fragments, as a result of weathering, reworking, transportation and diagenesis of the parent rock (Pettijohn et al., 1972). Weathering is the most important sediment producing process, and the rate of weathering is related to rock type, precipitation, climate, relief etc. (Bjørlykke, 2010). Mechanical weathering breaks rocks into smaller fragments, without significant change in chemical or mineralogical composition. Chemical weathering processes are the most important, since these processes alters both the chemical and the mineralogical composition of the rocks (Boggs, 2010). The most active of these weathering processes depends on factors such as climate, precipitation and relief (Nesbitt et al., 1997).

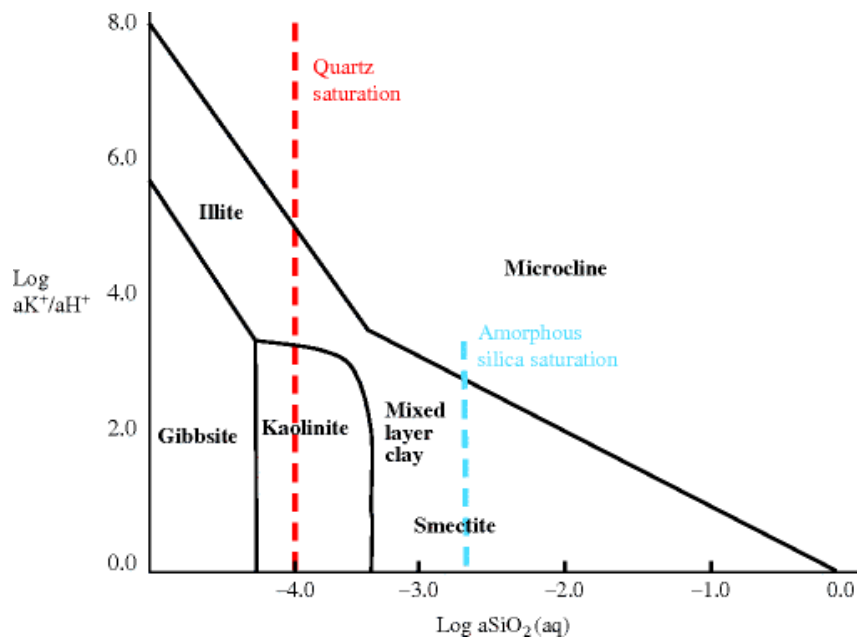
The following chapters discuss the petrography and the diagenetic history of the studied sandstones from field outcrops and cores. Upper Kipatimu Mb. will be discussed first, then Upper Mitole Mb. and Makonde Mb. will be discussed together due to similarities in petrography and diagenetic relations. Finally, cores from well sites 24 and 21 will be discussed together due to abundant similarities.

### 5.2.1 Field outcrops

#### Upper Kipatimu Mb.

Upper Kipatimu Mb. displays very coarse grain sizes with varying degree of sorting, and subrounded to angular grain shapes. The weathering degree of the framework grains is severe, and feldspar grains display a preservation grade of category 4-5 (Table 3.3). This preservation may be a result of intense weathering in a tropical climate, where the weathering is at a maximum (Carroll, 1970). Upper Kipatimu Mb. sandstone is the eldest succession studied, and has a longer exposure time in the weathering system compared to Upper Mitole Mb. and Makonde Fm. An average quartz/feldspar ratio of 7 indicates that this sandstone is more mature than the sandstones of Upper Mitole Mb. and Makonde Fm. Further, the lack of plagioclase indicates that the sandstone has been subjected to severe weathering compared to Upper Mitole Mb. and Makonde Fm., since plagioclase is one of the least resistant minerals when subjected to weathering (Ma and Liu, 1999). The coarse nature of the sandstone may imply a more proximal deposition compared to Upper Mitole and Makonde Fm.

Authigenic kaolinite is apparent as pore filling cement in optical microscopes studies. XRD analyses show that kaolinite constitutes an average of 8,3% of the bulk mineralogy. The authigenic kaolinite observed in the SEM analysis commonly displays the characteristic booklet stacks (Lanson et al., 2002). The coarse nature of the sandstone could allow meteoric water to flow easily through it due to high permeability, and leaching by meteoric water is generally strong in fluvial and alluvial sediments (Morad et al., 2010). Kaolinite can precipitate during meteoric water flushing as a result of dissolution of feldspar and mica. For kaolinite to precipitate, the silica ( $K^+$  and  $Na^+$ ) must constantly be removed from the system. A low  $K^+/H^+$  ratio and a constant removal of cations ( $Na^+$  and  $K^+$ ) is required, so that the porewater can remain in the stability field for kaolinite (Bjørlykke, 1997) (Figure 5.1). Furthermore, abundant kaolinite is typically developed as a weathering product in fluvial channel sediments within tropical and subtropical climates, where rainfall is abundant. Active percolation of unsaturated meteoric water causes dissolution of detrital silicates and precipitation of kaolinite (Potter et al., 1980, Morad et al., 2000). The abundant kaolinite in Upper Kipatimu Mb. is thought to have formed in periods of high meteoric flushing rates. The kaolinite in Upper Kipatimu Mb. is mostly pore filling and abundant within the primary intergranular pores, and is observed in relation to dissolved feldspar and mica.

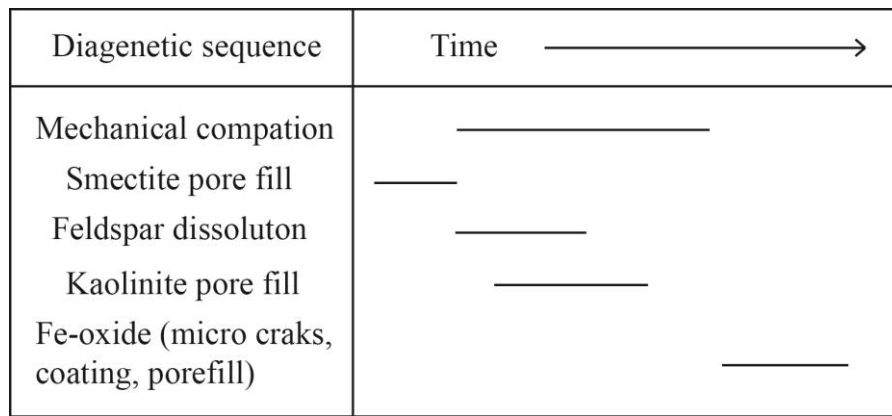


**Figure 5.1:** Logarithmic activity diagram showing stability of smectite and kaolinite as a function of silica and the  $K^+/H^+$  ratio, modified by Bjørlykke (2010) from Aagaard and Helgeson (1982).

The kaolinite examined in the EMP did not display any significant elemental variations between the inferred detrital kaolinite and the authigenic kaolinite (Figure 4.40) (Table 4.6). Several authors have studied similar intergrowths of kaolinite and muscovite, and most of them conclude that the kaolinite is authigenic and formed due to alteration of muscovite (Bjørlykke, 1986, Burkley and MacQuaker, 1992).

The abundant Fe-oxide, discussed in chapter 5.1.1, is thought to be formed as a late diagenetic process. The Fe-oxide occurs as pore filling cement, grain coating and within microcracks. Oxidizing conditions at a late stage, in connection with surface weathering, is interpreted to be the mechanism for the precipitated Fe-oxide. Further, the previously discussed kaolinite seems to predate the abundant Fe-oxide. A similar sequence is discussed by Khidir and Catuneanu (2003) of fluvial sandstones in the Red Deer Valley region of central Alberta.

The sequence of diagenetic events, determined from thin sections and SEM examinations is summarized in Figure 5.2. Early diagenesis includes (1) Initial mechanical compaction; (2) pore filling detrital smectite (3); dissolution of feldspar; (4) authigenic kaolinite; (5) formation of Fe-oxide as coatings, pore fill and precipitation within microcracks.



*Figure 5.2: Generalized diagenetic sequence of Upper Kipatimu Mb.*

### **Upper Mitole Mb. and Makonde Fm.**

Upper Mitole Mb. and Makonde Fm. are both interpreted to be channel deposits. Upper Mitole Mb. is slightly coarser in grain size, compared to Makonde Fm., with mainly well to moderately sorted sand. The quartz/feldspar ratios are 2 and 3 for Upper Mitole Mb. and Makonde Fm., respectively. Further, the plagioclase/K-feldspar ratio is between 1,2 and 1,4 for all the studied samples, and the feldspar preservation is mainly categorized as category 3 within both sandstones. The feldspars are better preserved in Upper Mitole Mb. and Makonde Fm. compared to Upper Kipatimu Mb., which is thought to be a combined effect of less meteoric water flushing, less exposure time in the weathering system, and the abundant clay coatings. The finer grain size, better sorting and less angular grains may indicate that these sandstones have a more distal deposition compared to Upper Kipatimu Mb. In addition, these sandstones are yellow/white in color, which infers that the sandstones have been flooded by water, compared to the red sandstones of Upper Kipatimu Mb.

The authigenic kaolinite is much less abundant in Upper Mitole Mb. and Makonde Fm., compared to Upper Kipatimu Mb. Only Upper Mitole Mb. displays kaolinite in one sample (NG-2-3-13) from the XRD analysis (4,5%). Studies in SEM and the light microscope display pore filling authigenic kaolinite in all the sandstone samples from both Upper Mitole Mb. and Makonde Fm. The amounts of kaolinite are probably below detection limit, and do not appear in the XRD analysis. Pore filling kaolinite in Upper Mitole Mb. and Makonde Fm. is probably a result of early diagenetic processes by meteoric water flow or surface weathering, as discussed previously for the Upper Kipatimu Mb.



Clay coatings in both Upper Mitole Mb. and Makonde Fm. consist of a mix of smectite and chlorite. Smectite-chlorite mixed clay described by Ku and Walter (2003) have a similar SEM energy dispersive spectrum as sandstones of Upper Mitole Mb. and Makonde Fm., which reinforces the interpretation of the analyzed clay coating being a smectite-chlorite mix. The clay coating appears to be authigenic, as indicated by crystal morphology and the radial orientation. Authigenic clays often exhibit crystalline habits and this observation is the most widely used criterion to distinguish authigenic clays from allogenic clays (Wilson and Pittman, 1977).

Authigenic clay may form through reactions between the precursor minerals on framework grains and the contained waters during regeneration. Authigenic clays generate and regenerate during burial diagenesis (Wilson and Pittman, 1977, Aagaard et al., 2000). The precursor mineral could in this case be a smectite obtained from mechanical infiltration. Mechanical infiltrated smectite is more abundant in coarser grained braided fluvial sands, compared to other fluvial deposits (Morad et al., 2010). Salem et al. (2000) discussed a smectite precursor in fluvial sandstones that regenerated into a mixed chlorite-smectite. The presence of smectite minerals in the sandstones of Upper Mitole Mb. and Makonde Fm. could be a result of early silica diagenesis, which is one of the fundamental reactions in clastic basins (Pettijohn et al., 1972). Silicon and aluminum have very low solubility, and form new silicate minerals. Since quartz displays very low precipitation rates at low temperatures, it allows precipitation of silica-rich phases, such as smectite. Smectites require a porewater composition with relatively high silica content (Figure 5.1) and are often found in sediments derived from volcanic rocks (Bjørlykke, 2010). Sediments found in the Mandawa basin could derive gneisses within the Mozambique belt east of the Tanzania craton (Nerbråten, 2014), which contain soluble silicate.

The smectite precursor present on the framework grains may have accumulated due to mechanical clay infiltration, by seepage of muddy waters through the coarse alluviums (Moraes and De Ros, 1990). Infiltration of muddy surface runoff, with a high abundance of clay particles, may deposit fine suspended loads within the alluvial sediments. The accumulation of these muds may be concentrated in the pheratic zone. When seepage reaches the water table, the percolation velocity decreases, and clay can accumulate. Accumulation of such clays may also develop above impermeable layers during periods of surface runoff and flooding. Evaporation of such suspended water tables accumulate clays (Moraes and De Ros, 1990). These mechanisms could explain for the accumulation of clay precursors in Upper

Mitole Mb. and Makonde Fm. Further, the distribution of the mechanically infiltrated clay is highly heterogeneous vertically and laterally within braided river systems (Morad et al., 2010). In Upper Mitole Mb. and Makonde Fm. the authigenic clay, originating from mechanically infiltrated clay, appears in all the studied samples.

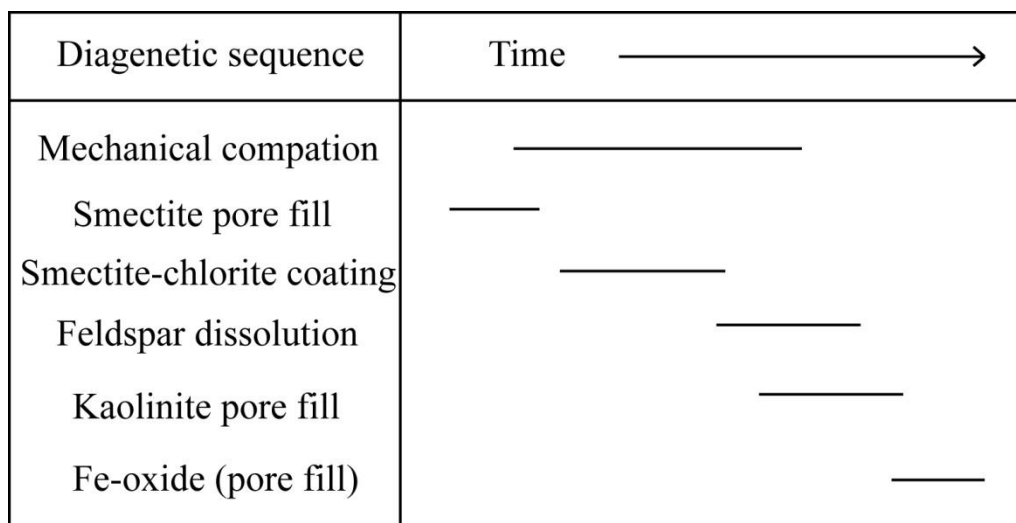
Mechanical mud infiltration is enhanced by proximity to the source of influent seepage, such as basin margin highs and channels. Infiltration beneath channels can accumulate large volumes and thick zones of clay, as the channel directions shift laterally and thereby the location of where the clay infiltrates (Morad et al., 2000). Crone (1975) found that infiltrated clays occurred as grain coatings, where the clay particles were orientated parallel to the grain surface. It is important to emphasize that the recognition of such infiltrated clays that have undergone burial diagenesis is difficult in ancient sandstones. Further, during burial the infiltrated clays will be subjected to diagenetic reactions that will result in transformation of recrystallization (Matlack et al., 1989). Moraes and De Ros (1992) described mechanical infiltrated smectite in fluvial sandstones, that changed composition to a smectite-chlorite during burial. It is therefore considered that the infiltrated clays acted as the precursor mineral on the framework grains, thus allowing regeneration of the smectite to a smectite-chlorite coating.

Comparing Upper Kipatimu Mb. with Upper Mitole Mb. and Makonde Fm. the sandstone of Upper Kipatimu Mb. does not display the same smectite-chlorite coating. The absence of clay coatings could be related to a more humid climate during deposition of Upper Kipatimu Mb., compared to the two other formations. This is inferred by the high amounts of kaolinite in Upper Kipatimu Mb. and relatively small amounts of smectite. Further, Upper Kipatimu Mb. displays coarser sand grains which may have led the fine suspended clay materials to seep through and not accumulate. In addition Upper Kipatimu Mb. display a slightly poorer sorting, which could affect the infiltration process (Matlack et al., 1989). Upper Kipatimu Mb. display a coarser grain size and would be expected to be exposed to a greater volume of pore fluid and thus accumulating infiltrated clay, but reworking of sediments in the upper zones of the alluvial setting commonly eliminates such accumulations (Moraes and De Ros, 1990).

From petrographic relations, the timing of the smectite coating is determined. Firstly, smectite coatings are typically absent along grain contacts, which point out that the coating was formed after the sand grains had come in contact, and adjusted to their present relative position by mechanical compaction. Secondly in certain places the smectite rims form hollow structures

outlining the original grain boundaries of dissolved grains, and most of the feldspars are moderately weathered. This indicates that the regeneration of smectite predates the feldspar grain dissolution. Smectite coating must have occurred after the sandstone framework had become stabilized, otherwise the delicate grain molds of feldspar would have collapsed (Ehrenberg and Boassen, 1993). The kaolinite are thus interpreted to have formed after the smectite coating, as observed in Figure 4.29 C, where the kaolinite seems to postdate the authigenic formed smectite-chlorite. Much of the present kaolinite may be a product of surface weathering in the outcrops as described by Baker (2000), who also studied fluvial sandstones from field outcrops and cores.

The sequence of diagenetic events, as determined from thin sections and SEM examinations is summarized in Figure 5.3. Early diagenesis includes (1) Initial mechanical compaction; (2) pore filling detrital smectite; (3) regeneration of mechanical infiltrated clay; (4) dissolution of feldspar; (5) authigenic kaolinite; (6) formation of minor pore filling Fe-oxide. A similar sequence is discussed by Billaut et al. (2003) who described a diagenetic sequence in grain-coated sandstone reservoirs.



**Figure 5.3:** Generalized diagenetic sequence of Upper Mitole Mb. and Makonde Fm.

Alteration during weathering of the sampled outcrops may have occurred, but it is difficult to differentiate weathering from diagenetic alteration. The diagenetic mineralogy of the sediments described from the outcrops differs considerably from the sediments sampled from the cored boreholes, presumably because of the direct influence of recent weathering processes, as observed by Strong and Mildowski (1987).

### 5.2.2 Well sites 24 and 21

Studied sandstone samples from the cores display medium to coarse grain sizes, where compaction is weak to moderate. Feldspars in the core samples are mostly classified as category 3 (Table 3.3). The quartz/feldspar ratio ranges from 4 up to 13, and the plagioclase/K-feldspar ratio ranges between 0,4 and 0,6. These ratios indicate more mature samples compared to the field samples of Upper Kipatimu Mb., Upper Mitole Mb. and Makonde Fm. Feldspar minerals are far more abundant than rock fragments in the core samples, and they classify as arkosic sandstones. In general monocrystalline quartz dominates the quartz fraction of the samples. In addition, the sandstone samples from the cores display a higher abundance of quartz with undulatory character compared to the field samples. The amount of undulatory quartz could reflect that these sandstones have been affected by higher stress compared to the field sandstones (Conolly, 1965).

Cores from well site 21 and 24 display the lowest kaolinite content of all the studied sandstones in the Mandawa Basin. This can be explained by less meteoric flushing in a distal shelf environment. Clay units within the cores are often located above sandy horizons, which could prevent meteoric water flushing. In addition, these sandstones have had the least exposure time in the weathering realm, which could affect the amount of kaolinite present.

Cementation by feldspar overgrowth is apparent in few samples of cores from well sites 24 and 21 (sample 24/16/3 and 21/24/1). Elemental analysis done by the EMP (Table 4.8) revealed a composition close to the pure end-member of K-feldspar, with an average composition of about 65% SiO<sub>2</sub>, 18% Al<sub>2</sub>O<sub>3</sub> and 17% K<sub>2</sub>O (Dypvik and Nesteby, 1992). Notably, there are only minor differences between the detrital core and the authigenic overgrowth. Another detected feature is minor amounts of BaO present within the detrital core, which is more or less absent in the overgrowth. The absence of BaO within the overgrowth is commonly observed in authigenic K-feldspars. The crystallization of authigenic K-feldspar requires an interstitial environment with a supply of potassium, aluminum and silica ion. The depositional environment of the sandstones within the cores is interpreted as marine, where the marine seawater provides the source of alkali metals (Ali and Turner, 1982). The feldspar overgrowths are present within the calcite cemented units, and could have formed before or contemporary with the calcite cementation. Feldspar overgrowth is considered to be near-surface and shallow subsurface cement as discussed by Loucks et al (1977).

Carbonate cement is the most abundant cement in the cores. Calcite is the predominant mineral determined by XRD analysis, which is the most common carbonate mineral cementing up sandstones (Pettijohn et al., 1972). Dolomite and ankerite cements are also found in the cores but in minor amounts compared to the calcite. Further, dolomite and ankerite appear to postdate the calcite cement, notably where calcite occurs together with dolomite and/or ankerite.

The interpreted marine depositional environment of the core sandstones fits well with the common perception of carbonate cement being an early diagenetic process in marine sandstones (Pettijohn et al., 1972). Calcite cement is interpreted to be the earliest diagenetic mineral, indicated by loosely packed framework grains “floating” in carbonate cement, thus preserving intergranular volume. Loose sediments are cemented in environments where there is a significant throughput of pore-fluid saturated with respect to the cement phase present (Tucker, 2001). In the samples where ankerite or dolomite dominate, the dolomite or ankerite is molded directly against the rounded edges of framework grains, thus indicating dolomite or ankerite being the first diagenetic mineral in the samples displaying these carbonate minerals.

Calcite occurs as sparitic cement and is easily differentiated from dolomite and ankerite rhombs in both optical microscope and SEM studies. The calcite cement studied in SEM appears to be composed of low-Mg calcite which is the most stable form, and the composition reflect pore water composition (Andersson et al., 2008). The sparitic carbonate cement in the turbiditic layers may have precipitated from a  $\text{CaCO}_3$  source in the porewater, but most likely in marine sandstones, the source of  $\text{CaCO}_3$  derived from dissolution of pelagic skeletal carbonate grains being mixed in with the turbiditic sands and recrystallizing into carbonate cement (Tucker, 2001, Bjørlykke and Jahren, 2010). Several authors have recognized sparry calcite to represent recrystallized products of earlier deposited and dissolved skeletal fragments in shelf sediments (Dypvik and Vollset, 1979, Hendry et al., 1996). Dolomite may form by replacement of calcite, or by direct precipitation from sea water. Precipitation of ankerite, the ferron variety of dolomite, may indicate precipitation in reducing environments (Tucker, 2001).

In addition, cores from both well sites display some sandstones units that lack carbonate cementation. Inferring that the carbonate precipitated from reworked shelf bioclasts, the different settling rates within the turbidites could lead to a concentration of the carbonate cement in specific layers (Morad et al., 2010). Dolomite zonation studied in EMP show



zonations of darker and lighter zones displaying higher values of Mg and FeO, respectively. This zonation displays a complex growth where darker zones display lower Fe concentrations and higher Mg concentrations, compared to the lighter zones. As discussed by Pye and Krinsley (1986) concentrically zoned rhombs of dolomite could have formed as a result of direct precipitation due to changing pore-fluid composition.

The authigenic kaolinite is observed to have precipitated within secondary pore space in connection with partly dissolved feldspar grains. The SEM examinations revealed that kaolinite overlies the carbonate cement; leading to the conclusion that kaolinite may be one of the latest diagenetic minerals to form in the sandstone. Observation of late diagenetic kaolinite in marine sandstones are described by Gier et al. (2008).

The minor amounts of barite and pyrite cements are also considered to be of the latest diagenetic minerals, and are presumed to have formed in reducing conditions (Pettijohn et al., 1972).

The sequence of diagenetic events is summarized in Figure 5.4. Early diagenesis includes (1) Initial mechanical compaction; (2) feldspar dissolution; (3) feldspar overgrowth; (4) calcite cement; (5) ankerite/dolomite cement; (6) pore filling kaolinite; (7) Pyrite/barite. A similar sequence is discussed by Loucks et al (1977) who described diagenetic sequences within sandstone reservoirs along the Texas Gulf Coast.

Diagenetic sequence	Time <span style="float: right;">—————&gt;</span>
Mechanical compaction	—————
Feldspar dissolution	———
Feldspar overgrowth	—————
Calcite cement	—————
Ankerite/dolomite cement	—————
Kaolinite pore fill	—————
Pyrite	———

**Figure 5.4:** Generalized diagenetic sequence of cores from well sites 24 and 21.

### **5.2.3 Offshore samples**

Thin section analysis of offshore sandstones samples (2/2/14\_a and 2/2/14\_b) show a greater abundance of rock fragments compared to the other sandstones analysed in this thesis, but they classifies as arkosic sandstone. Mica appears as small fragments that are partially altered to smectite-chlorite. The alteration reactions of mica release  $\text{Fe}^{2+}$   $\text{Mg}^{2+}$   $\text{K}^+$  and  $\text{Na}^+$  to pore fluids, from which the authigenic minerals precipitate (Morad, 1990). Clay minerals are absent in the bulk mineralogy analysis, but SEM studies of sample 2/2/14\_a reveal minor amounts of pore filling authigenic smectite-chlorite. The formation of this mixed-clay composition may be related to the long term substitution of K and Mg for Na and Ca. The substitution is a part of the geochemical “maturation process” that sediments of great age and long burial are subjected to (Pettijohn et al., 1972). The smectite-chlorite energy dispersive spectrum (Figure 4.30 and 4.38) is similar to the energy dispersive spectrum obtained from the smectite-chlorite coating in Upper Mitole Mb. and Makonde Fm.

## **5.3 Reservoir sandstones**

Reservoir properties in relation to depositional environments, diagenesis, area measurements and calculated IGV will briefly be discussed in the following chapters.

### **5.3.1 Field outcrops**

Upper Kipatimu Mb., Upper Mitole Mb. and Makonde Fm. are fluvial sandstones which displays relatively high intergranular primary porosities. Total porosity values obtained by point counting display an average porosity of 11,3% for Upper Kipatimu Mb. and 19% for Upper Mitole and Makonde Fm. Area measurements conducted on selected samples displays similar values obtained from point counting, and proved to be a good technique for measuring porosities. Upper Kipatimu Mb. displays slightly higher porosity values in the area measurements, compared to the point counting values. This difference could be obtained due to detection of microporosity within the abundant pore filling kaolinite. All samples have an IGV mean value above 30% indicating that these sandstones have not been buried more than 1000 m depth, which classifies as shallow burial (Paxton et al., 2002). This indicates that these sandstone are within the window of mechanical compaction (Bjørlykke and Jahren, 2010).

The main factors that determine the intergranular porosity are the sedimentological characteristics (grain size, sorting) and the extent of authigenic kaolinite and presence of smectite-chlorite coating. Authigenic clays may have profound effects on properties related to reservoir quality (Wilson and Pittman, 1977). Both kaolinite and smectite-coating in the fluvial sandstone will have a negative effect on the permeability in the sandstones. Kipatimu Mb. contain higher abundance of authigenic clay, in the form of kaolinite, compared to Upper Mitole Mb. and Makonde Fm. Wilson and Pittman (1977) argued that sporadic occurrence of authigenic clay in pores has a less influence on the permeability compared to pore lining clay that restrict pore throats. Upper Mitole Mb. and Makonde Fm. have a higher abundance of authigenic clay coating, combined with minor amounts of authigenic kaolinite. These three sandstones have similar porosity values, but Kipatimu Mb. could display higher permeability with respect to the discussed. The authigenic clay coatings of Upper Mitole Mb. and Makonde Fm. contain microporosity within the authigenic clay coatings. Further, the lateral extension and vertical interconnection of fluvial sand bodies have an impact on the reservoir properties the sandstones. Braided river systems may be laterally extensive due to the lateral accretion of channels and bars (Morad et al., 2010).

### **5.3.2 Well site 21 and 24**

The outer shelf and upper slope sandstones of cores from well site 21 and 24 display highly variable porosity values. Highly cemented layers displays average porosity values of 2,1-3,8%. Uncemented layers and layers with minor amounts of carbonate cement display average porosity values of 20,4%. The area measurements displays higher porosity values than point counting results, and the values are highly dependent on whether one measures an area of dense carbonate cement or not. Still, the point countings seems to better reflect the porosities present in the cored samples, due to less deviations of microporosity. Minor amounts of secondary porosity related to the dissolution of feldspars are present. These values reflect that carbonate cement is the main porosity reducing mechanism in the sandstone samples.

Cement textural relationships and high IGV values (up to 40%) within the carbonate cemented units, supports an interpretation of a early precipitated carbonate cement, and that the sediments are within the mechanical compaction realm (Bjørlykke and Jahren, 2010). In general the sandstones of the studied cores are highly carbonate cemented and display low porosities. Some units display good porosities, where carbonate cement is absent.

Considerable reservoir heterogeneity is obtained due to cemented and uncemented layers within these deposits.

#### **5.4 Offshore-onshore relation**

The offshore samples of Cenomanian age resemble the onshore samples in several ways. Offshore samples are arkosic in composition with low quartz/feldspar ratio, similar to the sandstone samples from Upper Mitole Mb. and Makonde Fm. The offshore samples have undergone weak to medium compaction, reflected in mainly tangential and straight contacts. The most striking feature is the chemical composition of the authigenic pore filling clay in the offshore samples. The SEM energy dispersive spectrum, for both offshore and onshore samples (Upper Mitole Mb. and Makonde Fm.), detected Si, Al and Mg tops, lower Fe tops, and minor amounts of Cl. This suggests a very similar composition as the EDS spectrum from the onshore samples. Further, the continental shelf of Tanzania is narrow (3-10 km) and much of the sediments could originate from the Rufiji and Ruvu deltas, and being transported down slope as turbiditic currents (McDonough et al., 2013). Block 2 is located 80 km offshore Tanzania, and a transport by these mechanisms could be a possibility. Another possibility is that the offshore sediments could have derived from coast parallel surface currents. Several currents are described being active along the coastal Tanzania in recent times (Sætre and Da Silva, 1984, Swallow et al., 1991). The uncertainty lies within how strong these currents were at the time of the sandstone deposition. If the sediments in the offshore reservoirs derived from the Mandawa Basin, it is critical that the sedimentary sequences in the onshore analogues are relatively similar to those in the subsurface with respect to primary mineral composition, as discussed by Bjørlykke (2014). With respect to the petrological findings in this study, the heavy mineral studies done by Nerbråten (2014) and the studies on the clays within the Kilwa Gp. by Mahmic (2014), the sediments in the offshore areas could have derived from the Mandawa Basin.

#### **Further work**

Further studies of the mechanical infiltrated clay in Upper Mitole Mb. and Makonde Fm. are necessary to obtain information about the origin of the clay coatings. Further studies should include analysis of clays within clay clast, mud drapes and clay matrix within the sandstones. Mechanical infiltrated clay is highly heterogeneous and the formations need to be studied in a broader sense. The mixed-layer clays within the formations were not the focus in this study,

and further studies are needed. In addition, only minor information about the onshore-offshore was obtained by this study. Future analysis must be conducted on the offshore samples. In the terms of reservoir potential of the sandstones, reservoir modeling should be done.

## 5.5 Conclusion

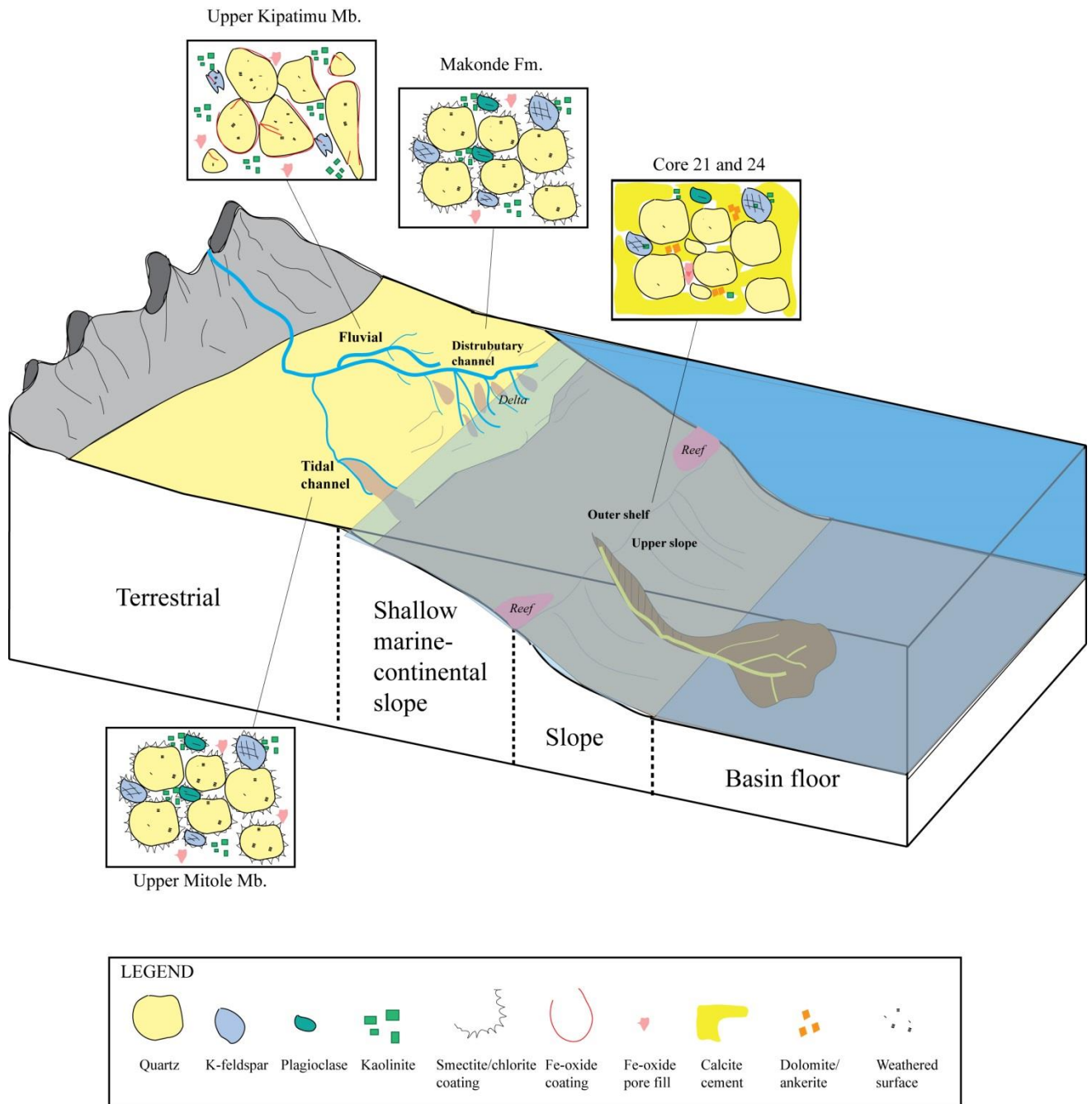
- **Upper Kipatimu Mb.:** The cross bedded very coarse sediments of Upper Kipatimu Mb. were probably deposited in a braided high energy fluvial system. After deposition, the fluvial sandstone experienced weak to moderate compaction. The sandstone has experienced shallow diagenesis where siliclastic minerals like feldspar and mica are highly dissolved. Abundant cement, consisting of pore filling kaolinite, precipitated from silica- and aluminum enriched solutions. In addition the sandstones have been subjected to intense weathering in a tropical climate, and kaolinite and abundant Fe-oxides may be a product of intense weathering. The porosities consist mainly of primary intergranular porosity, where the main pore reducing factors are mechanical compaction and kaolinite cementation. The abundant kaolinite is also the main permeability reducing factor. The sandstone may not have been buried deeper than 1000m.
- **Upper Mitole Mb.:** Upper Mitole Mb. sandstones are interpreted to be deposited in an tidal channel, where abundant double-mud drapes is the most prominent evidence for this interpretation. The diagenetic history of the sandstones comprises of mechanical compaction, mechanical infiltration of clay, authigenic growth of clay coatings and minor kaolinite cement. The sandstone has well preserve primary porosities, where authigenic clay coating and pore filling kaolinite is the porosity and permeability reducing factors. The sandstones display high IGV values, and may not have been buried deeper than 1000 m. Upper Mitole Mb. displays on of the most promising reservoir rocks of this study. High surface weathering has affected the sandstone, and it is difficult to differentiate chemical weathering from diagenetic alteration.
- **Makonde Fm.:** Makonde Fm. is interpreted to be deposited in a terminal distributary channel, where trough cross bedding is the dominant sedimentary structure. The diagenetic history is quite similar to Upper Mitole Mb. comprising weak to moderate mechanical compaction, mechanical infiltrated clay, and authigenic clay in the form of smectite-chlorite coating and pore filling kaolinite. The preserved porosity consists mainly of primary porosity, where the clay coatings and the pore filling clay are the main porosity and permeability reducing factors. The sandstone display high IGV val-

ues that inferred that the sandstone have not been buried deeper than 1000 m. Upper Mitole Mb. displays on of the most promising reservoir rocks of this study. High surface weathering have affected the sandstone, and it is difficult to differentiate chemical weathering form diagenetic alteration

- **Well site 24 and 21:** These sediments are equivalent in time with Kihuluhulu Fm., and could represent this formation. The depositional environment appear to fluctuate between an outer shelf and an upper slope environment, based on the interpretations of FA5, FA6, FA7 and FA8 associations done on the cores from well site 21 and 24. The sandstones are in general highly cemented by carbonate cements; calcite, dolomite and ankerite. The abundant sparry calcite cement is thought to be derived from reworked material, while the dolomite and ankerite are precipitated from porewaters in a reducing environment. The sandstones studied are thought to derive mainly from turbiditic currents on the upper slope. The diagenetic history display weak mechanical compaction, early feldspar and calcite cement, late dolomite, ankerite and kaolinite cement. The porosities are generally low, in the calcite cemented layers where secondary porosity make.
- **Offshore samples:** The two offshore samples display similar petrographical characteristics as the analysed onshore samples from the Mandawa Basin.

A summarizing illustration of the depositional environments and the diagenesis of the studied sedimentary sequences in the Mandawa Basin are presented in Figure 6.1.





**Figure 6.1:** Summarizing figure displaying the depositional environments and diagenesis of the studied sandstone sequences within the Mandawa Basin. Upper Kiptaimu Mb. deposited in a braided river system, with abundant authigenic kaolinite and Fe-oxides. Upper Mitole Mb. (tidal channel) and Makonde Fm. (distributary channel) displays mechanical infiltrated clays as smectite-chlorite coatings. Well sites 24 and 21 (Kihuluhulu Fm.) deposited in a marine environment on the outer shelf/upper slope, and are mostly carbonate cemented.

## References

- AAGAARD, P. & HELGESON, H. C. 1982. Thermodynamic and kinetic constraints on reaction rates among minerals and aqueous solutions; I, Theoretical considerations. *American journal of Science*, 282, 237-285.
- AAGAARD, P., JAHREN, J., HARSTAD, A., NILSEN, O. & RAMM, M. 2000. Formation of grain-coating chlorite in sandstones. Laboratory synthesized vs. natural occurrences. *Clay Minerals*, 35, 261-269.
- AERTS, M. 2014.
- ALI, A. & TURNER, P. 1982. Authigenic K-feldspar in the Bromsgrove sandstone formation (Triassic) of Central England. *Journal of Sedimentary Research*, 52.
- ALLEN, J. 1970. Studies in Fluvial Sedimentation: A Comparison of Fining-Upwards Cyclothems, with Special Reference to Coarse-member Composition and Interpretation. *Journal of Sedimentary Research*, 40.
- ANDERSSON, A. J., MACKENZIE, F. T. & BATES, N. R. 2008. Life on the margin: implications of ocean acidification on Mg-calcite, high latitude and cold-water marine calcifiers. *Mar. Ecol. Prog. Ser.*, 373.
- BAKER, J. C., HAVORD, P. J., MARTIN, K. R. & GHORI, K. A. R. 2000. Diagenesis and petrophysics of the Early Permian Moogooloo sandstone, southern Carnarvon basin, western Australia. *AAPG bulletin*, 84, 250-265.
- BESLY, B. & TURNER, P. 1983. Origin of red beds in a moist tropical climate (Etruria Formation, Upper Carboniferous, UK). *Geological Society, London, Special Publications*, 11, 131-147.
- BILLAULT, V., BEAUFORT, D., BARONNET, A. & LACHARPAGNE, J.-C. 2003. A nanopetrographic and textural study of grain-coating chlorites in sandstone reservoirs. *Clay Minerals*, 38, 315-328.
- BJØRLYKKE, K. 1986. Diagenesis of the Brent sandstone in the Statfjord field, North Sea.
- BJØRLYKKE, K. 2010. Sedimentary Geochemistry. *Petroleum Geoscience: From Sedimentary Environments to Rock Physics*. Heidelberg: Springer, 87-112.
- BJØRLYKKE, K. & JAHREN, J. 2010. Sandstone and Sandstone Reservoirs. *Petroleum Geoscience: From Sedimentary Environments to Rock Physics*. Heidelberg: Springer.
- BOGGS, S. J. 2010. Origin and Transportation of Sedimentary Materials. *Principles of Sedimentology and Stratigraphy*. United States of America: Pearson Education International.
- BOUMA, A. H. 2004. Key controls on the characteristics of turbidite systems. *Geological Society, London, Special Publications*, 222, 9-22.
- BOURGET, J., ZARAGOSI, S., GARLAN, T., GABELOTAUD, I., GUYOMARD, P., DENNIELOU, B., ELLOUZ-ZIMMERMANN, N. & SCHNEIDER, J.-L. 2008. Discovery of a giant deep-sea valley in the Indian Ocean, off eastern Africa: The Tanzania channel. *Marine Geology*, 255, 179-185.
- BRIERLEY, G. J. 1989. River planform facies models: the sedimentology of braided, wandering and meandering reaches of the Squamish River, British Columbia. *Sedimentary geology*, 61, 17-35.
- BURKLEY, S. D. & MACQUAKER, J. H. S. 1992. Authigenic clays, diagenetic sequences and conceptual diagenetic models in contrasting basin-margin and basin-centre north sea Jurassic sandstones and siltstones. In: PITTMAN, D. W. H. A. E. D. (ed.) *Origin, diagenesis, and petrophysics of clay minerals in sandstones*. U.S.A: SEPM (Society for Sedimentary Geology).
- CARROLL, D. 1970. *Rock Weathering*, New York, Plenum Press.

- CHEN, P.-Y. 1977. *Table of key lines in x-ray powder diffraction patterns of mineral in clays and associated rocks*, Geological Survey.
- CLIFTON, H. E. 1969. Beach lamination: nature and origin. *Marine Geology*, 7, 553-559.
- COLLINSON, J. D. 1986. Alluvial Sediments. In: READING, H. G. (ed.) *Sedimentary Environments and Facies*. Oxford: Blackwell Scientific Publications, 49-54.
- COMPTON, R. R. 1962. Manual of field geology. *Soil Science*, 93, 295.
- CONOLLY, J. R. 1965. The occurrence of polycrystallinity and undulatory extinction in quartz in sandstones. *Journal of Sedimentary Research*, 35, 116-135.
- CROCKETT, J. & NITTROUER, C. 2004. The sandy inner shelf as a repository for muddy sediment: an example from Northern California. *Continental Shelf Research*, 24, 55-73.
- DALRYMPLE, R. W. 2010. Interpreting Sedimentary Successions: Facies, Facies Analysis and Facies Models. In: DALRYMPLE, R. W. (ed.) *Facies Models 4*. Canada: Geological Association of Canada, 3-18.
- DE MOWBRAY, T. & VISSER, M. J. 1984. Reactivation surfaces in subtidal channel deposits, Oosterschelde, Southwest Netherlands. *Journal of Sedimentary Research*, 54.
- DOTT JR, R. H. 1964. Wacke, Graywacke and Matrix--What Approach to Immature Sandstone Classification? *Journal of Sedimentary Research*, 34.
- DYPVIK, H. & NESTEBY, H. 1992. The diagenesis of continental (Karoo-Tertiary?) siliciclastics from an East African rift valley (Rukwa-Tukuyu area), Tanzania. *Sedimentary geology*, 78, 251-266.
- DYPVIK, H. & VOLLSET, J. 1979. Petrology and Diagenesis of Jurassic Sandstones from Norwegian Danish Basin, North Sea. *AAPG Bulletin*, 63, 182-193.
- EHRENBERG, S. 1995. Measuring sandstone compaction from modal analysis of thin sections: how to do it and what the results mean. *Journal of Sedimentary Research*, 65.
- EHRENBERG, S. & BOASSEN, T. 1993. Factors controlling permeability variation in sandstones of the Garn Formation in Trestakk Field, Norwegian continental shelf. *Journal of Sedimentary Research*, 63.
- EKDALE, A. 1984. Trace fossils and mid-Cretaceous anoxic events in the Atlantic Ocean.
- ELLIOT, T. 1986. Deltas. In: READING, H. G. (ed.) *Sedimentary environments and facies*. Oxford: Blackwell Scientific Publications, 113 - 154.
- ESRI. 2014. *Basemaps, Reference Maps, and Specialty Maps*.
- GIER, S., WORDEN, R. H., JOHNS, W. D. & KURZWEIL, H. 2008. Diagenesis and reservoir quality of Miocene sandstones in the Vienna Basin, Austria. *Marine and Petroleum Geology*, 25, 681-695.
- GOLDSTEIN, J., NEWBURY, D. E., JOY, D. C., LYMAN, C. E., ECHLIN, P., LIFSHIN, E., SAWYER, L. & MICHAEL, J. R. 2003. *Scanning electron microscopy and X-ray microanalysis*, Springer.
- HENDRY, J. P., TREWIN, N. H. & FALLICK, A. E. 1996. Low-Mg calcite marine cement in Cretaceous turbidites: origin, spatial distribution and relationship to seawater chemistry. *Sedimentology*, 43, 877-900.
- HILL, P. R. 1984. Sedimentary facies of the Nova Scotian upper and middle continental slope, offshore eastern Canada. *Sedimentology*, 31, 293-309.
- HJELLBAKK, A. 1997. Facies and fluvial architecture of a high-energy braided river: the Upper Proterozoic Segloden Member, Varanger Peninsula, northern Norway. *Sedimentary Geology*, 114, 131-161.
- HUDSON, W. 2011. *The Geological Evolution of the Petroleum Prospective Madawa Basin Southern Coastal Tanzania*. Doctor of Philosophy, The University of Dublin.

- HUDSON, W. & NICHOLAS, C. 2014. The Pindi Group (Triassic to Early Jurassic Mandawa Basin, Southern Coastal Tanzania): definition, palaeoenvironment, and stratigraphy. *Journal of African Earth Sciences*.
- JIMÉNEZ BERROCOSO, Á., MACLEOD, K. G., HUBER, B. T., LEES, J. A., WENDLER, I., BOWN, P. R., MWENEINDA, A. K., ISAZA LONDOÑO, C. & SINGANO, J. M. 2010. Lithostratigraphy, biostratigraphy and chemostratigraphy of Upper Cretaceous sediments from southern Tanzania: Tanzania drilling project sites 21–26. *Journal of African Earth Sciences*, 57, 47-69.
- JOHNSON, H. D. & BALDWIN, C. T. 1986. Shallow Siliclastic Sea. In: READING, H. G. (ed.) *Sedimentary Environments and Facies*. Oxford: Blackwell Scientific Publications, 229-282.
- KAGYA, M. L. 1996. Geochemical characterization of Triassic petroleum source rock in the Mandawa basin, Tanzania. *Journal of African Earth Sciences*, 23, 73-88.
- KENT, P. E., HUNT, J. A. & JOHNSTONE, D. W. 1971. *The geology and geophysics of coastal Tanzania*, HM Stationery Office.
- KU, T. & WALTER, L. 2003. Syndepositional formation of Fe-rich clays in tropical shelf sediments, San Blas Archipelago, Panama. *Chemical geology*, 197, 197-213.
- LAMING, D. 1966. Imbrication, paleocurrents and other sedimentary features in the lower New Red Sandstone, Devonshire, England. *Journal of Sedimentary Research*, 36.
- LANSON, B., BEAUFORT, D., BERGER, G., BAUER, A., CASSAGNABERE, A. & MEUNIER, A. 2002. Authigenic kaolin and illitic minerals during burial diagenesis of sandstones: a review. *Clay Minerals*, 37, 1-22.
- LOUCKS, R., BEBOUT, D. & GALLOWAY, W. E. 1977. Relationship of Porosity Formation and Preservation to Sandstone Consolidation History--Gulf Coast Lower Tertiary Frio Formation (1).
- LOWE, D. R. 1976. Subaqueous liquefied and fluidized sediment flows and their deposits. *Sedimentology*, 23, 285-308.
- MA, Y. & LIU, C. 1999. Trace element geochemistry during chemical weathering. *Chinese Science Bulletin*, 44, 2260-2263.
- MAHMIC, O. 2014. *RE: Composition and trace-element geochemistry of clays of the Upper Cretaceous to Paleogene Kilwa Group, Tanzania: A provenance study*.
- MATLACK, K. S., HOUSEKNECHT, D. W. & APPLIN, K. R. 1989. Emplacement of clay into sand by infiltration. *Journal of Sedimentary Research*, 59.
- MCDONOUGH, K.-J., BOUANGA, E., PIERARD, C., HORN, B., EMMET, P., GROSS, J., DANFORTH, A., STERNE, N. & GRANATH, J. 2013. Wheeler-transformed 2D seismic data yield fan chronostratigraphy of offshore Tanzania. *The Leading Edge*, 32, 162-170.
- MIALL, A. D. 2003. Sands, gravels, and their lithified equivalents. *Sedimentology*. Springer, 960-966.
- MORAD, S. 1990. Mica alteration reactions in Jurassic reservoir sandstones from the Haltenbanken area, offshore Norway. *Clays and Clay Minerals*, 38, 584-590.
- MORAD, S., AL-RAMADAN, K., KETZER, J. M. & DE ROS, L. 2010. The impact of diagenesis on the heterogeneity of sandstone reservoirs: A review of the role of depositional facies and sequence stratigraphy. *AAPG bulletin*, 94, 1267-1309.
- MORAD, S., KETZER, J. & DE ROS, L. F. 2000. Spatial and temporal distribution of diagenetic alterations in siliclastic rocks: implications for mass transfer in sedimentary basins. *Sedimentology*, 47, 95-120.
- MORAES, M. A. 1992. Depositional infiltrated and authigenic clays in fluvial sandstones of the Jurassic Sergi Formation, Reconcavo Basin, northeastern Brazil.

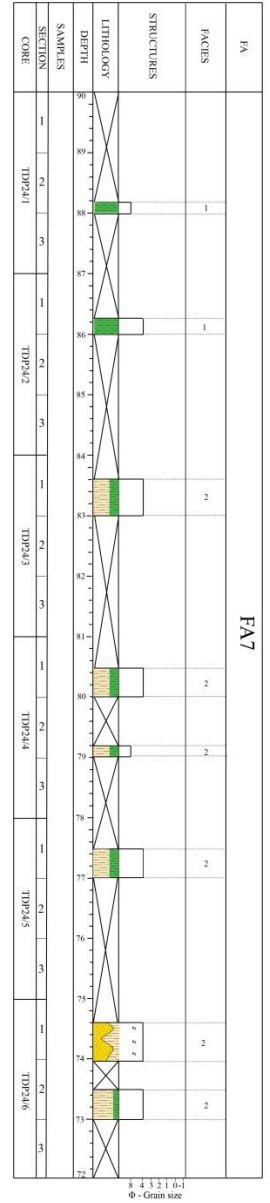
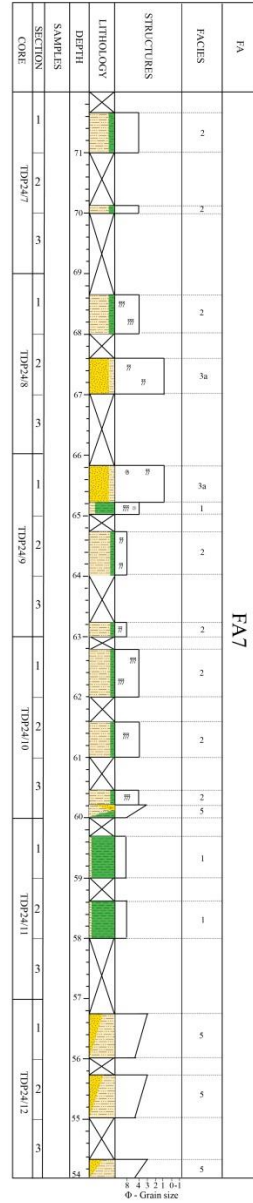
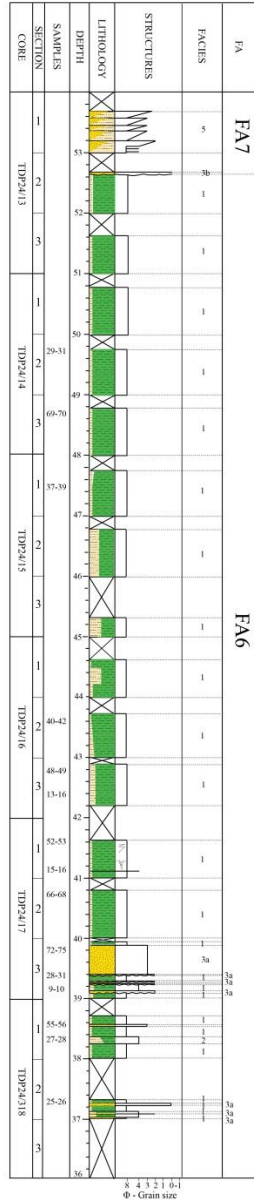
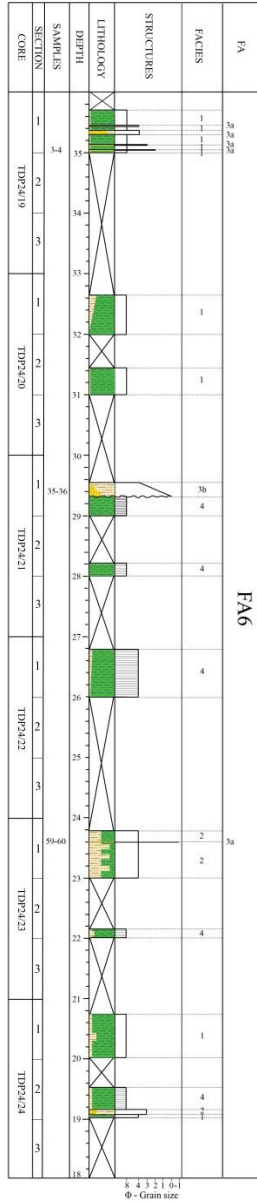
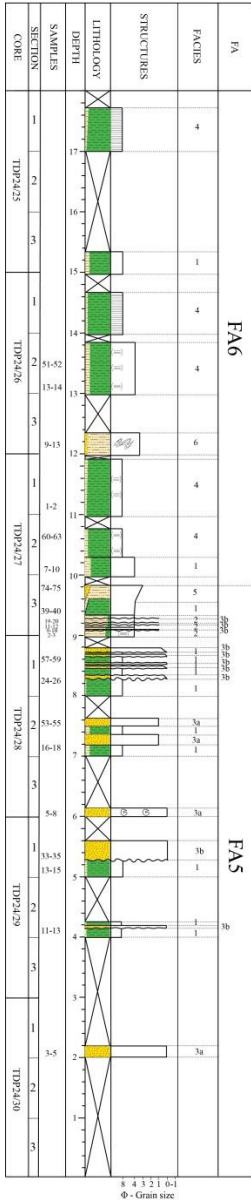
- MORAES, M. A. & DE ROS, L. F. 1990. Infiltrated clays in fluvial Jurassic sandstones of Recôncavo Basin, northeastern Brazil. *Journal of Sedimentary Research*, 60.
- MORRIS, K. A. 1979. A classification of Jurassic marine shale sequences: an example from the Toarcian (Lower Jurassic) of Great Britain. *Palaeogeography, Palaeoclimatology, Palaeoecology*, 26, 117-126.
- MORTON, A. C. & HALLSWORTH, C. R. 1999. Processes controlling the composition of heavy mineral assemblages in sandstones. *Sedimentary Geology*, 124, 3-29.
- MPANDA, S. 1997. Geological development of the East African coastal basin of Tanzania.
- MULDER, T. & ALEXANDER, J. 2001. The physical character of subaqueous sedimentary density flows and their deposits. *Sedimentology*, 48, 269-299.
- MYROW, P. M. 1990. A New Graph for Understanding. *Journal of Geological Education*, 38, 16.
- NELSON, P. H. 1994. Permeability-porosity relationships in sedimentary rocks. *The log analyst*, 35.
- NERBRÅTEN, K. 2014. Petrology and Sedimentary Provenance of Mesozoic and Cenozoic Sequences in the Mandawa Basin.
- NESBITT, H. W., FEDO, C. M. & YOUNG, G. M. 1997. Quartz and feldspar stability, steady and non-steady-state weathering, and petrogenesis of siliciclastic sands and muds. *The Journal of Geology*, 105, 173-192.
- NICHOLAS, C. 12th December 2013. RE: Rifting along the southern coastal Tanzania margin and development of the petroleum prospective Mandawa Basin.
- NICHOLAS, C. J., PEARSON, P. N., BOWN, P. R., JONES, T. D., HUBER, B. T., KAREGA, A., LEES, J. A., MCMILLAN, I. K., O'HALLORAN, A. & SINGANO, J. M. 2006. Stratigraphy and sedimentology of the Upper Cretaceous to Paleogene Kilwa Group, southern coastal Tanzania. *Journal of African Earth Sciences*, 45, 431-466.
- NICHOLAS, C. J., PEARSON, P. N., MCMILLAN, I. K., DITCHFIELD, P. W. & SINGANO, J. M. 2007. Structural evolution of southern coastal Tanzania since the Jurassic. *Journal of African Earth Sciences*, 48, 273-297.
- NIO, S.-D. & YANG, C.-S. 1991. Diagnostic attributes of clastic tidal deposits: a review.
- OLARIU, C. & BHATTACHARYA, J. P. 2006. Terminal distributary channels and delta front architecture of river-dominated delta systems. *Journal of Sedimentary Research*, 76, 212-233.
- PATTISON, S. A. 2005. Storm-influenced prodelta turbidite complex in the Lower Kenilworth Member at Hatch Mesa, Book Cliffs, Utah, USA: implications for shallow marine facies models. *Journal of Sedimentary Research*, 75, 420-439.
- PAXTON, S., SZABO, J., AJDUKIEWICZ, J. & KLIMENTIDIS, R. 2002. Construction of an intergranular volume compaction curve for evaluating and predicting compaction and porosity loss in rigid-grain sandstone reservoirs. *AAPG bulletin*, 86, 2047-2067.
- PEARSON, P. N., NICHOLAS, C. J., SINGANO, J. M., BOWN, P. R., COXALL, H. K., VAN DONGEN, B. E., HUBER, B. T., KAREGA, A., LEES, J. A. & MSAKY, E. 2004. Paleogene and Cretaceous sediment cores from the Kilwa and Lindi areas of coastal Tanzania: Tanzania Drilling Project Sites 1-5. *Journal of African Earth Sciences*, 39, 25-62.
- PETTIJOHN, F. J., POTTER, P. E. & SIEVER, R. 1972. Diagenesis. *Sand and Sandstones*. Berlin: Springer - Verlag, 383-434.
- PIPER, D. J., NORMARK, W. R. & INGLE, J. C. 1976. The Rio Dell Formation: a Plio-Pleistocene basin slope deposit in Northern California. *Sedimentology*, 23, 309-328.
- POTTER, P. E., MAYNARD, J. B. & PRYOR, W. A. 1980. *Sedimentology of shale: study guide and reference source*, Springer-Verlag Berlin.

- POWERS, M. C. 1953. A new roundness scale for sedimentary particles. *Journal of Sedimentary Research*, 23.
- PYE, K. & KRINSLEY, D. 1986. Diagenetic carbonate and evaporite minerals in Rotliegend aeolian sandstones of the southern North Sea: their nature and relationship to secondary porosity development. *Clay Minerals*, 21, 443-457.
- REEVES, C., SAHU, B. & DE WIT, M. 2002. A re-examination of the paleo-position of Africa's eastern neighbours in Gondwana. *Journal of African Earth Sciences*, 34, 101-108.
- SALEM, A. M., MORAD, S., MATO, L. F. & AL-AASM, I. 2000. Diagenesis and reservoir-quality evolution of fluvial sandstones during progressive burial and uplift: Evidence from the Upper Jurassic Boipeba Member, Reconcavo Basin, Northeastern Brazil. *AAPG bulletin*, 84, 1015-1040.
- SALMAN, G. & ABDULA, I. 1995. Development of the Mozambique and Ruvuma sedimentary basins, offshore Mozambique. *Sedimentary Geology*, 96, 7-41.
- SHANMUGAM, G. 1997. The Bouma sequence and the turbidite mind set. *Earth-Science Reviews*, 42, 201-229.
- SMITH, D. G. 1988. Tidal Bundles and Mud Couplets in the McMurray Formation, Northeastern Alberta, Canada: GEOLOGICAL NOTES. *Bulletin of Canadian Petroleum Geology*, 36, 216-219.
- STATOIL. 2014. *Vellykket produksjonstest av Zafarani-reservoaret i Tanzania* [Online]. Available: [http://www.statoil.com/no/NewsAndMedia/News/2014/Pages/03Mar\\_Tazania.aspx](http://www.statoil.com/no/NewsAndMedia/News/2014/Pages/03Mar_Tazania.aspx).
- STRONG, G. & MILODOWSKI, A. 1987. Aspects of the diagenesis of the Sherwood Sandstones of the Wessex Basin and their influence on reservoir characteristics. *Geological Society, London, Special Publications*, 36, 325-337.
- SWALLOW, J. C., SCHOTT, F. & FIEUX, M. 1991. Structure and transport of the East African coastal current. *Journal of Geophysical Research: Oceans (1978–2012)*, 96, 22245-22257.
- SÆTRE, R. & DA SILVA, A. J. 1984. The circulation of the Mozambique Channel. *Deep Sea Research Part A. Oceanographic Research Papers*, 31, 485-508.
- TUCKER, M. E. 2001. Limestones. *Sedimentary petrology: an introduction to the origin of sedimentary rocks*. United Kingdom: Blackwell Science, 110-151.
- VAN HEERDEN, I. L. & ROBERTS, H. H. 1988. Facies development of Atchafalaya Delta, Louisiana: a modern bayhead delta. *AAPG Bulletin*, 72, 439-453.
- VISSER, M. 1980. Neap-spring cycles reflected in Holocene subtidal large-scale bedform deposits: a preliminary note. *Geology*, 8, 543-546.
- WELTON, J. E. 1984. *SEM petrology atlas*, American Association of Petroleum Geologists Tulsa, OK.
- WENTWORTH, C. K. 1922. A scale of grade and class terms for clastic sediments. *The Journal of Geology*, 377-392.
- WILSON, M. D. & PITTMAN, E. D. 1977. Authigenic clays in sandstones: recognition and influence on reservoir properties and paleoenvironmental analysis. *Journal of Sedimentary Research*, 47.
- WOPFNER, H. 2002. Tectonic and climatic events controlling deposition in Tanzanian Karoo basins. *Journal of African Earth Sciences*, 34, 167-177.
- ZAKARIASSEN, E. 2014.

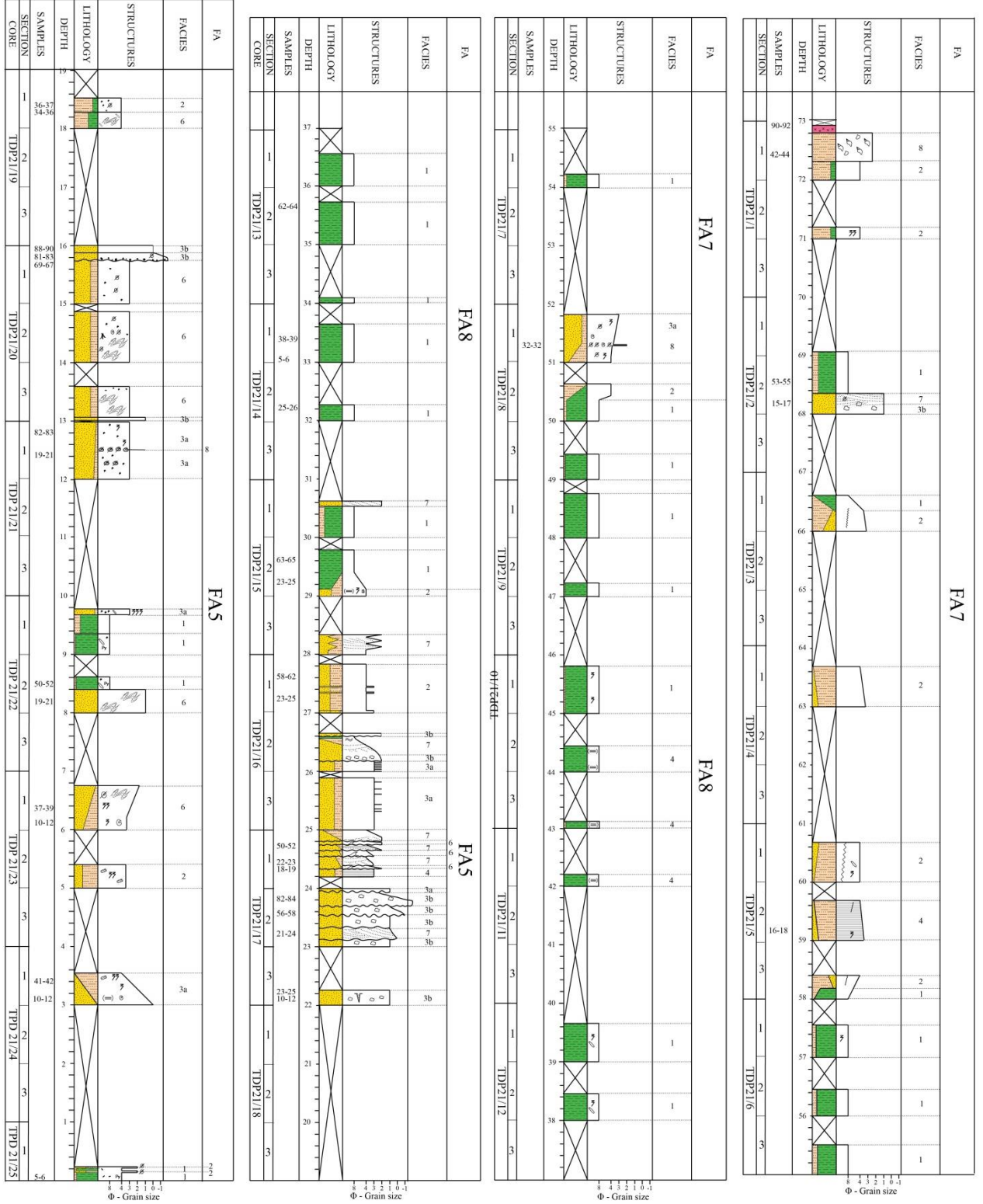


# Appendix

## Appendix A – Sedimentary log of well site 24.



# Appendix B – Sedimentary of log well site 21



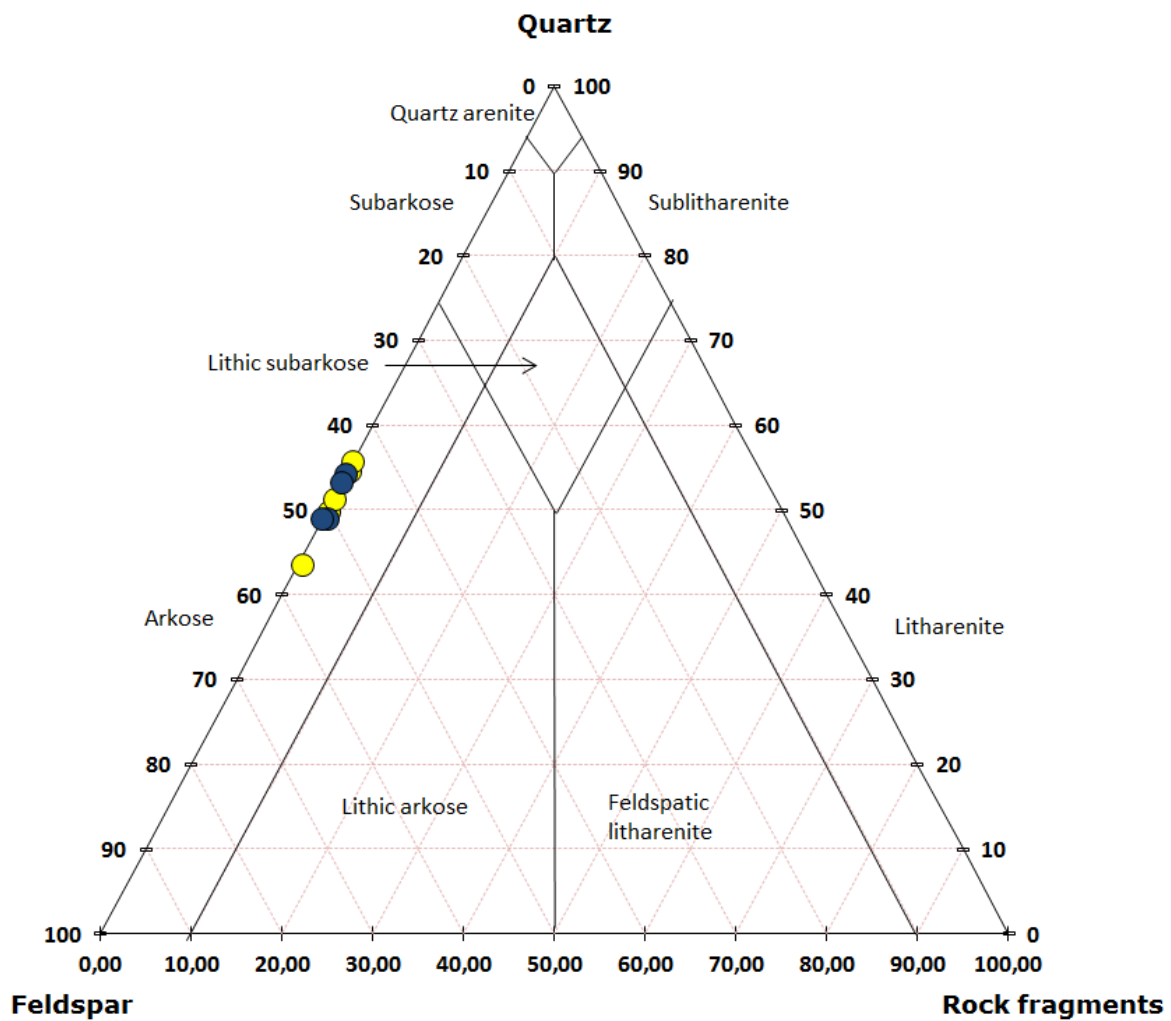
Appendix C – Point counting.

Prøvenr.	%	Quartz tot.	Quartz				Feldspar tot.	K-feldspar					Plagioclase					Clay cen.	Carb. cen.	Porosity	Pyrite	Kaolin	Mica	RF	Coating	HM	Dolomite	Fe oxide	Matrix					
			MonoM	MonoU	PolyM	PolyU		1	2	3	4	5	1	2	3	4	5																	
TDP241703_9-10	%	66,0	58,5	4,8	1,5	1,3	3,0	0,0	0,0	2,0	0,8	0,3	0,0	0,0	0,0	0,0	2,5	24,7	2,2	1,5	0,0	0,0	0,0	0,0	0,0	0,0	0,0	0,0	0,0	0,0	0,0	0,0	0,0	
TDp241603_13-16	%	37,7	32,3	2,8	2,5	0,3	5,0	0,0	0,0	0,8	3,3	1,0	0,0	0,0	0,0	0,0	0,7	49,2	8,0	0,2	0,0	0,0	0,0	0,0	0,0	0,0	0,0	0,0	0,0	0,0	0,0	0,0	0,0	
TDp242803_5-8	%	66,1	62,3	2,5	1,0	0,3	2,2	0,0	0,0	1,3	0,0	0,5	0,0	0,0	0,0	0,0	0,5	14,7	16,0	0,0	0,2	0,0	0,0	0,0	0,0	0,0	0,0	0,0	0,0	0,0	0,0	0,0	0,0	
TDP242801_57-59	%	66,5	52,0	9,8	3,5	1,3	0,2	0,0	0,0	0,3	0,0	0,0	0,0	0,0	0,0	0,0	32,7	0,5	0,0	0,0	0,0	0,0	0,0	0,0	0,0	0,0	0,0	0,0	0,0	0,0	0,0	0,0	0,0	
TDP241302_62-64	%	41,5	40,3	0,3	0,3	0,3	6,0	0,0	0,0	0,0	0,0	0,0	0,0	0,0	0,0	9,5	14,2	4,5	24,2	0,0	0,0	0,0	0,0	0,0	0,0	0,0	0,0	0,0	0,0	0,0	0,0	0,0	0,0	
TDP243001_3-5	%	71,5	65,8	3,8	0,3	1,8	1,0	0,0	0,0	0,3	0,8	0,0	0,0	0,0	0,0	0,0	9,0	17,7	0,0	0,0	0,0	0,0	0,0	0,0	0,0	0,0	0,0	0,0	0,0	0,0	0,0	0,0	0,0	
TDP211702_82-84	%	61,2	53,3	5,3	2,5	0,3	1,2	0,0	0,0	0,8	0,5	0,0	0,0	0,0	0,0	0,0	0,5	11,0	25,7	0,0	0,0	0,0	0,0	0,0	0,0	0,0	0,0	0,0	0,0	0,0	0,0	0,0	0,0	
TDP211702_56-58	%	49,7	34,8	9,3	2,0	3,8	9,7	0,0	0,0	0,8	3,8	4,5	0,0	0,0	0,0	15,0	22,7	1,2	0,0	0,5	0,0	1,0	0,0	0,0	0,0	0,0	0,0	0,0	0,0	0,0	0,0	0,0	0,0	
TDP212401_10-12	%	54,7	32,0	4,5	1,8	1,0	4,0	0,0	0,5	2,3	1,0	0,3	0,0	0,0	0,0	0,0	39,9	1,2	0,0	0,0	0,0	0,0	0,0	0,0	0,0	0,0	0,0	0,0	0,0	0,0	0,0	0,0	0,0	
TDP212501_5-6	%	41,0	38,0	2,3	0,0	0,8	3,2	0,0	0,0	1,5	1,0	0,5	0,0	0,0	0,0	28,2	0,0	21,2	0,0	0,0	0,0	0,0	0,0	0,0	0,0	5,0	0,0	0,0	0,0	0,0	0,0	0,0	0,0	
TDP212001_88-90	%	51,0	48,5	1,8	0,8	0,0	4,5	0,0	0,0	0,0	0,0	0,0	0,0	0,0	0,0	0,0	40,0	4,5	0,0	0,0	0,0	0,0	0,0	0,0	0,0	0,0	0,0	0,0	0,0	0,0	0,0	0,0	0,0	
TDP211703_23-25	%	35,0	33,3	1,5	0,0	0,5	1,2	0,0	0,0	0,3	1,0	0,0	0,0	0,0	0,0	23,7	31,5	1,7	0,2	0,0	0,0	0,0	0,0	0,0	0,0	0,0	0,0	6,5	0,0	0,0	0,0	0,0	0,0	
NG-1-2-13	%	53,2	49,5	2,0	1,5	0,3	5,2	0,0	0,0	0,0	0,0	0,0	0,0	0,0	2,3	2,0	1,2	0,0	26,7	0,0	1,5	0,0	0,0	11,5	0,0	0,0	0,0	0,5	0,0	0,0	0,0	0,0	0,0	
NG-1-5-13	%	49,0	44,3	2,5	1,3	1,0	8,5	0,0	0,0	1,3	4,0	2,3	0,0	0,0	0,0	0,3	20,5	0,0	21,2	0,0	0,0	0,0	0,0	0,0	0,2	0,0	0,0	0,0	0,0	0,0	0,0	0,0	0,0	
NG-1-1-13	%	54,2	44,5	5,5	2,8	1,5	7,2	0,0	0,0	5,8	0,0	1,5	0,0	0,0	0,0	0,0	2,7	0,0	19,0	0,0	0,0	0,0	0,0	15,7	0,0	0,0	0,0	1,0	0,0	0,0	0,0	0,0	0,0	
NG-2-1-13	%	49,0	46,5	2,0	0,5	0,0	12,5	0,0	0,0	5,5	0,0	3,5	0,0	0,0	0,0	0,0	9,0	0,0	11,0	4,5	0,0	0,0	0,0	13,2	0,0	0,0	0,0	0,6	0,0	0,0	0,0	0,0	0,0	
MN-1-6-13	%	54,5	51,0	1,8	5,5	1,8	9,0	0,0	0,0	0,0	0,0	0,0	0,0	0,0	0,0	20,7	0,0	8,7	1,5	0,0	0,2	0,2	0,0	1,0	0,0	0,0	4,0	0,0	0,0	0,0	0,0	0,0		
MN-1-5-13	%	51,2	46,8	2,3	2,3	0,0	10,2	0,0	0,3	0,0	8,0	2,3	0,0	0,0	0,0	0,0	0,0	0,0	21,5	0,0	13,2	0,0	0,2	1,7	0,2	0,0	1,2	0,0	0,0	0,0	0,0	0,0	0,0	
MN-1-3-13	%	48,7	40,3	5,8	2,3	1,5	5,2	0,0	0,0	1,8	2,3	1,5	0,0	0,0	0,0	0,0	0,0	0,0	13,5	0,0	21,5	0,2	0,2	5,2	0,0	0,0	4,2	0,0	0,0	0,0	0,0	0,0	0,0	
MN-2-1-13	%	43,5	40,3	1,8	1,0	0,5	0,8	0,0	0,0	0,0	0,5	0,3	0,0	0,0	0,0	24,5	0,0	7,5	0,2	0,0	0,0	0,0	0,0	0,0	0,5	0,0	0,0	0,0	0,0	0,0	0,0	0,0	0,0	
MN-2-3-13	%	55,7	48,3	4,8	1,8	1,0	6,0	0,0	0,0	0,0	0,8	5,3	0,0	0,0	0,0	29,5	0,0	5,5	0,2	0,0	0,0	0,0	0,0	0,2	0,0	0,2	0,0	2,5	0,0	0,0	0,0	0,0	0,0	
MB-2-2-13	%	48,2	45,5	2,5	0,3	0,0	9,5	0,0	0,0	6,3	1,5	1,3	0,0	0,3	0,3	0,0	2,2	0,0	16,5	0,0	0,0	0,0	0,0	13,0	0,0	0,0	0,0	0,0	0,0	0,0	0,0	0,0	0,0	0,0
MB-2-1-13	%	58,0	50,0	4,8	1,8	1,5	2,5	0,0	0,0	0,0	0,0	0,0	0,0	0,0	0,0	7,5	0,0	14,7	0,0	0,0	0,0	0,0	0,7	0,0	0,0	0,0	2,2	0,0	0,0	0,0	0,0	0,0	10,7	
MB-2-4-13	%	55,5	48,3	5,8	1,5	0,0	9,2	0,0	0,5	4,8	0,8	2,5	0,0	0,3	0,0	0,0	0,0	0,0	27,2	0,0	0,0	0,0	0,0	7,5	0,5	0,0	0,0	0,0	0,0	0,0	0,0	0,0	0,0	
MB-1-7-13	%	49,5	45,3	2,5	1,5	0,3	14,7	0,0	1,3	6,0	0,8	2,3	0,0	0,0	0,0	0,0	0,0	0,0	14,7	0,0	1,0	0,5	0,0	22,2	1,5	0,0	0,0	0,0	0,0	0,0	0,0	0,0	0,0	
MB-1-4-13	%	46,2	39,3	3,3	3,3	0,5	8,2	0,0	0,0	4,3	0,0	3,5	0,0	0,0	0,0	0,0	5,2	0,0	19,2	0,0	2,2	0,2	0,0	13,5	0,2	0,0	4,2	0,0	0,0	0,0	0,0	0,0	0,0	

Appendix D – XRD.

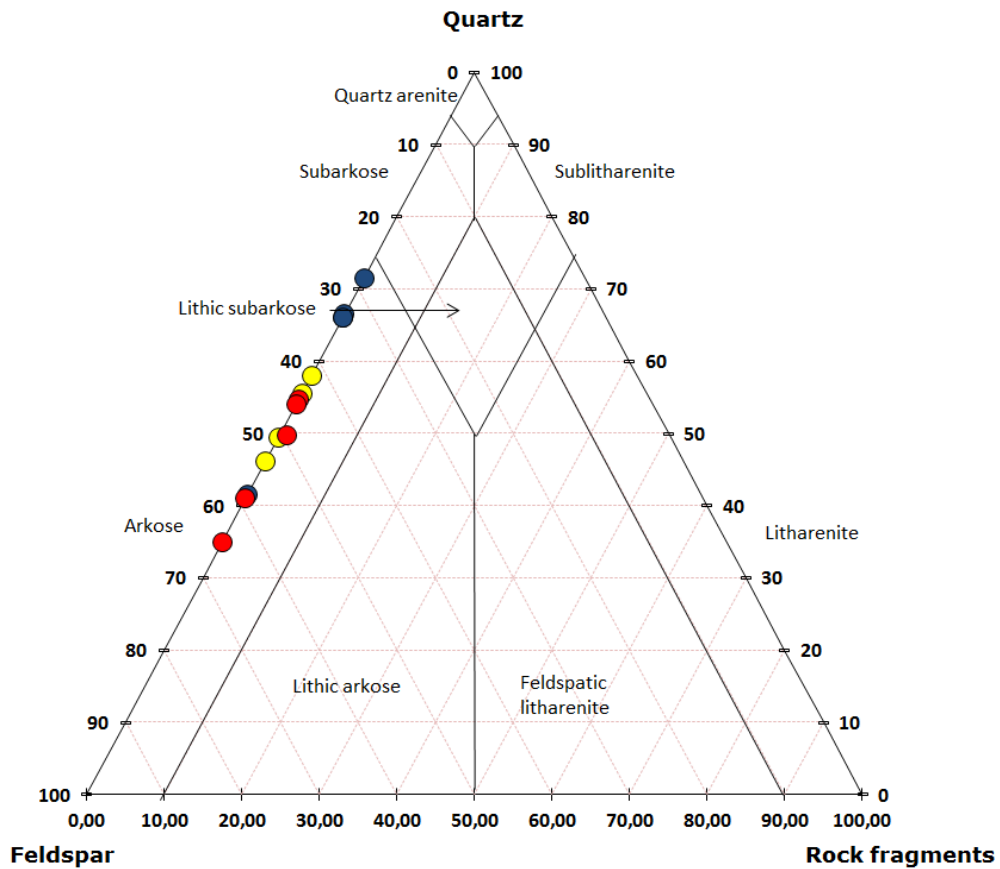
Prøvenr.	Mixed layered clay minerals	Illite	Chlorite	Kaolinite	Halite	Mica	Quartz	K-feldspar	Plagioclase	Calcite	Dolomite	Ankerite	Pyrite	Chi Squared
MN-1-3-13	0,0	0,0	0,0	6258,0	0,0	455,0	15789,0	4547,0	0,0	0,0	0,0	0,0	0,0	3,9
MN-1-5-13	0,0	0,0	0,0	2822,0	0,0	0,0	16599,0	3878,0	0,0	0,0	0,0	0,0	0,0	4,0
MN-1-6-13	0,0	0,0	0,0	4986,0	0,0	0,0	16750,0	4777,0	0,0	0,0	0,0	0,0	0,0	4,1
MN-2-1-13	0,0	0,0	0,0	3805,0	0,0	555,0	12803,0	3563,0	0,0	851,0	0,0	0,0	0,0	4,4
MN-2-3-13	0,0	0,0	0,0	4291,0	0,0	392,0	16435,0	3284,0	0,0	778,0	0,0	0,0	0,0	5,2
NG-1-1-13	0,0	0,0	0,0	0,0	0,0	0,0	12935,0	3519,0	4090,0	0,0	0,0	0,0	0,0	4,9
NG-1-2-13	0,0	0,0	0,0	601,0	0,0	0,0	13892,0	3534,0	3476,0	730,0	0,0	0,0	0,0	5,1
NG-1-5-13	566,0	0,0	0,0	439,0	0,0	0,0	12237,0	4162,0	4505,0	0,0	0,0	0,0	0,0	5,3
NG-2-1-13	0,0	0,0	0,0	0,0	0,0	0,0	12746,0	4070,0	3874,0	0,0	0,0	0,0	0,0	5,0
MB-1-0-13	1097,0	0,0	0,0	0,0	0,0	706,0	6260,0	2139,0	3251,0	0,0	0,0	0,0	0,0	3,9
MB-1-3-13	817,0	0,0	0,0	0,0	0,0	0,0	9654,0	2870,0	4949,0	0,0	0,0	0,0	0,0	4,3
MB-1-4-13	442,0	0,0	0,0	523,0	0,0	0,0	10513,0	4684,0	5809,0	0,0	0,0	0,0	0,0	4,8
MB-1-7-13	0,0	0,0	0,0	484,0	0,0	539,0	9893,0	6190,0	6925,0	0,0	0,0	0,0	0,0	5,1
MB-2-1-13	0,0	0,0	0,0	0,0	0,0	0,0	17402,0	0,0	4267,0	4100,0	0,0	0,0	0,0	5,3
MB-2-2-13	0,0	0,0	0,0	0,0	760,0	465,0	8925,0	5182,0	7098,0	827,0	0,0	0,0	0,0	5,1
MB-2-4-13	0,0	0,0	0,0	0,0	0,0	416,0	14763,0	4045,0	4336,0	719,0	0,0	0,0	0,0	5,1
24/30/1, 3-5	0,0	0,0	0,0	0,0	0,0	0,0	78,9	4,7	1,2	0,0	9,4	5,8	0,0	5,6
24/28/3, 5-8	0,0	0,0	0,0	0,0	0,0	0,0	73,9	5,8	2,0	0,0	18,3	0,0	0,0	4,9
4/28/1, 57-5	0,0	0,0	0,0	0,0	0,0	0,0	60,0	5,3	1,8	0,0	0,0	32,9	0,0	5,0
24/26/3, 9-13	19,2	0,0	0,0	0,0	0,0	0,0	17,2	6,2	3,0	38,8	15,7	0,0	0,0	3,1
24/17/3, 9-10	0,0	0,0	0,0	0,0	0,0	0,0	76,2	4,6	1,7	17,5	0,0	0,0	0,0	4,5
4/16/3, 13-1	0,0	0,0	0,0	0,0	0,0	0,0	41,5	7,8	10,8	39,9	0,0	0,0	0,0	4,2
21/25/1, 5-6	2,9	10,5	0,0	0,3	0,0	0,0	69,5	10,7	4,0	0,0	0,0	0,0	2,3	4,4
1/24/1, 10-1	0,0	0,0	0,0	0,0	0,0	0,0	48,7	6,7	3,6	41,0	0,0	0,0	0,0	4,5
1/20/1, 88-9	0,0	0,0	0,0	0,0	0,0	0,0	50,5	12,9	1,7	34,9	0,0	0,0	0,0	4,6
1/17/3,23-2	0,0	0,0	0,0	0,0	0,0	0,0	53,2	9,7	2,9	34,4	0,0	0,0	0,0	4,4
1/17/2, 82-8	0,0	0,0	0,0	0,0	0,0	0,0	70,4	16,2	1,3	0,0	11,1	11,1	0,0	5,0
1/17/2,56-5	0,0	0,0	0,0	0,0	0,0	0,0	52,8	11,1	5,8	29,3	0,3	0,3	0,0	5,2

Appendix E – Classification: Upper Kipatimu Mb. And Upper Mitole Mb.



Stratigraphical unit	Samples	Clay matrix (%)	Classification
Upper Kipatimu Mb.	MN-1-3-13	0,00	Arkose
	MN-1-5-13	0,00	Arkose
	MN-1-6-13	20,7	Feltspatic wacke
	MN-2-1-13	24,5	Feltspatic wacke
	MN-2-3-13	29,5	Feltspatic wacke
Upper Mitole Mb.	NG-1-1-13	2,7	Arkose
	NG-1-2-13	1,2	Arkose
	NG-1-5-13	20,5	Feltspatic wacke
	NG-2-1-13	9	Arkose

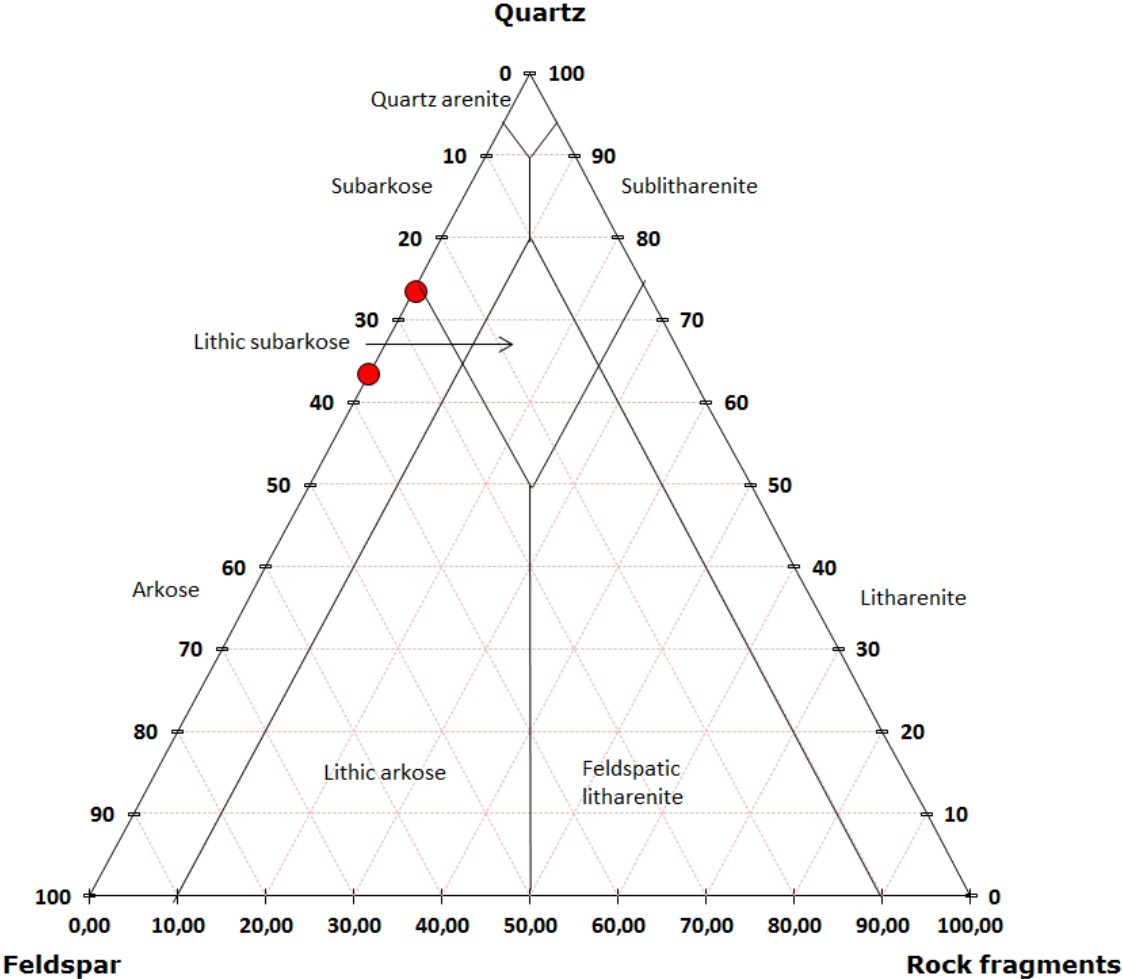
Appendix F - Classification: Makonde Fm., well sites 21 and 24.



Stratigraphical unit	Samples	Clay matrix (%)	Classification
Makonde Fm.	MB-1-4-13	5,20	Arkose
	MB-1-7-13	0,00	Arkose
	MB-2-1-13	7,50	Arkose
	MB-2-4-13	0,00	Arkose
Kihuluhulu Fm.	24/30/1_3-5	0,00	Arkose
	24/28/3_5-8	0,50	Arkose
	24/28/1_57-57	0,00	Arkose
	24/17/3_9-10	2,50	Arkose
	24/13/2_62-64	9,50	Arkose
	21/25/1_5-6	0,00	Arkose
	21/24/1_10-12	0,00	Arkose
	21/20/1_88-90	0,00	Arkose
	21/17/3_23-25	0,00	Arkose
21/17/2_56-58	15,00	Arkose	



Appendix G – Classification offshore.



Stratigraphical unit	Samples	Clay matrix (%)	Classification
Cenomanian	2/2/14_a	0,00	Arkose
	2/2/14_b	11,8	Arkose

Appendix H - IGV

Sample	Porosity	Cement	Matrix	Fe oxide	Coating	IGV
MN-1-6-13	8,70	20,70	2,50	0,00	0,00	31,90
MN-1-5-13	21,50	13,20	0,00	0,00	0,00	34,70
MN-1-3-13	13,50	21,50	0,70	0,00	0,00	35,70
MN-2-1-13	7,50	24,50	0,50	0,00	0,00	32,50
MN-2-3-13	5,50	29,50	9,50	0,00	0,00	44,50
NG-1-2-13	26,70	2,70	0,50	0,00	11,50	29,90
NG-1-5-13	21,20	20,50	0,00	0,00	0,00	41,70
NG-1-1-13	19,00	2,70	1,00	0,00	15,70	22,70
NG-2-1-13	11,00	9,00	0,60	0,00	13,20	20,60
MB-2-2-13	16,50	2,20	0,00	0,00	13,00	18,70
MB-2-1-13	14,70	7,50	10,70	2,20	0,70	35,10
MB-2-4-13	27,20	0,00	0,00	0,00	7,50	27,20
MB-1-7-13	14,70	0,00	0,00	0,00	22,20	14,70
MB-1-4-13	19,20	6,40	0,00	4,20	13,50	29,80
P241703_9	2,20	24,70	1,50	0,00	0,00	28,40
p241603_13	8,00	32,30	0,20	0,00	0,00	40,50
Dp242803_5	16,00	14,70	0,20	0,00	0,00	30,90
P242801_57	0,50	32,70	0,00	0,00	0,00	33,20
P241302_62	4,50	14,20	24,20	0,00	0,00	42,90
DP243001_3	17,70	9,00	0,00	0,00	0,00	26,70
P211702_82	25,70	11,50	0,00	0,00	0,00	37,20
P211702_56	1,20	37,70	0,50	0,00	0,00	39,40
P212401_10	1,20	39,90	0,00	0,00	0,00	41,10
DP212501_5	21,20	14,00	5,00	0,00	0,00	40,20
P212001_88	4,50	40,00	0,00	0,00	0,00	44,50
P211703_23	1,70	0,00	6,70	0,00	0,00	8,40

Appendix I – EMP: Dolomite.

Dolomite							
DataSet/Point	CaO wt%	FeO wt%	MnO wt%	MgO wt%	SrO wt%	SiO2 wt%	Total wt%
13 / 1 .	30,2922	3,0417	0,3463	17,8354	-0,1464	0,1015	51,4706
14 / 1 .	31,7566	3,8306	0,4148	15,5634	-0,0925	0,0238	51,4967
15 / 1 .	30,5596	3,1085	0,3251	17,3843	-0,1621	0,0438	51,2592
16 / 1 .	29,9405	3,8537	0,398	17,1643	-0,1293	0,0627	51,29
17 / 1 .	29,6887	3,095	0,3276	18,1357	-0,1525	0,2628	51,3572
18 / 1 .	31,5099	3,5348	0,4735	16,0174	-0,1703	0,0721	51,4374
19 / 1 .	30,1097	2,8399	0,3592	17,4664	-0,1304	0,0748	50,7196
20 / 1 .	31,9314	3,5585	0,4022	15,5766	-0,1977	0,0462	51,3172
21 / 1 .	29,7622	2,9523	0,3381	17,7677	-0,1363	0,0729	50,7568
22 / 1 .	32,0818	3,4378	0,4422	15,6234	-0,1559	0,0257	51,455
23 / 1 .	29,8842	2,959	0,3759	17,354	-0,1305	0,0416	50,4842
24 / 1 .	31,7939	3,5122	0,3361	15,966	-0,1632	0,0332	51,4782
25 / 1 .	29,6979	2,8765	0,3496	18,1128	-0,1311	0,0242	50,93
26 / 1 .	30,1437	3,2751	0,4655	17,1004	-0,1882	0,0251	50,8217
27 / 1 .	29,5769	3,0003	0,3495	17,8709	-0,1946	0,0105	50,6135
28 / 1 .	30,7848	3,0075	0,322	16,9103	-0,1519	0,0303	50,903
29 / 1 .	29,6228	2,9097	0,3307	18,1689	-0,1226	0,0284	50,9379
30 / 1 .	31,2752	3,396	0,3976	16,1109	-0,1654	0,0187	51,033
31 / 1 .	30,1759	3,0976	0,4087	17,5336	-0,1383	0,0042	51,0817
32 / 1 .	29,8065	2,8393	0,3052	17,7115	-0,1347	0,0347	50,5624
33 / 1 .	32,2774	3,3485	0,4188	15,3578	-0,1421	0,0548	51,3153
34 / 1 .	29,7559	3,0803	0,3304	17,9164	-0,1595	0,0347	50,9581
35 / 1 .	30,499	2,7969	0,337	17,2934	-0,1342	0,0084	50,8004
36 / 1 .	30,3709	2,5469	0,2864	17,612	-0,1732	0,0712	50,7143
37 / 1 .	32,1531	3,7009	0,431	14,9881	-0,0991	0,031	51,205
38 / 1 .	29,7726	2,6914	0,2736	18,0449	-0,1177	0,1251	50,7899
39 / 1 .	32,311	3,7496	0,4754	15,6989	-0,1236	0,0301	52,1413
40 / 1 .	31,1513	3,1951	0,3639	15,833	-0,1371	0,0426	50,4488

Appendix J – EMP: Smectite/chlorite, kaolinite and feldspar.

Smectite/chlorite	Oxide										
DataSet/Point	SiO2	Al2O3	CaO	FeO	MnO	Cr2O3	MgO	Na2O	K2O	TiO2	Total
1 / 1 .	47,2306	22,1823	0,7069	6,8715	0,0296	0,0553	1,6235	0,0912	1,1249	0,4686	80,3844
2 / 1 .	46,4481	30,1204	0,3266	5,3023	0,0339	0,0858	1,7025	0,1226	0,2581	0,0624	84,4627
3 / 1 .	46,1143	37,0215	0,0833	1,2754	0,0064	0,0385	0,0799	0,1214	1,0135	0,0737	85,828
4 / 1 .	25,9351	12,2244	0,5405	10,0572	0,0333	-0,0193	1,1497	0,0698	0,5506	0,102	50,6434
5 / 1 .	47,8631	22,6182	0,4079	6,1524	0,0232	0,0376	1,5374	0,0776	0,9221	0,3621	80,0016
6 / 1 .	31,7203	12,712	0,8456	17,7062	0,1348	-0,0304	2,1106	0,1525	0,4701	0,1251	65,9468
7 / 1 .	19,063	8,2847	0,6334	32,1416	0,3113	0,0064	1,2668	0,0846	0,3981	0,4294	62,6193
8 / 1 .	38,5738	17,8941	1,3102	14,8218	0,0955	0,0169	3,0495	0,145	0,1618	0,0964	76,1649
9 / 1 .	39,9188	19,7481	0,5491	5,8352	0,0401	0,0576	1,3185	0,1338	1,1164	0,79	69,5076
10 / 1 .	46,1304	19,4836	0,502	6,6769	0,0316	0,025	1,2219	0,1084	1,0904	0,3646	75,6347
11 / 1 .	44,9958	18,4634	0,4985	5,9095	0,0255	0,1211	1,1651	0,0992	1,1895	1,0495	73,5171
12 / 1 .	39,9315	27,3185	0,2383	3,2156	0,0128	-0,0255	1,1489	0,1081	0,1867	0,0623	72,1972

Kaolinite	Oxide										
DataSet/Point	SiO2	Al2O3	CaO	FeO	MnO	Cr2O3	MgO	Na2O	K2O	TiO2	Total
1 / 1 .	45,9804	37,4565	0,0335	0,8207	-0,0085	-0,0129	0,0371	0,0422	0,0543	0,0194	84,4227
2 / 1 .	46,058	38,2118	-0,0324	0,1341	0,0429	0,044	0,0216	0,0105	0,0235	-0,0264	84,4877
3 / 1 .	48,6955	35,4539	0,0298	0,6613	0,0086	0,0103	0,1547	0,0114	0,1019	0,0063	85,1336
4 / 1 .	47,4542	33,8636	0,0922	1,3862	0,0386	0,018	0,2501	0,1149	0,2164	0,0119	83,446
5 / 1 .	45,9705	37,2757	0	0,3785	-0,0086	-0,0156	0,1778	0,0379	0,8248	0,017	84,6581
6 / 1 .	46,2787	37,3406	-0,0275	0,4198	0,0021	0,0517	0,0794	0,0229	0,3424	0,0188	84,5291
7 / 1 .	48,1843	36,0177	0,0948	0,91	0,015	0,0077	0,3131	0,0327	0,3867	0,0941	86,0561
8 / 1 .	46,8397	37,9766	0,0038	0,3235	0,0043	-0,0182	-0,001	0,0035	0,0249	0,0088	85,1658
9 / 1 .	45,5376	37,4877	0,0464	0,2003	0,0539	-0,0078	0,0475	0,0009	0,0305	0,0227	83,4196
10 / 1 .	46,8263	25,5814	-0,04	5,9838	0,1589	-0,0253	2,5983	0,1046	11,0347	0,7757	92,9983
11 / 1 .	50,0689	34,0535	0,0273	0,6417	0	-0,0077	0,1495	0,0264	0,179	-0,0169	85,1218

Feldspar	Oxide									
DataSet/Point	SiO2	Al2O3	CaO	FeO	MnO	Na2O	K2O	BaO	Total	
16 / 1 .	65,1492	18,4241	0,0195	0,0306	-0,0343	0,0359	16,8182	0,0094	100,453	
17 / 1 .	64,5243	18,7141	-0,0508	0,0229	-0,0257	0,9963	15,4654	0,7145	100,361	
18 / 1 .	64,0638	18,3562	-0,0881	0,0305	0,0157	0,717	16,0629	0,719	99,8771	
19 / 1 .	64,3473	18,1717	-0,0128	0,0191	-0,0143	0,0383	16,8776	-0,0232	99,4038	
20 / 1 .	64,8071	18,1298	-0,0502	0,0013	-0,0229	0,0158	17,2678	0,0378	100,187	
21 / 1 .	64,2016	18,7916	-0,044	0,0483	-0,0271	0,8618	15,6472	0,9692	100,449	
22 / 1 .	64,8056	18,2196	-0,04	-0,0242	0	0,0322	17,1736	-0,0129	100,154	
23 / 1 .	64,1806	18,6288	-0,0339	0,0356	-0,0243	0,6162	16,107	0,7267	100,237	
24 / 1 .	64,7929	18,2143	-0,0128	0,0115	0,0544	0,0681	17,1972	-0,0215	100,304	
25 / 1 .	63,569	18,8656	-0,0244	0,0178	0,0114	1,482	14,3111	1,9507	100,183	
26 / 1 .	64,5958	18,3116	0,114	0,0013	0,0286	0,0146	17,2748	-0,0704	100,27	
27 / 1 .	64,3394	18,3867	-0,0153	-0,0445	0,0243	0,5728	16,347	0,7141	100,325	
28 / 1 .	65,3411	18,1792	-0,0425	-0,014	-0,0172	0,062	16,9721	-0,0129	100,468	
29 / 1 .	63,8806	18,5521	-0,0051	0,028	-0,0257	0,8191	15,5824	1,2656	100,097	
30 / 1 .	65,3879	18,456	0,141	0,0242	-0,0229	0,0262	16,6295	0,2018	100,844	
31 / 1 .	63,6655	18,7867	0,0989	-0,028	-0,0386	1,4972	14,6378	1,0988	99,7183	
32 / 1 .	64,578	18,4771	0,068	-0,0051	0,0272	0,0602	17,0579	0,018	100,281	
33 / 1 .	63,7754	18,4531	-0,0432	0,0153	-0,0029	0,6002	16,168	0,6524	99,6182	